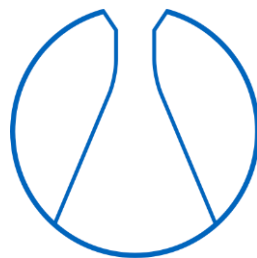




TECHNISCHE UNIVERSITÄT MÜNCHEN  
FAKULTÄT FÜR CHEMIE  
LEHRSTUHL FÜR ORGANISCHE CHEMIE II



**Phenyl Esters as Inhibitors of *S. aureus* ClpP  
and  
Hydroxylamine-based Reverse Polarity ABPP**

Dissertation zur Erlangung des akademischen Grades eines Doktors der  
Naturwissenschaften von

Mathias Willibald Hackl

München 2018





TECHNISCHE UNIVERSITÄT MÜNCHEN  
FAKULTÄT FÜR CHEMIE  
LEHRSTUHL FÜR ORGANISCHE CHEMIE II

**Phenyl Esters as Inhibitors of *S. aureus* ClpP  
and  
Hydroxylamine-based Reverse Polarity ABPP**

Mathias Willibald Hackl

Vollständiger Abdruck der von der Fakultät für Chemie der Technischen Universität München zur Erlangung des akademischen Grades eines

Doktors der Naturwissenschaften (Dr. rer. nat.)

genehmigten Dissertation.

Vorsitzender: Prof. Dr. Michael Groll  
Prüfer: 1. Prof. Dr. Stephan A. Sieber  
2. Priv.-Doz. Dr. Klaus Richter

Die Dissertation wurde am 5.12.2017 bei der Technischen Universität München eingereicht und durch die Fakultät für Chemie am 16.01.2018 angenommen.



Für meine Eltern  
Für meine Frau



„Und alles zusammen, alle Stimmen, alle Ziele, alles Sehnen, alle Leiden, alle Lust, alles Gute und Böse, alles zusammen war die Welt.“

- Hermann Hesse



## Danksagung

An erster Stelle gilt mein Dank Herrn Prof. Dr. Stephan A. Sieber für die Möglichkeit meine Dissertation an seinem Lehrstuhl anzufertigen. Die interessante und herausfordernde Themenstellung, seine persönliche und engagierte Betreuung, exzellente Ausstattung sowie sein Auge für ein ausgewogenes, motiviertes Team haben die letzten Jahre zu einem enorm positiven Erlebnis gemacht. Ich werde mich immer mit Freude an diese Zeit erinnern. Seine Begeisterung für die bearbeiteten Themen, bei gleichzeitiger größtmöglicher persönlicher Freiheit für meine eigenen Arbeiten waren von fundamentaler Bedeutung für den Erfolg dieser Arbeit.

Ich danke meiner Prüfungskommission für Ihre Zeit und Bemühungen bei der Bewertungen dieser Arbeit. Des Weiteren danke ich allen an den Projekten beteiligten Kooperationspartnern. Besonders hervorheben möchte ich hierbei Markus Lakemeyer für die gemeinsame Arbeit am Phenylester-Projekt, ohne seine Neugier, wissenschaftliche Exzellenz und Genauigkeit wären wir mit diesem Projekt nie so weit gekommen. Auch gilt ein besonderer Dank Dr. Nina Bach für die Initiierung des Phosphoaspartat-Projektes und die Betreuung im Verlauf. Ohne die engagierte tägliche Arbeit unserer Technischen Assistenten Frau Katja Bäuml und Frau Mona Wolff wäre eine erfolgreiche Arbeit nicht möglich gewesen. Vielen Dank für eure Geduld und Ausdauer auch die x-te Generation an Doktoranden in die Geheimnisse und Kniffe der täglichen Laborarbeit einzuführen.

Vielen Dank möchte ich darüber meinen aktuellen und ehemaligen Laborkollegen ausrichten, die in den vergangenen Jahren die gemeinsame Zeit erfolgreich und höchst unterhaltsam gestaltet haben. Allen voran den von meiner Anwesenheit direkt betroffenen Kollegen aus Labor B: Dr. Franziska Mandl, Dr. Weining Zhao, Thomas Gronauer, Barbara Hofbauer und Dr. Johannes Kreuzer. Ebenso danke ich: Matthias Stahl, Christian Fetzer, Dr. Johannes Lehmann, Volker Kirsch, Dóra Balogh, Elena Kunold, Philipp Kleiner, Wolfgang Heydenreuter, Dr. Megan Wright, Dr. Max Koch, Annabelle Hoegl, Dr. Katrin Lorenz-Baath, Dr. Axel Pahl, Dr. Maria Dahmen, Dr. Malte Gersch, Dr. Vadim Korotkov, Dr. Pavel Kielkovski und Dr. Georg Rudolph. Viele von euch sind in den letzten Jahren zu guten Freunden geworden, ich hoffe diese Freundschaften werden uns noch länger verbinden. Vielen Dank gilt dem AK Sieber Fußballteam für die legendären Spiele und mehr oder weniger erfolgreichen Turnierteilnahmen. Ebenso gilt mein Dank allen neuen Laborkollegen, die das in den letzten Jahren erreichte nun erhalten und hoffentlich weiter ausbauen werden. Viel Erfolg wünsche ich hierbei besonders Patrick Allihn, bei der Weiterführung des Phosphoaspartat-Projektes.

Zu guter Letzt gilt mein aufrichtiger Dank meiner Familie. Meinen Eltern für die bedingungslose Unterstützung auf allen Wegen in den letzten 30 Jahren, die stete Förderung und das gute Gefühl immer einen sicheren Halt zu haben. Meiner Ehefrau Ruoyu Sun danke ich für ihre

Zuneigung und Liebe, ihren beständigen Ansporn, ihre Inspiration immer nach mehr zu streben und das Eröffnen neuer, spannender Welten. Durch dich habe ich neue, ungeahnte Perspektiven kennen gelernt, die Erde inzwischen mehrmals umrundet und phantastische Menschen getroffen. Vielen Dank für Alles!

INTRODUCTORY REMARKS .....	1
ABSTRACT .....	3
ZUSAMMENFASSUNG .....	5
I — BIOCHEMICAL EVALUATION OF PHENYL ESTER-BASED INHIBITORS OF CASEINOLYTIC PROTEASE P .....	7
1 INTRODUCTION .....	8
1.1 Overcoming antimicrobial resistance by exploiting novel molecular targets .....	8
1.2 Structure and biology of <i>Staphylococcus aureus</i> ClpP .....	9
1.2.1 A proteolytic complex regulates bacterial virulence .....	9
1.2.2 ClpP is highly dynamic and samples multiple conformations .....	9
1.2.3 ClpP and ClpX form a proteolytic complex .....	11
1.3 Small molecule modulators of ClpP .....	12
2 SCOPE OF THIS WORK .....	15
3 RESULTS AND DISCUSSION .....	16
3.1 High-throughput screening and hit filtering .....	16
3.2 Species selectivity and activity in protease assay .....	17
3.3 Mechanism of action and inhibition kinetics .....	18
3.4 <i>In situ</i> target identification .....	20
3.5 Structure-activity relationship of compound stability and binding site occupancy .....	21
3.6 A stereogenic switch for deoligomerization .....	23
3.7 Biological activity .....	25
4. CONCLUSION AND OUTLOOK .....	26
5. EXPERIMENTAL SECTION .....	28
5.1 High-throughput screening .....	28
5.2 Biochemical procedures .....	29
5.2.1 Protein purification .....	29
5.2.2 Peptidase and protease activity assays .....	30
5.2.3 Analytical gel filtration .....	31
5.2.4 High resolution intact protein mass spectrometry .....	31
5.2.5 Determination of acyl-enzyme intermediate stability .....	31
5.2.6 Hemolysis assay .....	32
5.2.7 MTT assay .....	33
5.2.8 <i>In situ</i> analytical labeling .....	33
5.2.9 Western-Blot .....	34
5.2.10 Gel-free <i>in situ</i> target identification of ML16 .....	34
5.2.11 Peptide mass spectrometry and data evaluation .....	35
5.3 <i>In silico</i> studies .....	36

## TABLE OF CONTENTS

5.3.1 Protein and compound preparation .....	36
5.3.2 Docking calculations .....	36
5.3.3 Simulation settings .....	37
II — HYDROXYLAMINE-BASED REVERSE POLARITY ACTIVITY-BASED PROTEIN PROFILING .....	39
1. INTRODUCTION .....	40
1.1 Post-translational modifications and protein phosphorylation.....	40
1.2 Chemistry and biology of phosphoaspartate .....	40
1.3 Activity-based proteome profiling.....	44
2 SCOPE OF THIS WORK .....	46
3 RESULTS .....	47
3.1 Conversion of phosphoaspartate in <i>E. coli</i> PhoB .....	47
3.2 Development of an rp-ABPP protocol based on hydroxylamine .....	52
3.3 Target identification in exponentially growing <i>B. subtilis</i> .....	57
3.4 Target identification in <i>P. aeruginosa</i> under dynorphin treatment .....	59
4 CONCLUSION AND OUTLOOK .....	61
5 EXPERIMENTAL SECTION .....	63
5.1 <i>In vitro</i> studies on <i>E. coli</i> PhoB .....	63
5.1.1 Protein purification .....	63
5.1.2 Generation of PhoBD53N .....	64
5.1.3 <i>In vitro</i> phosphorylation and phosphoaspartate conversion of PhoB .....	64
5.1.4 Intact protein mass spectrometry .....	65
5.1.5 Phosphoaspartate conversion in PhoB in complex proteomic background.....	65
5.2. rp-ABPP method development on analytical scale .....	66
5.3 Gel-free target identification.....	67
5.3.1 Labeling in exponentially growing <i>B. subtilis</i> .....	67
5.3.2 Labeling in dynorphin-treated <i>P. aeruginosa</i> .....	68
5.3.3 Label free quantification LC-MS/MS and data evaluation .....	69
BIBLIOGRAPHY.....	71
CURRICULUM VITAE .....	81
LICENSE AGREEMENT .....	83

## INTRODUCTORY REMARKS

The present doctoral dissertation was accomplished between January 2014 and December 2017 under the supervision of Prof. Dr. Stephan A. Sieber at the Chair of Organic Chemistry II of the Technische Universität München.

Parts of this thesis have been published in:

Hackl, M. W., Lakemeyer, M., Dahmen, M., Glaser, M., Pahl, A., Lorenz-Baath, K., Menzel, T., Sievers, S., Böttcher, T., Antes, I., Waldmann, H. and Sieber, S.A. Phenyl Esters Are Potent Inhibitors of Caseinolytic Protease P and Reveal a Stereogenic Switch for Deoligomerization, *J. Am. Chem. Soc.*, **2015**, 137, 8475.

Publications not highlighted in this thesis:

Gersch, M., Hackl, M.W., Dubiella, C., Dobrinevski, A., Groll, M. and Sieber, S.A. A Mass Spectrometry Platform for a Streamlined Investigation of Proteasome Integrity, Posttranslational Modifications, and Inhibitor Binding, *Chem. Biol.*, **2015**, 22, 404.

Pahl, A., Lakemeyer, M., Vielberg, M.-T., Hackl, M.W., Vomacka, J. Korotkov, V.S., Stein, M. L., Fetzer, C., Lorenz-Baath, K., Richter, K., Waldmann, H., Groll, M. and Sieber, S.A. Reversible Inhibitors Arrest ClpP in a Defined Conformational State that Can Be Revoked by ClpX Association, *Angew. Chem. Int. Ed.*, **2015**, 54, 15892.



## ABSTRACT

Spreading of antimicrobial resistance is a major threat for human health in the 21<sup>st</sup> century. With more and more bacteria becoming insensitive towards classical antibiotics, novel molecular targets are becoming increasingly important to overcome the anti-infectives crisis. During active infections, bacteria produce virulence factors, causing devastating effects in the host. Therefore, understanding and manipulating virulence regulation has become a promising approach in the fight against resistant bacteria over the last years. In the present thesis, chemical biology is used to investigate two very distinct aspects of bacterial virulence:

(1) Caseinolytic protease P (ClpP) is a central virulence regulator in the opportunistic pathogen *Staphylococcus aureus*. Genetic and chemical knock-out of ClpP has been linked to reduced virulence by previous studies. To overcome the limitations of  $\beta$ -lactones, the previous gold standard inhibitors of ClpP, an unbiased high-throughput screen of over 137000 compounds against ClpP was conducted. Phenyl ester-based inhibitors were identified as novel chemical entities for the inhibition of ClpP. The compounds displayed unprecedented potency and target selectivity towards *S. aureus* ClpP. Mechanistic studies showed that the inhibitors trap the protease in the acyl-enzyme intermediate state and induce the deoligomerization of the tetradecameric complex into two heptameric rings. The stereochemistry of a methyl group in *alpha*-position to the central ester moiety was identified to be essential for the oligomerization state of ClpP. The intrinsic instability of the phenyl ester core motif limits their biological applicability, however, phenyl ester-based inhibitors could be established as novel tool compounds for the manipulation of *S. aureus* ClpP.

(2) Bacterial virulence and resistance is often regulated by two-component signaling systems via protein aspartate phosphorylation. Analysis of the phosphoproteome, however, mostly focusses on the most prominent serine, threonine and tyrosine phosphorylation sites. The intrinsic lability of the mixed anhydride bond makes global analysis of the phosphoaspartate proteome extremely challenging. To overcome this challenge, conversion of phosphoaspartate by small molecule nucleophiles to a stable derivative was applied. First, a model system based on the *Escherichia coli* response regulator PhoB for the conversion of phosphoaspartate was established. Subsequently, a reverse polarity activity-based proteome profiling platform using a hydroxylamine-derived probe was developed. The methodology was further applied for the identification of probe-reactive proteins in exponentially growing *Bacillus subtilis*. A subset of chemotaxis and motility-associated proteins was identified as the most promising targets. Finally, the workflow was used to study, how the virulence-enhancing hormone dynorphin changes the reactivity of the proteome of the human pathogen *Pseudomonas aeruginosa* towards the probe.



## ZUSAMMENFASSUNG

Die zunehmende Ausbreitung antimikrobieller Resistenzen stellt eine der zentralen Herausforderungen für die menschliche Gesundheit im 21. Jahrhundert dar. Da immer mehr Bakterien gegen klassische Antibiotika resistent werden, gewinnen neue molekulare Angriffsziele zunehmend an Bedeutung, um diese Antibiotika-Krise zu überwinden. Während aktiven Infektionsprozessen produzieren Bakterien Virulenzfaktoren, die dem Wirt erheblichen Schaden zufügen. Das Verständnis und die Beeinflussung der Virulenzregulation haben sich im Laufe der letzten Jahre zu einem vielversprechenden Ansatz im Kampf gegen resistente Bakterien entwickelt. In der hier vorliegenden Dissertationsschrift werden chemisch-biologische Methoden beschrieben um zwei verschiedene Aspekte bakterieller Virulenzregulation zu untersuchen.

(1) Die caseinolytische Protease P (ClpP) ist ein zentraler Virulenzregulator des opportunistischen Krankheitserregers *Staphylococcus aureus*. Frühere Studien konnten zeigen, dass die genetische und chemische Deletion von ClpP in einer Reduktion der Virulenz resultiert.  $\beta$ -Lactone stellten bisher den Goldstandard für die Inhibition von ClpP dar. Um deren limitierende Faktoren zu überwinden, wurde ein ergebnisoffenes Hochdurchsatz-Screening mit über 137000 Verbindungen gegen die Aktivität von ClpP durchgeführt. Phenylester-basierte Verbindungen wurden dabei als neue chemische Klasse zur Inhibition von ClpP identifiziert. Die Verbindungen zeigten noch nie dagewesene Potenz und Selektivität gegenüber *S. aureus* ClpP. Weitere Untersuchungen zeigten, dass die Inhibitoren die Protease im Azyl-Enzym-Intermediat arretieren und so die Deoligomerisierung des tetradecamerischen Komplexes in zwei heptamerische Ringe auslösen. Dabei hat die Stereochemie an einer Methylgruppe in *alpha*-Position zur zentralen Estereinheit einen essentiellen Einfluss auf den Oligomerisierungszustand von ClpP. Die intrinsische Instabilität des zentralen Phenylester-Motivs begrenzt zwar die biologische Anwendbarkeit der Substanzklasse, nichtsdestotrotz konnten die Inhibitoren als neuer Goldstandard für die Manipulation von *S. aureus* ClpP etabliert werden.

(2) Bakterielle Virulenz und Resistenz werden häufig über Zwei-Komponenten-Signaltransduktionssysteme unter Verwendung von Aspartatphosphorylierung reguliert. Dennoch beschränken sich phosphoproteomische Studien häufig auf die Analyse der bekanntesten Phosphorylierungsstellen an Serin, Threonin und Tyrosin. Die intrinsische Instabilität des gemischten Säureanhydrids des Phosphoaspartates macht die globale Analyse extrem anspruchsvoll. Um dieser Herausforderung zu begegnen wurden die Phosphoaspartate durch Reaktion mit niedermolekularen Nucleophilen zu stabileren Derivaten umgesetzt. Hierfür wurde zunächst ein Modellsystem für die Umsetzung, basierend

## ZUSAMMENFASSUNG

auf dem Protein PhoB aus *Escherichia coli*, etabliert. Anschließend wurde eine aktivitätsbasierte Proteinprofiling Methode für Moleküle mit inverser Polarität entwickelt, wofür eine Hydroxylamin-basierte Sonde eingesetzt wurde. Diese Methode wurde anschließend eingesetzt, um die Zielproteine der Sonde in *Bacillus subtilis* während der exponentiellen Wachstumsphase zu bestimmen. Dabei wurde eine Gruppe von Chemotaxis und Motilitäts-assoziierten Proteinen als die vielversprechendsten Zielproteine identifiziert. Zu guter Letzt wurde die Methode benutzt, um zu untersuchen wie das Virulenz-verstärkende Hormon Dynorphin die Reaktivität des Proteoms des Humanpathogens *Pseudomonas aeruginosa* gegenüber der Sonde verändert.

## I — BIOCHEMICAL EVALUATION OF PHENYL ESTER-BASED INHIBITORS OF CASEINOLYTIC PROTEASE P

The following chapters are based upon work published in: Hackl, M. W.\* , Lakemeyer, M.\* , Dahmen, M., Glaser, M., Pahl, A., Lorenz-Baath, K., Menzel, T., Sievers, S., Böttcher, T., Antes, I., Waldmann, H. and Sieber, S.A. Phenyl Esters Are Potent Inhibitors of Caseinolytic Protease P and Reveal a Stereogenic Switch for Deoligomerization, *J. Am. Chem. Soc.*, **2015**, 137, 8475. \* contributed equally. M.W.H.: peptidase activity assays of initial hit compounds, SEC, IP-MS, protein purification, gel-free quantitative target-ID, acyl-enzyme stability, cytotoxicity and hemolysis assays. M.L.: synthesis, peptidase activity assays of AV170-derivatives and gel-based ABPP. M.D.: protease activity assays of initial hit compounds, protein purification. M.G.: QM-MM studies. A.P., M.T., S.S.: high-throughput screening. K.L.-B.: plasma stability testing.

Reproduced in part with permission from Hackl, M. W.\* , Lakemeyer, M.\* , Dahmen, M., Glaser, M., Pahl, A., Lorenz-Baath, K., Menzel, T., Sievers, S., Böttcher, T., Antes, I., Waldmann, H. and Sieber, S.A. Phenyl Esters Are Potent Inhibitors of Caseinolytic Protease P and Reveal a Stereogenic Switch for Deoligomerization, *J. Am. Chem. Soc.*, **2015**, 137, 8475. Copyright 2015 American Chemical Society.

## 1 INTRODUCTION

### 1.1 Overcoming antimicrobial resistance by exploiting novel molecular targets

At the 2017 G20 summit the world's leaders highlighted that the development and spreading of antimicrobial resistance poses a growing threat to public health and economic growth worldwide.<sup>1</sup> The accidental discovery of penicillin in 1928 marked the beginning of the antibiotic era. Previously fatal bacterial infections seemed to become easily controllable and therefore antibiotics were regarded as miracle drugs.<sup>2-3</sup> However, already in the original publication of Fleming some bacteria were found to be insensitive towards penicillin, which could later be ascribed to penicillin-inactivating enzymes termed penicillinases.<sup>4</sup> As early as 1941 it was shown that bacteria such as *Staphylococcus aureus* could be rendered penicillin-resistant by multiple passaging in the presence of the drug.<sup>5</sup> First reports of penicillin-resistant clinical isolates emerged soon after these *in vitro* findings.<sup>6-7</sup> The peak of antibiotic drug discovery in the 1960s marked at the same time the end of the golden era of the antibiotics.<sup>8</sup> Since then misguided use of antibiotic agents in humans as well as in animal livestock led to the accelerated spread of resistant bacteria while at the same time antimicrobial drug discovery pipelines were drying up.<sup>9-10</sup> Today, up to 50000 deaths in Europe and the United States alone are attributed to antimicrobial resistance, with global numbers as high as 700000.<sup>11</sup>

*Staphylococcus aureus* is a wide-spread opportunistic human pathogen, with up to 37% of the general population being asymptomatic nasal carriers of *S. aureus*.<sup>12</sup> The ability to colonize healthy individuals without causing any symptoms makes *S. aureus* a normal part of the commensal microbiome. However, *S. aureus* can also cause severe to fatal infections of the skin, soft tissue or the blood stream.<sup>13</sup> The ease of spreading through skin-to-skin contact and the readiness with which *S. aureus* acquires antimicrobial resistance makes it a severe threat to public health.<sup>3</sup> The WHO identified methicillin- and vancomycin-resistant *S. aureus* strains as one of their twelve priority pathogens for the development of novel therapeutics and listed them under "high" priority.<sup>9</sup> Beyond the development of novel "classical" antibiotics which aim to eradicate bacteria via a bactericidal or bacteriostatic mode of action, novel therapeutic options are sought.<sup>14</sup> Anti-virulence drugs aim to disturb bacterial virulence to render the bacteria less harmful and allow the immune system of the host to cure the infection.<sup>15</sup> This approach thereby exploits novel molecular targets, exerts less selective pressure and should preserve the host's microbiome. Anti-virulence approaches include the direct inhibition of toxins, secretory systems, cell-to-cell signaling, biofilm formation and the inhibition of virulence regulation systems.<sup>16-17</sup> One promising target to address virulence regulation in the pathogen *S. aureus* is the caseinolytic protease P (ClpP).

## 1.2 Structure and biology of *Staphylococcus aureus* ClpP

### 1.2.1 A proteolytic complex regulates bacterial virulence

Proteolytic events are vital processes for all living organisms and are therefore often tightly regulated.<sup>18</sup> The controlled degradation of proteins plays a central role in protein quality control, unfolded protein response and regulatory events.<sup>19-20</sup> The serine protease ClpP was first identified as the proteolytic subunit of a two-component protease complex isolated from *Escherichia coli*.<sup>21-25</sup> ClpP associates with AAA+ (ATPases associated with diverse cellular activities) ATPases belonging to the Hsp100 family, such as ClpA and ClpX, to form the proteolytic active complex.<sup>26-29</sup> ClpP is an evolutionary highly conserved protease and homologs of the first identified *E. coli* protein can not only be found in almost all bacteria but also in a variety of eukaryotes and even in *Homo sapiens* where it is localized in the mitochondria.<sup>30-32</sup> When studying the biological relevance of ClpP in the pathogen *S. aureus*, *Frees et al.* found that knockout of the *clpP* gene leads to reduced unfolded protein removal, growth defects and reduced virulence.<sup>33</sup> In particular it could be shown that *clpP* deletion mutants are less infective in a murine skin abscess model and that the secretion of the two hemolytic exoproteins  $\alpha$ - and  $\beta$ -hemolysin is greatly reduced.<sup>33</sup> The lower levels of hemolysin  $\alpha$  secretion are caused by a diminished transcription of the corresponding gene *hla*, indicating that hemolysin expression is influenced by ClpP-mediated regulatory proteolytic events further upstream. A possible route is the *agr* virulence regulatory network involving RNAlII and the HTH-type transcriptional regulator Rot, which is a putative ClpP substrate.<sup>34</sup> ClpP-mediated virulence regulation is not only limited to *S. aureus* but is also found in other human pathogens such as *Yersinia enterocolytica*, *Salmonella typhimurium* and *Listeria monocytogenes*.<sup>35-37</sup> These findings make ClpP an attractive target for the exploration of anti-virulence strategies.

### 1.2.2 ClpP is highly dynamic and samples multiple conformations

Detailed biochemical knowledge of the structure and function of the protease is essential to successfully exploit it as a drug target. Several crystal structures of ClpP from a variety of organisms have been solved so far, and all reveal a highly similar, compartmentalized architecture.<sup>30</sup> *S. aureus* ClpP forms homo-tetradecamers that build up the barrel-shaped peptidolytic active complex. The barrel is formed by two heptameric rings that are stacked upon each other, establishing a confined reaction chamber for the 14 active sites (Fig. 1A-B).<sup>38</sup> Every ClpP monomer consist of three distinct regions: N-terminal loops, a central head domain and a flexible handle domain (Fig. 1C).<sup>39</sup> The axial N-terminal loops are highly dynamic and play a role in the binding of ClpP-associated chaperones like ClpX.<sup>40</sup> The catalytic triad Ser98, His123 and Asp172 resides within the central head domain. Furthermore, intra-ring monomer-to-monomer contacts are established by neighboring head domains. Inter-ring contacts, however, are mediated by the highly dynamic handle region formed by  $\alpha$ -helix E and  $\beta$ -strand 9.

Different conformations of this handle region directly impact the alignment of the catalytic triad, thereby influencing the activity of the complex.<sup>38-39, 41</sup>

To understand the tight connection of protease conformation and activity, it is worthwhile to take a look at the generally accepted mechanism of serine proteases.<sup>42</sup> The aspartate-histidine charge relay system of serine proteases increases the nucleophilic reactivity of the active site serine by polarization of the  $\beta$ -hydroxyl group proton. The oxygen atom of the hydroxyl group attacks the carbonyl-C of a substrate peptide bond resulting in the formation of a first tetrahedral reaction intermediate. The histidine, acting as a base, accepted the hydroxyl group's proton and now carries a positive charge which, in turn, is stabilized by the  $\gamma$ -carbonyl group of the catalytic triad aspartate. The tetrahedral intermediate carries a negative charge at the carbonyl oxygen which is stabilized by the oxyanion hole of the protease. After electron pair rearrangement the tetrahedral intermediate is resolved and the novel aminoterminal part of the substrate accepts the proton from the catalytic histidine and is finally expelled. The novel C-terminal part of the substrate remains attached to the active site as an acyl-enzyme intermediate. In order to complete peptide bond cleavage, this intermediate needs to be deacylated. Water is activated by the catalytic histidine, which acts again as a base. The activated water attacks the acyl-enzyme intermediate, resulting in the formation of a second tetrahedral intermediate. The reaction cycle is finalized with the expulsion of the novel C-terminal part of the peptide substrate and protonation of the active site serine.<sup>42</sup> This catalytic cycle illustrates that the activity of serine protease is highly dependent on the accurate alignment of the active site residues to each other. If this charge relay system is disturbed, catalytic activity will be lost.

Three different conformations of *S. aureus* ClpP have been observed in crystallographic experiments: extended, compact and compressed.<sup>38-39, 41, 43</sup> Only the extended conformation represents an active state of ClpP, since the catalytic triad is not aligned in the latter two states. Differences are most striking between compressed and extended state. In the compressed state the ClpP barrel is about 10 Å smaller in height than in the extended state, since the handle domain helix E adopts a kinked conformation and is not fully straightened (Fig. 1C). The handle kink leads to abolition of a hydrogen bond network of three highly conserved glycine residues (Gly127, Gly128, Gly131), which mediates contacts between  $\beta$ -strand 9 of the handle domains in the opposing rings of the barrel. Furthermore the kink of the helix leads to a change of orientation of Arg171. This residue usually links one subunit with its adjacent neighbor inside the same heptameric ring via Gln132 and with its neighbor in the opposing ring by hydrogen bonding to Asp170. All these interactions of Arg171 are lost in the compressed state of ClpP. Finally, this shift of Arg171 in the compressed conformation leads to a protrusion of the catalytic triad Asp172 next to it, which then results in a 3.5 Å shift of His123 away from

the active site Ser98 (Fig. 1D). Therefore charge relay, and by this catalytic activity, is only possible in the extended state.<sup>39</sup>

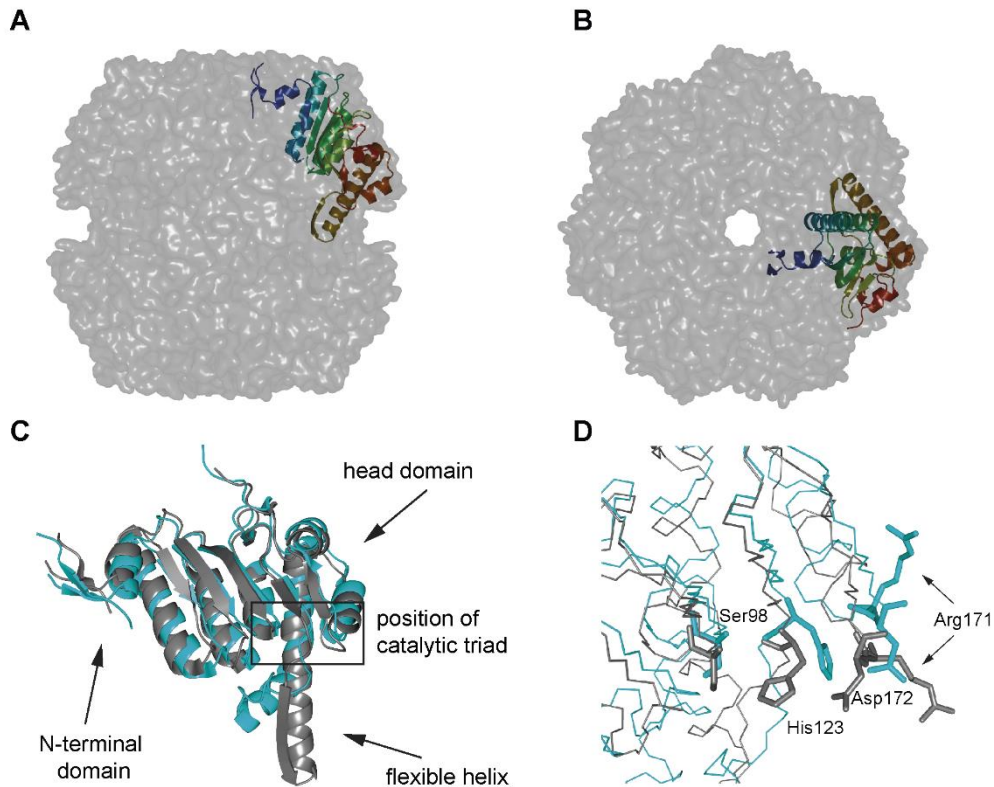


**Figure 1:** ClpP samples extended (PDB: 3V5E) and compressed (PDB: 3QWD) conformations. **(A-B)** Tetradecameric ClpP in the active extended conformation in side view and top view in gray surface representation. One monomer is highlighted in colors from blue (N-terminus) to red (C-terminus). **(C)** Structure alignment of the extended, active conformation (gray) and the compressed, inactive conformation (cyan). **(D)** Comparison of the active site and the deoligomerization sensor Arg171 in extended and compressed conformation.

Mutational studies of the residues involved in interring contacts underlined the crystallography results and could establish a direct connection between oligomerization state and catalytic activity. If the tetradecameric assembly is lost, catalytic activity is also abolished.<sup>39, 41</sup> Biomolecular NMR studies and computational simulations both indicate that ClpP samples several conformations in solution.<sup>40-41, 44</sup> Conformational switching might occur spontaneously or as part of the catalytic cycle of ClpP. No structural data is yet available to prove the exact mechanism, but it is speculated that product release might either occur via orchestrated formation of equatorial side pores or a simultaneous switch of all 14 subunits resulting in transient loss of interring contacts.<sup>39, 41</sup>

### 1.2.3 ClpP and ClpX form a proteolytic complex

Since ClpP alone possesses only limited peptidolytic capabilities, associated co-chaperones like ClpX are required to form the fully functional proteolytic complex.<sup>27, 45-46</sup> ClpX is a disassembly chaperone - also called an unfoldase - of about 46 kDa that belongs to the Hsp100 protein family.<sup>28</sup> It forms ring-shaped homo hexamers and exhibits ATPase activity.<sup>47</sup>

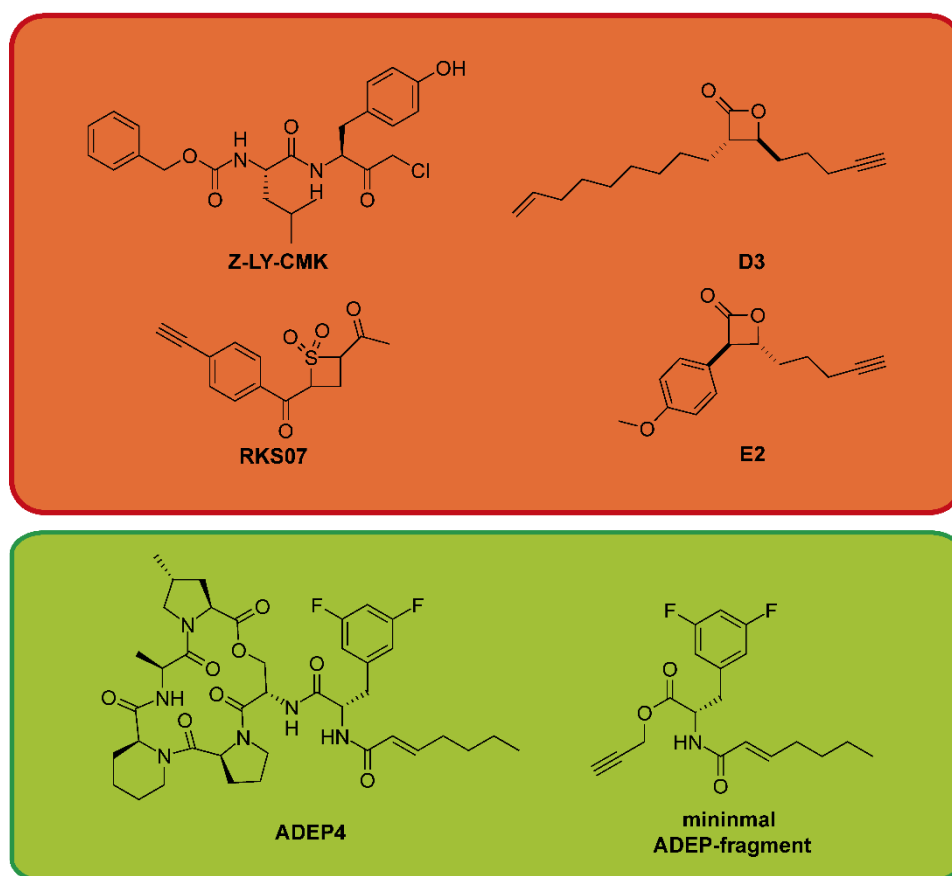
The N-terminal domain plays a role in the recognition of substrate and adaptor proteins and for the stability of the hexamer, whereas the mechanical work of protein unfolding and threading towards ClpP is carried out by two AAA+ domains.<sup>48-49</sup> ClpX recognizes substrate proteins with short unstructured protein degradation sequences, so called degrons, and ssrA-tagged proteins.<sup>50-52</sup> This hydrophobic, C-terminal tag is added when nascent polypeptide chains stall during ribosomal protein biosynthesis and thereby marks the stalled protein for proteolytic degradation by ClpXP.<sup>53</sup> Bound substrates are unfolded under ATP hydrolysis by mechanical pulling events and then threaded through the central pore of the ClpX hexameric ring.<sup>54</sup> During unfolding, ClpX pulls on N- or C-terminal and local structural elements in order to overcome the energy barrier of the stable folded protein.<sup>55</sup> Many of the pulling events are futile, so that dwell phases of unsuccessful pulling and burst phases of translocation alternate, rather than substrate processing being a continuous process.<sup>56</sup> The exact details of ClpX-ClpP binding still remain elusive due to a lack of high-resolution structural data. It is of special interest to solve the question how the symmetry mismatch between the hexameric ClpX ring and its heptameric ClpP counterpart is resolved during binding. However, it is already known that 14-meric ClpP can bind one hexameric ClpX ring on each of its opposing apical sides, but also single-capped ClpXP species have been observed.<sup>57</sup> Tripeptide IGF loops of ClpX are crucial for the interaction of ClpP and ClpX and complex formation requires binding of ATP to ClpX.<sup>29</sup> The IGF loops bind to cavities located between adjacent monomers on the apical sides of ClpP. Electron microscopy studies showed that the formation of the ClpAP proteolytic complex leads to an opening of the axial pores of ClpP.<sup>58</sup> This pore widening increases the accessibility of the proteolytic chamber for translocated substrates. Detailed biochemical studies demonstrated that binding of ClpX exerts conformational control over ClpP beyond axial pore opening by locking the protease in an overactivated conformation with increased catalytic activity.<sup>59</sup>

### 1.3 Small molecule modulators of ClpP

Its biological relevance and thorough biochemical characterization make the ClpP proteolytic machinery an attractive target in drug discovery, and numerous small molecules have been developed to manipulate the protease (Fig. 2). Chloromethyl ketones (CMK) are highly reactive moieties targeting active sites in proteases.<sup>60</sup> Nucleophilic attack on the CMK warhead leads to the displacement of chloride as a leaving group and results in irreversible alkylation of the active site.<sup>61</sup> A dipeptide **Z-LY-CMK** was used to examine the transition state of the proteolytic cycle of ClpP.<sup>62</sup> Although this structural study revealed insights in the mode of action of ClpP, the general applicability of CMK-based inhibitors is limited due to their high reactivity towards all kinds of nucleophilic bio-molecules, such as glutathione, and limited selectivity over non-catalytic proteins.<sup>61</sup> In the course of a proteomic profiling study in bacterial lysates,  $\beta$ -lactones,

strained 4-membered cyclic esters with substituents at the C2 and C3 position, were identified to bind to ClpP.<sup>63</sup> Further studies showed that  $\beta$ -lactones can be applied in pathogenic bacteria like *S. aureus* to inhibit the function of ClpP *in vivo*. Such a chemical knock-down of ClpP results in a phenotype similar to the genetic knock-out observed by *Frees*<sup>33</sup> and coworkers.<sup>64</sup> Virulence factor production is reduced and hemolytic, proteolytic, lipolytic and DNase capabilities are impaired after treatment of *S. aureus* with  $\beta$ -lactones.<sup>65</sup> *In vivo* studies in mice showed a beneficial effect of lactone treatment in a *S. aureus* skin infection model.<sup>66</sup> Lactones were further successfully applied in the context of parasitic and human ClpP. Chemical knock-down of ClpP by lactones leads to reduced growth and development arrest of the malaria-causing pathogen *Plasmodium falciparum*.<sup>67</sup> A lactone-based inhibitor was also used to target ClpP-dependent leukemic cells and promising results on human acute myeloid leukemia were achieved in a xenograft mouse model.<sup>68</sup>

### Inhibitors



### Activators

**Figure 2:** Inhibitors and activators of *S. aureus* ClpP. **Z-LY-CMK** was used in a mechanistic study to elucidate the reaction mechanism of ClpP. Lactone-based inhibitors work either by blockade of all active sites (**D3**) or compound-induced deoligomerization after partial active site modification (**E2**). Sultam **RKS07** leads to dehydroalanine formation at the active site serine. Activators like **ADEP4** dysregulate proteolysis and have strong antibiotic potential. A minimalistic ADEP-fragment was found to be necessary and sufficient for the antibiotic effect.

Mechanistic studies revealed that aliphatic substituted  $\beta$ -lactones, like the initial hit ABPP probe **D3**, perfectly bind to the hydrophobic S1 pocket of *S. aureus* ClpP. Variation of the aliphatic chain length leads to decreased target engagement. ClpP attacks the lactone by its active site serine at the C1 position and induces ring opening of the strained ester. The result is an acyl-enzyme complex that resembles the key intermediate in the natural catalytic cycle of the protease.<sup>69</sup> By this mechanism of action aliphatic lactones, like **D3**, block the active site serines of the ClpP subunits and render them inaccessible for natural substrates. However, this approach needs to block all 14-active sites of a ClpP homotetradecamer to completely inhibit its activity and is non-permanent, since the acyl-enzyme complex can be resolved by attack of water. Beyond active site blockade by acylation, induction of complex deoligomerization and compound-induced dehydroalanine formation at the active site serine are two further mechanisms of ClpP inhibition.<sup>70</sup> Sultams are, like lactones, strained four-membered heterocycles. Treatment of ClpP with sultam-containing inhibitor **RKS07** first leads to sulfonylation of the active site serine followed by an elimination which yields dehydroalanine. Since this reaction is irreversible, the inhibition of ClpP is permanent. However, the low selectivity and high reactivity of the sultam-based inhibitors limit their applicability.<sup>71</sup> Deoligomerization of the tetradecameric complex into two heptameric rings has been observed for diverse compounds such as peptidic CMK, diisopropyl fluorophosphate (DFP), dichloroisocoumarin (DCI), a sultam and lactone **E2**. The latter is a *p*-methoxy phenyl substituted derivative of **D3**. Despite their structural similarity, both lactones possess different modes of action. **E2** only partially acylates the active sites of the tetradecameric complex, but is a more efficient inhibitor of ClpP since it induces complex disassembly into inactive heptamers. Therefore, lower inhibitor concentrations are sufficient to completely abolish the functionality of ClpP. The structural basis for the induction of deoligomerization remains elusive. Inhibition of ClpP has been studied intensively over the last years, however, compound-induced overactivation of the protease is another promising approach in anti-infective research. Natural product-derived acyldepsipeptides (ADEPs) such as **ADEP4** were found to possess potent antibacterial activity against multidrug-resistant Gram-positive bacteria like *S. aureus*, *Streptococcus pneumoniae* and *Enterococcus faecium*. Their activity could be linked to an ATPase-independent activation of ClpP, leading to dysregulation of proteolysis in the treated cells.<sup>72</sup> As a consequence, the degradation of the cell division protein FtsZ ultimately leads to a filamentous phenotype and impaired bacterial growth.<sup>73</sup> The dysregulation of ClpP is caused by uncoupling the proteolytic activity from AAA+ ATPase association. ADEPs bind to the same apical and distal hydrophobic pockets of the ClpP barrel as the associated chaperones like ClpX or ClpA do. A co-crystal structure of a ClpP tetradecamer with 14 bound ADEP molecules has been reported.<sup>74</sup> Investigation of the ADEP chemical space revealed that a minimal *N*-acyldifluorophenylalanine core unit of the ADEP structure is necessary and sufficient to trigger

the activation of ClpP (Fig. 2).<sup>75</sup> Unfortunately resistance development to ADEPs is easily observed, especially in strains where ClpP is not essential or strains that have several slightly different ClpP genes.<sup>72, 76</sup> However, application of ADEPs in combination with classical antibiotic rifampicin shows high potency and even eradicates persister cells and biofilms.<sup>77</sup>

## 2 SCOPE OF THIS WORK

With  $\beta$ -lactones being the only specific ClpP inhibitors known so far, novel compound classes are needed to overcome the intrinsic limitations of lactone-based inhibitors. All lactone-based compounds have only limited target selectivity paired with poor stability in blood plasma, limiting their *in vivo* applicability.<sup>63, 66</sup> Previous rational approaches to replace the lactone warhead by acyclic esters, carbamates, oxetanes or  $\beta$ -lactams only yielded inactive compounds.<sup>69</sup> An unbiased high-throughput screening (HTS) of a library containing over 137000 compounds was conducted against the peptidase activity of *S. aureus* ClpP. Hit evaluation identified six structurally very similar compounds as the most potent ClpP inhibitors: five phenyl esters and one triazole amide. The inhibitors were further validated and characterized regarding their species selectivity, their mechanism of action, inhibition kinetics and biological activity. An alkyne-tagged probe was used to elucidate the *in situ* targets of lead compound **AV170**. These studies revealed an unprecedented selectivity for ClpP as the only covalent target of the phenyl ester in living *S. aureus*. In order to increase the plasma and acyl-enzyme intermediate stability of the compounds, structure-activity relationship studies were carried out. In the course of these studies it was discovered that the stereochemistry of a methyl group in *alpha*-position to the central ester moiety decides whether the compound induces ClpP deoligomerization or the tetradecameric state is retained. Molecular docking experiments were carried out to gain more mechanistic insights into this intriguing behavior.

### 3 RESULTS AND DISCUSSION

#### 3.1 High-throughput screening and hit filtering

To overcome the limitations of rational compound design based on the previously identified  $\beta$ -lactone inhibitors, an unbiased high-throughput screen based on the well-established ClpP peptidase assay was conducted and a total number of 137793 compounds were tested at 12.5  $\mu$ M. In the assay, ClpP catalyzes the hydrolytic cleavage of the model dipeptide substrate N-succinyl-Leu-Tyr-7-amido-4-methylcoumarin (Suc-LY-AMC) which leads to the liberation of fluorogenic AMC. The assay was validated by dose-dependent ClpP inhibition using the  $\beta$ -lactone-based inhibitor Palmostatin M (Fig. 3A). The overall Z factor of the screen was determined to be  $0.69 \pm 0.14$  and the overall signal-to-background ratio was  $25 \pm 9$ .

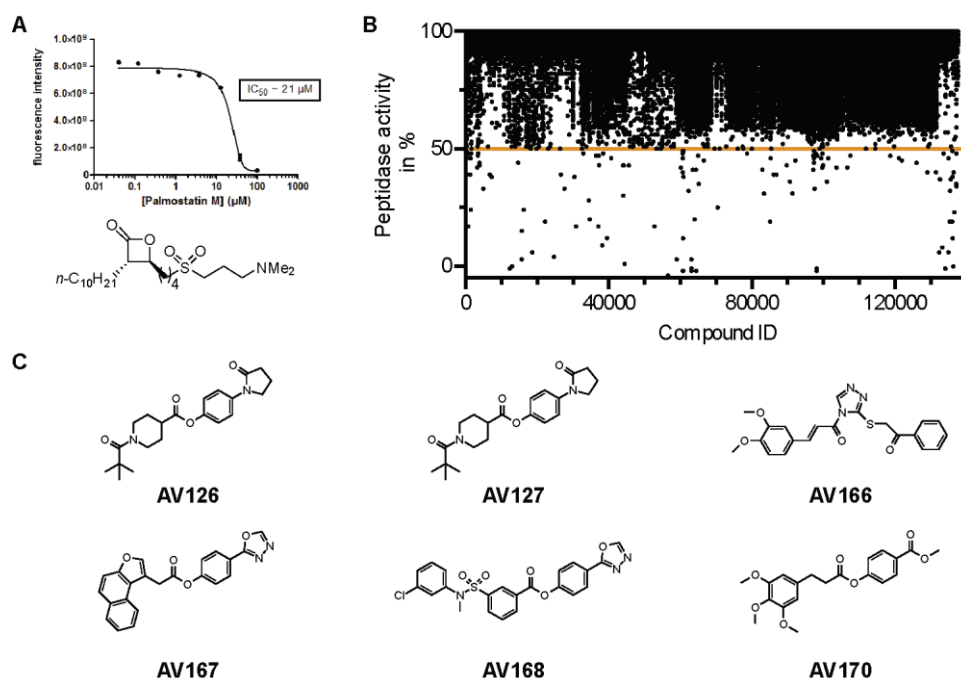


**Figure 3:** ClpP peptidase high-throughput screening. (A) Validation of the HTS assay using  $\beta$ -lactone-based inhibitor Palmostatin M. (B) Screening of more than 137000 compounds identified 161 initial hits with peptidase inhibition of more than 50%. (C) After validation and filtering, six final hits with an  $IC_{50} < 2 \mu$ M remained.

Compounds which reduced the fluorescence signal by at least 50% were defined as primary hits (Fig. 3B). 161 compounds matched this criteria and were further validated in a dose-dependent inhibition assay. Compounds with  $IC_{50}$  values  $< 2 \mu$ M and desirable pharmacological properties were selected for detailed examination. Compounds with a molecular weight below 200 or above 600 Da were excluded as well as organometallic compounds. Furthermore, eight compounds were eliminated because of technical reasons. Out of the 161 primary hits only six compounds were obtained as final hits after this strict filtering process (Fig. 3C). Strikingly, the compounds share high structural similarity: five possess a highly reactive phenyl ester moiety and the sixth compound bears a very similar

triazole amide as its reactive center. Although 1780 phenyl esters were present in the assay, only five (0.28%) of them were identified as hits. This demonstrates that general compound reactivity is not sufficient, but that access to the active site of ClpP is limited and structurally very challenging. The aromatic stabilization of the phenyl or triazole leaving group of the hit compounds seems to be a crucial aspect that favors them over previously rationally designed inhibitors. Consequently, it is not surprising that all rational attempts to replace the lactone warhead by acyclic esters have failed so far.<sup>69</sup>

### 3.2 Species selectivity and activity in protease assay

To test whether the identified hits also act on ClpPs from other species, three-point peptidase assays (100  $\mu$ M, 10  $\mu$ M and 1  $\mu$ M) were performed with ClpP from *S. aureus*, *E. coli* and *L. monocytogenes* (Fig. 4A-C). In the case of *L. monocytogenes*, which encodes two ClpP isoforms, the catalytic active ClpP2-homocomplex was used. **AV170**, followed by **AV126** and **AV166** were identified as the most active compounds against *S. aureus* ClpP.

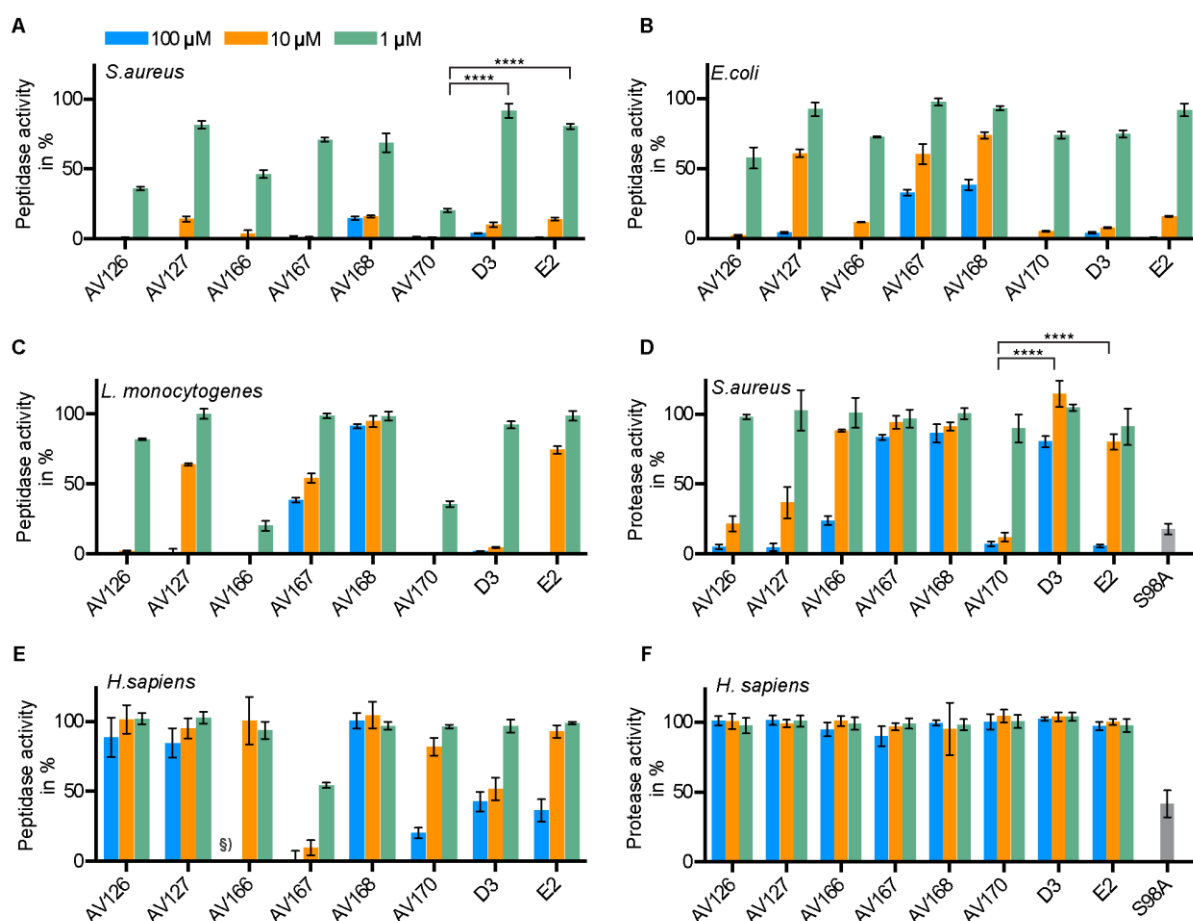


**Figure 4:** Determination of species selectivity and protease inhibition. The six final HTS hits were examined regarding their selectivity for ClpPs from different organisms, including *S. aureus* (A), *E. coli* (B), *L. monocytogenes* (C) and *H. sapiens* (E). Inhibition of the ClpXP proteolytic complex was assessed for *S. aureus* (D) and *H. sapiens* (F). Experiments were carried out in triplicates or duplicates of triplicates (*S. aureus*). \*\*\*\* indicates a p-value of  $\leq 0.0001$  determined by Student's t-test. §) Due to internal fluorescence of **AV166**, measurements at 100  $\mu$ M were omitted from analysis.

All hits showed their highest potency against *S. aureus* ClpP, with exception to **AV166** which was slightly more active against *L. monocytogenes* ClpP2. These results indicate a high species selectivity of the phenyl esters even among highly similar bacterial ClpPs. This further underlines that not the general reactivity of the phenyl ester motif is responsible for the high potency of the compounds, but rather a very narrow target profile defined by structural requirements. Compared to the previous gold standard  $\beta$ -lactone-based inhibitors **D3** and **E2**, phenyl ester **AV170** showed a 4.5 to 4-fold higher potency against *S. aureus* ClpP at the lowest tested concentration of 1  $\mu$ M. Remarkably, **AV170** was also found to be a potent inhibitor in the GFP-ssrA degradation assay as well (Fig. 4D). This assay surveys the proteolytic activity of the *S. aureus* ClpXP complex. ClpX was shown to exert conformational control over ClpP which might weaken the inhibitor's residence time in the active site or even completely revoke inhibitor binding.<sup>59, 78</sup> However, **AV170** was shown to fully inhibit the ClpXP complex at 10  $\mu$ M, whereas lactone **E2** barely had any effect on the complex at this concentration. Strikingly, the non-deoligomerizing lactone **D3** was completely inactive in the protease assay. The residual GFP fluorescence decay observed in the proteolytic inactive ClpXP(S98A) complex is caused by ClpX-mediated unfolding and not by proteolytic degradation (Fig. 4D). The most potent phenyl esters **AV126**, **AV127** and **AV170** abolished also this unfolding-mediated fluorescence decay, suggesting a mechanism of action that also impairs ClpX-mediated substrate unfolding. The activity of the phenyl esters was also tested against human ClpP and ClpXP (Fig. 4E-F). On the one hand, human ClpP is an attractive novel anti-cancer target for treatment of AML, on the other hand mutations in human ClpP are also known to cause the *Perrault* syndrome associated with sensorineural hearing loss and ovarian failure.<sup>68, 79-80</sup> For a potential antibacterial medical application, target selectivity for bacterial over human ClpP is therefore deemed favorable. Satisfyingly, all tested compounds except **AV167** were much less potent against human ClpP than they were against *S. aureus* ClpP. **AV170** did not inhibit human ClpP activity up to a concentration of 10  $\mu$ M, whereas lactone **D3** reduced activity by 50%. All tested compounds showed no activity at all in the human ClpXP assay. Based on the high potency of the compounds and the favorable reactivity profile with discrimination against human ClpP, the binding mode and mechanism of action were examined in more detail.

### 3.3 Mechanism of action and inhibition kinetics

To test whether phenyl esters work as covalent inhibitors, an excess of **AV170** was incubated with ClpP and intact protein mass spectrometry experiments were conducted (Fig. 5A). The spectra showed adduct formation on about 40% of ClpP monomers. The mass of the observed adduct corresponds to the formation of an acyl-enzyme intermediate under simultaneous liberation of the inhibitor's phenol leaving group. Only one adduct was formed, hinting for a site specific reaction. No covalent adducts were observed when the catalytic site mutant S98A was

used, demonstrating that the inhibitors are active site directed. Analytical size exclusion chromatography was employed to monitor the oligomerization state of ClpP. After compound treatment under saturating conditions only heptameric ClpP was observed, whilst DMSO treated control samples retained tetradecameric oligomerization (Fig 5C). All tested inhibitors induced deoligomerization into heptamers under only partial modification of the active sites of about 20 to 50%. Only **AV167**, with its large naphthofuran moiety, modified all active sites but nonetheless also followed a deoligomerization route.

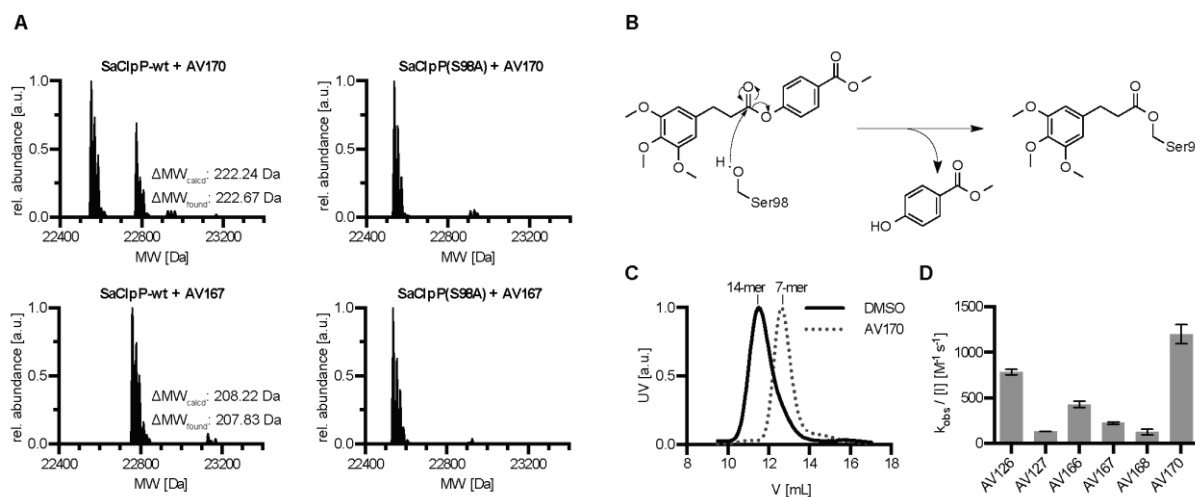


**Figure 5:** Mechanism of action of phenyl ester and triazole amide based inhibitors. **(A)** Intact protein mass spectrometry of ClpP wt and S98A after compound treatment reveals an active site directed, covalent inhibition mechanism. **(B)** Proposed reaction mechanism requires nucleophilic attack of Ser98 at the reactive ester moiety under liberation of a stabilized phenol leaving group. The active site serine is trapped in the acyl-enzyme intermediate state. **(C)** Analytical size exclusion chromatography shows that phenyl esters follow a deoligomerizing inhibition principle **(D)** Phenyl ester compounds demonstrate very fast inactivation kinetics.

The tested phenyl ester compounds and the triazole amide **AV166** share a common mechanism of action. They covalently modify the active site serine of ClpP through nucleophilic attack of Ser98 at the reactive core motif and trap the enzyme in the acyl-enzyme intermediate (Fig. 5B). The stabilized phenol or triazole leaving group is liberated in this process, leaving only the acid part of the inhibitor attached to ClpP. This acylation of the active site induces separation of the two stacked, tetradecameric rings of the protease and disassembly of the barrel. The resulting heptameric ClpP is catalytically inactive. ClpX-ClpP interaction is presumably also affected by ClpP deoligomerization and substrate proteins are stalled at ClpX, since GFP unfolding was found to be abolished under compound treatment in the protease assay (Fig 4D). Since not all active sites need to be modified to induce deoligomerization, this mechanism of inhibition is more efficient than acylation of the active sites without deoligomerization. This could be confirmed by measurement of the apparent inactivation constant  $k_{\text{obs}}/[I]$  (Fig. 5D). Previously reported gold standard inhibitors **D3** and **E2** have  $k_{\text{obs}}/[I]$ -values of  $78 \pm 6 M^{-1} s^{-1}$  and  $64 \pm 3 M^{-1} s^{-1}$ , respectively.<sup>70</sup> Phenyl ester **AV170** exhibits extremely fast inactivation kinetics of  $1200 \pm 105 M^{-1} s^{-1}$ . The inactivation rate constant

surpasses not only the one of non-deoligomerizing **D3**, but is also almost 19-times faster than that of deoligomerizing lactone **E2**. The high reactivity of the phenyl ester core motif paired with high binding preference for the ClpP active site and a favorable deoligomerizing mode of action make **AV170** a very promising candidate for further biological validation.

### 3.4 *In situ* target identification

Activity-based proteome profiling was used to determine the intracellular target profile of **AV170** in living *S. aureus* cells. **AV170** was synthetically modified and an alkyne handle was introduced at the site of the *p*-methoxy group in the acid part of the inhibitor: This part of the molecule remains covalently bound to the target molecules of the phenyl ester after nucleophilic attack. The bioorthogonal alkyne motif enables the selective introduction of reporter groups such as rhodamine azide or biotin azide by copper-catalyzed azide-alkyne cycloaddition (CuAAC).

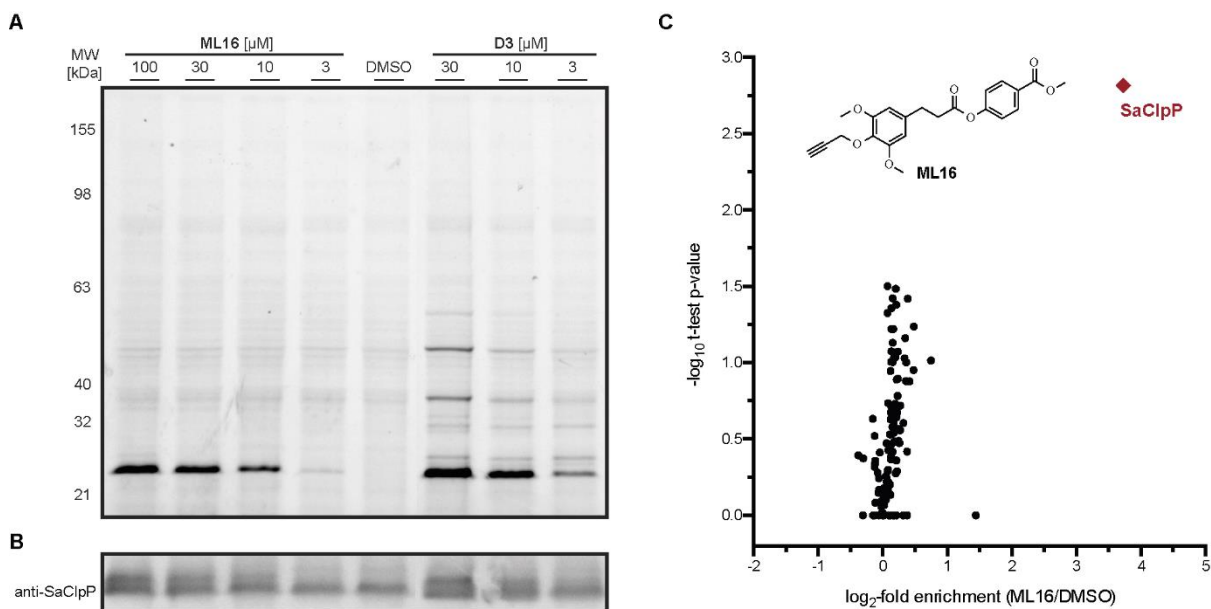


**Figure 6:** *In situ* target identification in *S. aureus* using ABPP technology. (**A-B**) Gel-based fluorescence detection of protein targets of **ML16** compared to lactone probe **D3**. ClpP was confirmed by Western blotting. (**C**) Gel-free quantitative MS analysis of the target profile of **ML16** validates ClpP as the only covalent target of the phenyl ester probe. Quantitative experiments were carried out in biological triplicates.

Living *S. aureus* cells were incubated with different concentrations of **ML16** or **D3** and the labeled proteome was isolated. The fluorescent rhodamine azide reporter tag was introduced and the proteomes were analyzed by SDS-PAGE with subsequent fluorescence visualization (Fig. 6A). The obtained labeling pattern revealed that, even at high concentrations of up to 100  $\mu$ M, labeling with **ML16** gives only one prominent fluorescent band with a molecular weight of about 23 kDa. Lactone **D3**, on the other hand, labels several protein bands already at 30  $\mu$ M compound concentration. The same protein band at about 23 kDa can be found as the main target in the **D3** treated samples and this band has been identified as ClpP by previous studies.

Western blotting and detection with an *anti*-SaClpP antibody colocalized with the fluorescent band, confirming the reported results (Fig. 6B). Since low-abundant targets might be elusive from gel-based fluorescence detection, gel-free quantitative mass spectrometry-based (MS) target identification was performed with probe **ML16** (Fig. 6C). Biotin azide was introduced as a reporter tag and the inhibitor-bound proteins were enriched on avidin beads. Tryptic digestion, followed by liquid-chromatography MS-based analysis revealed that ClpP is the sole and only covalent target of **ML16** in living *S. aureus* cells. ClpP was 13 times enriched over the DMSO treated control sample with a *p*-value of 0.0015. The data show that phenyl ester **AV170** is cell permeable, addresses ClpP in its native environment and possesses unprecedented target selectivity.

### 3.5 Structure-activity relationship of compound stability and binding site occupancy

Lead compound **AV170** traps ClpP in the acyl enzyme intermediate, leading to the generation of a putatively labile ester bond between compound and enzyme. In order to test whether the enzyme-inhibitor complex is reversible, ClpP was incubated with saturating excess of inhibitor and compound-bound ClpP was separated from free inhibitor by size exclusion chromatography. The isolated enzyme-inhibitor complex was analyzed by time-resolved intact protein mass spectrometry (Fig. 7C). It was found that the acyl-enzyme intermediate is prone to hydrolysis and the half-life time of the **AV170**-adduct in the ClpP active site was determined to be  $8.2 \pm 0.8$  h. This is a more stable half-life time than that of lactone-based inhibitor **D3** which was used as the reference system ( $5.0 \pm 0.4$  h).

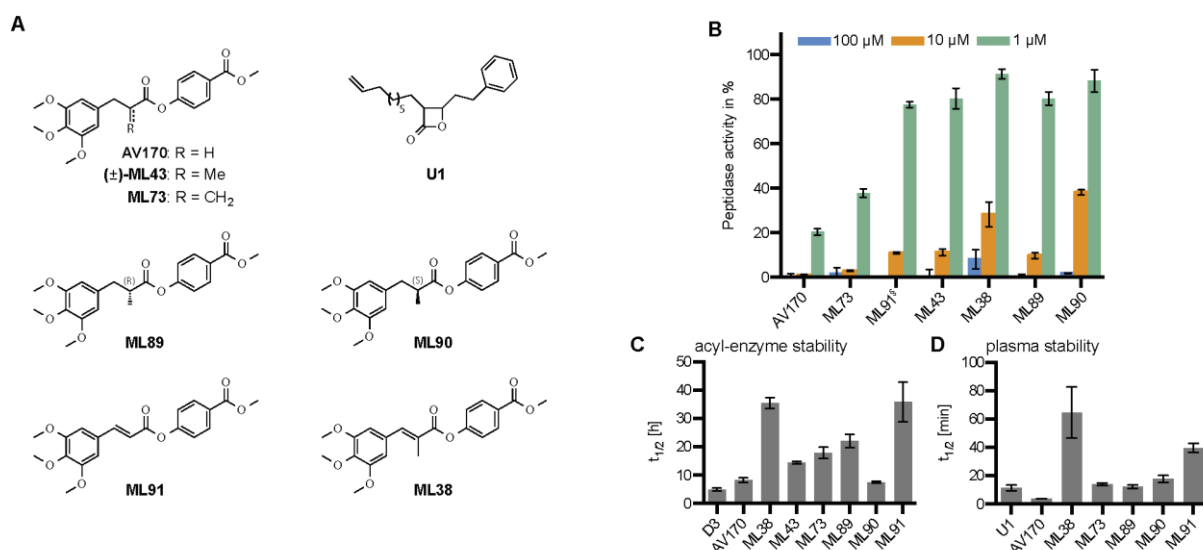


**Figure 7:** SAR studies for the enhancement of acyl-enzyme intermediate and blood plasma stability. (A) Structures of stabilized **AV170**-derivatives and reference lactone **U1**. (B) Peptidase inhibition data of the stabilized derivatives. Experiments were carried out in duplicates of triplicates. (C) Acyl-enzyme intermediate stability. (D) Compound stability in human blood plasma.

To prolong the residence time of the inhibitor on the active site serine, structure-activity relationship studies were carried out. In order to sterically shield the ester bond, a methyl (**ML43**, **ML89** and **ML90**) or methylene group (**ML73**) was introduced in  $\alpha$ -position to the ester bond (Fig. 7A). The methyl group can be placed in (*R*) or (*S*) absolute configuration. The racemic mixture **ML43** had a half-life time of  $14.4 \pm 0.4$  h, whereas enantiomeric pure (*R*)-configured **ML89** and (*S*)-configured **ML90** had half-life times of  $22.0 \pm 2.4$  and  $7.5 \pm 0.4$  h, respectively. Electronic stabilization of the ester by introduction of a double bond at the  $\alpha$ -position further increased the stability to  $35.4 \pm 2.0$  (**ML38**) and  $35.7 \pm 7.0$  h (**ML91**). Similar trends were observed when the compound stability in human blood plasma was determined (Fig. 7D). Plasma stability is a critical factor for potential therapeutic compounds, since it might be limiting the bioavailability of the drug. Lead compound **AV170** had a half-life time of only  $3.7 \pm 0.1$  min, which is roughly a third of the half-life time of reference lactone **U1** ( $11.4 \pm 2.0$  min). Steric shielding (**ML73**, **ML89**, and **ML90**) had moderate effects on blood plasma stability and increased the half-life to time spans comparable to the half-life of lactone **U1**. Mesomeric stabilization (**ML91**) extended the half-life further to  $39.6 \pm 3.2$  min. When both steric and electronic stabilization were combined (**ML38**) the most pronounced effect was observed and blood plasma stability was increased to  $64.6 \pm 18.0$  min. Unfortunately all stabilizing efforts resulted in reduced inhibitory potency of the compounds when tested against ClpP peptidase activity (Fig. 7B), since the stabilizing modifications also reduces the reactivity of the phenyl ester core moiety toward nucleophilic attack by Ser98. Shortened derivatives of lead compound **AV170** were generated to probe how the compound might bind into the S1 binding pocket of ClpP. Two methylene units separate the reactive ester core from the trimethoxyphenyl moiety. Removal of both methylene groups (**ML74**) resulted in almost complete loss of inhibition, while removal of only one unit (**ML21**) retained the inhibitory potential (Fig. 8A-B). Replacement of Leu154 by tyrosine shortens the S1 binding pocket of ClpP significantly. This mutant was used to gain further insight in the binding site occupancy of phenyl ester compounds. While  $100 \mu\text{M}$  **AV170** abolished activity in wt ClpP completely, the L154Y mutant could only be inhibited by about 40%. No such reduction in inhibitory potency was observed with the shortened derivative **ML21**, leading to the conclusion that the trimethoxyphenyl moiety of **AV170** must reside within the S1 binding pocket of ClpP (Fig. 8C) to enable for nucleophilic attack by Ser98. **AV170** cannot be accommodated sufficiently in the shortened S1 binding pocket so that inhibition of ClpPL154Y is impaired.

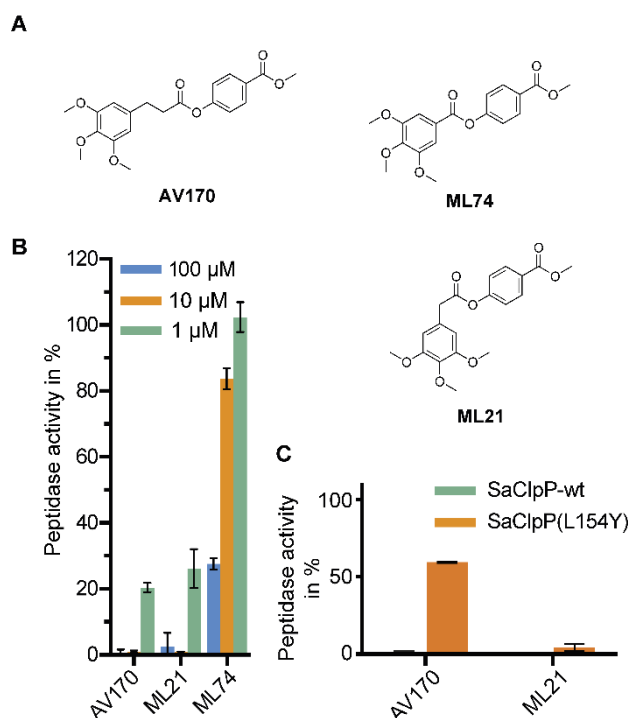


**Figure 8:** Structure-activity relationship studies to probe for the binding mode of **AV170** in the S1 pocket of ClpP. **(A)** **AV170** and derivatives with shortened linker length. **(B)** Peptidase inhibition data reveals a minimum linker length of one methylene unit is required for sufficient target engagement. Experiments were carried out in duplicates or triplicates. **(C)** ClpPL154Y, with its shortened S1 pocket, cannot be inhibited by **AV170** (100  $\mu$ M).

### 3.6 A stereogenic switch for deoligomerization

When the methyl substituted derivatives **ML89** and **ML90** were checked for their influence on ClpP oligomerization state it was found that (*R*)-configured **ML89** follows the known deoligomerizing route described for **AV170** and all other HTS final hits. However, the (*S*)-enantiomer **ML90** does not induce deoligomerization and retains the tetradecameric state of ClpP (Fig. 9A).

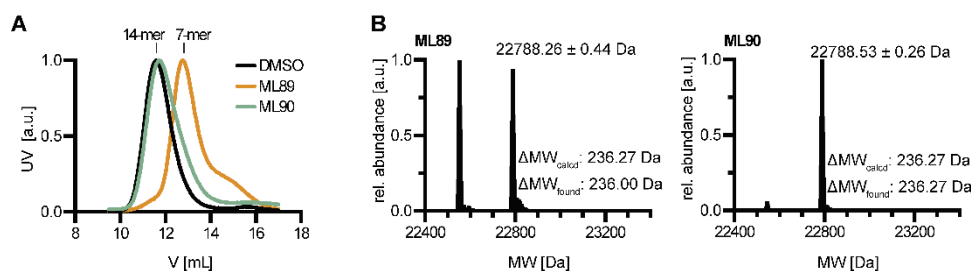


**Figure 9:** Methyl substituted **AV170** derivatives uncover a stereogenic switch for deoligomerization of ClpP. **(A)** Size exclusion chromatography of compound treated ClpP shows different oligomerization states depending on the configuration of the methyl substituted derivatives (*R*)-**ML89** and (*S*)-**ML90**. **(B)** Intact protein mass spectrometry analysis of the degree of active site modification under saturating conditions. Deoligomerizing **ML89** causes only partial modification whereas **ML90** acylates all active sites.

Furthermore, it modifies all active sites of the protease in order to completely shut down catalytic activity, rather than partially modifying ClpP like **ML89** (Fig. 9B). This explains the weaker inhibitory potency of (*S*)-configured **ML90** compared to (*R*)-configured **ML89**.

Henceforth, the stereoconfiguration of a single methyl group in the inhibitor is sufficient to influence the overall oligomeric assembly of a 300 kDa proteolytic machinery. In order to gain further insights into the structural basis of phenyl ester binding, molecular docking experiments were conducted (Fig. 10). Consistent with the experiments with the shortened **AV170**-derivatives **ML21** and **ML74**, it was found that the trimethoxyphenyl moiety of **AV170** resides within the hydrophobic S1 binding pocket of ClpP (Fig. 10A-B). **ML21** also adopts a similar conformation (Fig. 10C). **ML74** on the other hand, with the trimethoxyphenyl directly attached to the ester, is repulsed from the active site (Fig. 10F). Since the entrance to the active site is sterically restricted and the linker between ester and trimethoxyphenyl moiety is needed to span the constricted region, the trimethoxyphenyl moiety of **ML74** is not able to reach the S1 pocket. Therefore, no stable position, in which the nucleophilic attack by Ser98 could occur, can be reached and the compound leaves the binding site.

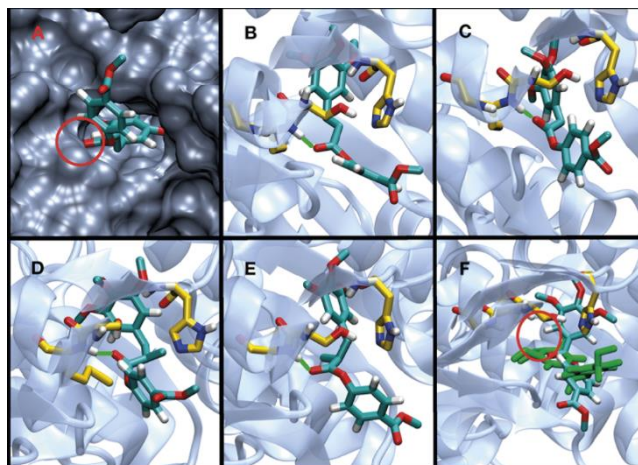


**Figure 10:** Molecular docking experiments. (A) **AV170** bound to the ClpP active site in surface representation. (B-F) Final poses of 5 different phenyl ester compounds after molecular dynamics refinement. Ser98, Met99 (oxyanion hole), His123 and compounds are given in stick representation. ClpP is given in cartoon representation. (B) **AV170**. (C) **ML21**. (D) **ML89**. (E) **ML90**. (F) **ML74** (green: final pose after repulsion from active site).

Docking experiments of the methyl substituted compounds **ML89** and **ML90** gave insights into the molecular basis of the stereogenic deoligomerization switch. The relative orientation of the methyl group differs greatly between both enantiomers. For non-deoligomerizing **ML90** the methyl group adopts a stable position in the constricted area near the oxyanion hole (Fig. 10E). For **ML89**, however, the methyl group directly points toward the histidine of the catalytic triad (Fig. 10D). This might lead to conformational changes in the catalytic triad and thereby trigger deoligomerization. The correct alignment of the catalytic triad has previously been shown to be directly linked to helix E conformation and the oligomeric state. However, it still remains elusive why the non-substituted lead compound **AV170** also induces deoligomerization of the ClpP barrel.

### 3.7 Biological activity

To test whether the excellent *in vitro* inhibitory potency and supreme *in vivo* target selectivity also translate into a beneficial effect on ClpP virulence, hemolysis assays were performed (Fig. 11A). *S. aureus* cells were grown in presence of compound and the culture supernatant was isolated. This supernatant, containing the hemolytic factors, was given to an erythrocyte solution and red blood cell integrity was monitored by absorbance measurement. Satisfyingly, all tested compounds (**AV170**, **ML21**, **ML89** and **ML90**) showed an inhibitory effect on the hemolytic potential of *S. aureus*. The EC<sub>50</sub>-values ranged from 60 to 200 μM for all compounds.

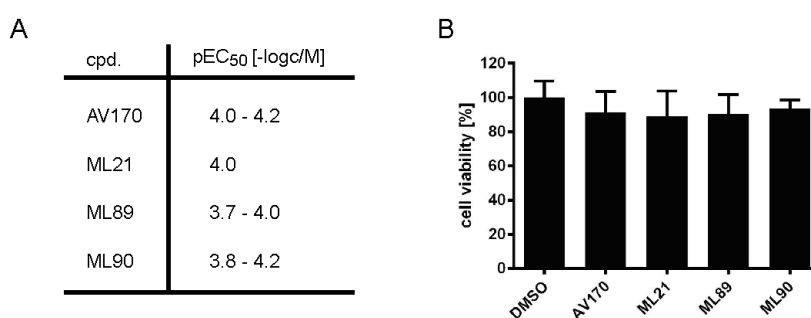


**Figure 11:** Biological activity of selected phenyl ester compounds. **(A)** Anti-hemolytic activity in living *S. aureus* NCTC 8325 cells. Results are given as the range of pEC<sub>50</sub>-values obtained from three independent biological replicates. **(B)** Cytotoxicity was tested by MTT assay in human epithelial lung cancer cell lines A549 at 100 μM compound concentration.

No difference between the tested substances could be detected. Since prolonged incubation of the supernatant still led to an onset of hemolysis even at highest concentrations, it can be assumed that production of hemolytic factors such as  $\alpha$ -hemolysin was not inhibited completely. In order to check for potential cytotoxic effects of the compounds, MTT assays in human epithelial lung cancer cell line A549 were performed (Fig. 11B). High compound concentrations of 100 μM were applied, which corresponds to the EC<sub>50</sub>-values obtained in the hemolysis assay. However, there was no to only very mild reduction in cell viability in human cells at this high concentration. These results are in line with the data obtained from human ClpP peptidase and protease assays, underlining the species selectivity of the phenyl ester compounds.

## 4. CONCLUSION AND OUTLOOK

Derived from a high-throughput screen, five phenyl ester and one triazole amide-based compound were identified as novel and privileged inhibitors of *S. aureus* caseinolytic protease P. The screening hits were further validated regarding their species selectivity and inhibitory potency on the ClpXP proteolytic complex. The compounds displayed high potency towards ClpPs originating from *Gram*<sup>+</sup> (*S. aureus*, *L. monocytogenes*) as well as *Gram*<sup>-</sup> (*E. coli*) bacteria. The more challenging proteolytic ClpXP complex was also inhibited very efficiently by the most potent compounds **AV170**, **AV126** and **AV127**, making these compounds the first highly potent and selective inhibitors of the *S. aureus* ClpXP complex. Human ClpP, on the other hand, was not efficiently inhibited by all compounds except for **AV167**. The selectivity of most compounds for bacterial over human ClpP is a beneficial property, since ClpP is linked to the hereditary *Perrault* syndrome. On the other hand, ClpP has been shown to be an essential target in some leukemic cancers like AML.<sup>68</sup> This makes **AV167** a promising starting point for the exploitation of a phenyl ester-based scaffold in the context of ClpP-dependent cancer cells.

Active site acylation at Ser98 accompanied by complex deoligomerization into heptamers was identified as the common mode of action of all HTS hits. This reaction mechanism also explains the very fast inactivation kinetics observed. Modification of some active sites is necessary and sufficient for most hit compounds to achieve deoligomerization of the ClpP complex into heptamers, making this a more efficient inhibition principle than acylation of all active sites under retention of the tetradecameric assembly. Based on its superior reactivity and potency, **AV170** was selected for structure-activity relationship studies and *in situ* target profiling. Using ABPP technology it could be shown that ClpP is the sole covalent target of **AV170**-based probe **ML16** in living *S. aureus* cells. This unprecedented target selectivity made **AV170** an excellent candidate for further application-driven studies. Unfortunately, the intrinsic acyl-enzyme intermediate stability as well as blood plasma stability of **AV170** proved to be rather low. Structure-activity relationship studies were used to identify more stable derivatives. Mesomeric stabilization and steric shielding strategies were applied to protect the reactive ester moiety. The protective effect of introducing a double bond in *alpha*-position to the ester was found to have the most profound influence on compound stability. Unfortunately, all efforts to increase the stability led to a more or less pronounced reduction in inhibitory potency of the compounds. Further studies should be applied to identify possibilities to stabilize the compound without reducing its inhibitory potency. Computational studies that allow to gain detailed insights in the quantum mechanical details of the acylation and hydrolysis steps will help to rationally design more stable but still potent derivatives in the future.

Further SAR studies revealed that the linker length between the trimethoxyphenyl moiety and the reactive ester of **AV170** is essential for correct positioning in the S1 binding pocket of *S. aureus* ClpP.

A stereogenic switch for deoligomerization was uncovered when the methyl-substituted derivatives (*R*)-**ML89** and (*S*)-**ML90** were investigated in detail. Molecular docking studies revealed that the stereoconfiguration of the methyl substituent leads to widely different positioning of the compound in the active site, which in turn might cause rearrangement of the catalytic triad, triggering down-stream effects that lead to disassembly of the complex. Since the *alpha* substituted ester resembles a native peptide backbone, it is worthwhile to speculate that the stereogenic switch might also have biological relevance *in vivo*. The (*S*)-configuration depicts the same absolute stereoconfiguration as found in native substrate peptides, whereas D-amino acids have the same absolute configuration as (*R*)-**ML89**. Future studies will have to focus on detailed SAR studies of more peptide-like inhibitors and identifying potential endogenous small molecule modulators of ClpP.

Testing the anti-hemolytic and cytotoxic profile of **AV170** and derivatives revealed that the translation of the excellent target profile and superior inhibitory potency of the compounds into a pharmacologically exploitable anti-virulence strategy remains a great challenge. Although severe cytotoxic effects were not observed, the anti-hemolytic effect was only moderate. Challenges are most certainly the limited hydrolytic stability of the compounds in aqueous systems as well as the transient nature of the active site acylation in ClpP. In the future, structural biology and computational studies will be needed to deliver further insights into the mechanism of inhibition and will thereby help to develop more suitable pharmacological candidates. Up to that, phenyl esters have been identified as the new state-of-the-art ClpP inhibitors and will serve as excellent tool compounds to study the protease.

## 5. EXPERIMENTAL SECTION

### 5.1 High-throughput screening

The activity of the ClpP protease was studied *in vitro* by its peptidase activity for the fluorogenic substrate N-succinyl-Leu-Tyr-7-amido-4-methylcoumarin (Suc-Leu-Tyr-AMC = Suc-LY-AMC, Bachem). After peptide bond cleavage the fluorophore 7-amino-4-methylcoumarin is liberated and can be quantified. The HTS assay was carried out in 1536 well format with an assay volume of 6  $\mu$ l. Briefly, 4  $\mu$ l of ClpP in assay buffer (50 mM MES 7.0, 100 mM KCl) were dispensed into black 1536 well plates (Corning 3728) using Multidrop Combi (Thermo Fisher Scientific); 7.5 nl of 10 mM compound were added by the acoustic dispenser Echo 520 (Labcyte Inc.) and incubated for 15 min. Then, 2  $\mu$ l of Suc-LY-AMC substrate were added, again by Multidrop Combi. Final concentration of ClpP was 2  $\mu$ M and of Suc-LY-AMC was 33  $\mu$ M. After 2 h incubation, fluorescence was measured at 360 nm excitation and 460 nm emission wavelengths in the Spectramax Paradigm reader (Molecular Devices). Using this assay, 137793 compounds were screened at 12.5  $\mu$ M concentration. HTS data analysis was carried out using Quattro Workflow software (Quattro Research GmbH) and included normalization of data; as well as calculation of plate statistics and generation of heat maps for quality control purposes. Positive (DMSO only) and negative controls (Palmostatin M 66.66  $\mu$ M) were included on every plate and were used to assess the performance of the primary screen: the overall Z factor was calculated as  $0.69 \pm 0.14$  and the overall signal-to-background ratio as  $25 \pm 9$ . Primary hits were defined as compounds that induced a decrease in the fluorescent signal of at least 50%. 161 compounds were thus chosen for dose response analysis (corresponding to a primary hit rate of 0.117%). Dose response analyses were carried out using a three-fold dilution series over eight steps; starting at 10  $\mu$ M. 37 compounds were found to have an  $IC_{50}$  value below 10  $\mu$ M.

## 5.2 Biochemical procedures

### 5.2.1 Protein purification

C-terminal STREP-II affinity tagged ClpP (*S. aureus*, *E. coli*, *L. monocytogenes*, *H. sapiens*) constructs were cloned in pET301 expression vectors via the Gateway® cloning system (Life Technologies) (*H. sapiens* ClpP: amino acids 57-277).<sup>39</sup> Proteins were expressed overnight at 25 °C in *E. coli* BL21(DE3) cells (*H. sapiens* ClpP was expressed in *E. coli* Rosetta2 cells providing enhanced codon usage) after induction at OD<sub>600</sub> of 0.6 with 0.5 mM IPTG. Cells were harvested, resuspended in binding buffer (100 mM Tris/HCl, pH 8.0, 150 mM NaCl, 1 mM EDTA) and lysed by sonication (2x (7 min, 30% int.; 3 min, 80% int.), Bandelin Sonopuls) under constant cooling on ice. The lysate was cleared by centrifugation at 18.000 rpm and the soluble fraction was loaded on a pre-equilibrated 5 mL StrepTrap HP column (GE Healthcare) using an Äkta purifier 10 system (GE Healthcare). The column was washed with 7 column volumes binding buffer. Elution was performed over 4 column volumes binding buffer + 2.5 mM desthiobiotin. The fractions containing ClpP were pooled, concentrated and subjected to preparative size exclusion chromatography (HiLoad 16/60 Superdex 200 pg (GE Healthcare)) in ClpP storage buffer (*S. aureus*, *E. coli*, *H. sapiens* ClpP: 20 mM HEPES, pH 7.0, 100 mM NaCl; *L. monocytogenes* ClpP2: 20 mM HEPES, pH 7.0, 100 mM NaCl, 5% (v/v) glycerol). Fractions containing ClpP were pooled, concentrated and stored at -80 °C.

eGFP-ssrA was cloned as a fusion protein with an ssrA tag (AANDENYALAA) at the C-terminus in vector pDEST007 and was purified as described previously.<sup>59, 81</sup> In short, the cells were overexpressed for 4 h at 37 °C after induction with anhydrotetracycline (0.2 mg/L). After harvest and cell disruption the cleared lysates were purified by Strep column using ice-cold lysis/wash buffer (100 mM Tris, pH 8.0, 150 mM NaCl, 1 mM EDTA, + 2.5 mM desthiobiotin for elution). eGFP-ssrA containing fractions were pooled, concentrated and purified with a HiLoad 16/60 Superdex 200 pg gel filtration column (GE Healthcare) in GF buffer (100 mM NaCl, 20 mM Tris, 10% glycerol, pH = 7.0).

EcClpX was purified as described previously.<sup>82</sup> SaClpX was cloned into vector pET300 with an N-terminal His<sub>6</sub>-tag and a TEV cleavage site and purified as described previously.<sup>59</sup> In short both ClpX enzymes were expressed in BL21(DE3) cells (SaClpX) or in Rosetta (DE3) cells (EcClpX) at 25 °C over night after induction with IPTG (0.5 mM) The cells were lysed in ClpX lysis buffer (50 mM HEPES pH 7.5, 300 mM KCl, 15% glycerol, 1 mM DTT, 5 mM MgCl<sub>2</sub>) and ClpX was purified by affinity chromatography. Following digestion with His<sub>6</sub>-tagged TEV protease, a second affinity purification was carried out and the flow through was buffer exchanged to ClpX lysis buffer by 10 kDa spin column devices.

## 5.2.2 Peptidase and protease activity assays

*In vitro* inhibition of ClpP peptidase activity was measured by monitoring the cleavage of fluorogenic Suc-Leu-Tyr-AMC (Bachem) substrate as described previously.<sup>70</sup> 1  $\mu$ L of inhibitor (100x stocks in DMSO; final concentrations 1  $\mu$ M, 10  $\mu$ M and 100  $\mu$ M) or DMSO as a control were added to a black flat-bottom 96-well plate (Greiner) and mixed with 98  $\mu$ L buffer-enzyme mix (final ClpP monomer concentration: *S. aureus* ClpP, *H. sapiens* ClpP, *L. monocytogenes* ClpP2: 1  $\mu$ M; *E. coli* ClpP: 0.1  $\mu$ M; reaction buffers: *S. aureus* ClpP: 100 mM HEPES, pH 7.0, 100 mM NaCl; *H. sapiens* ClpP: 50 mM HEPES, pH 7.5, 300 mM KCl, 1 mM DTT, 15% (v/v) glycerol; *L. monocytogenes* ClpP2: 100 mM HEPES, pH 7.0, 100 mM KCl, 15% (v/v) glycerol; *E. coli* ClpP: 100 mM HEPES, pH 7.5, 100 mM NaCl) and incubated for 1 h at 32 °C (hClpP 37 °C) in an infinite M200 plate reader (Tecan). The reaction was started by addition of 1  $\mu$ L (20 mM in DMSO, final concentration: 200  $\mu$ M) Suc-Leu-Tyr-AMC. Fluorescence was recorded for 90 min (excitation: 380 nm; emission: 440 nm). The slope of the fluorescence over time signal was calculated from  $t = 500$  s to  $t = 2000$  s via linear regression using Microsoft Excel. DMSO treated control samples were normalized to 100% activity and the residual activity of inhibitor treated samples was determined. To determine  $k_{obs}/[I]$  values of the inhibitors against *S. aureus* ClpP, 1  $\mu$ L inhibitor (100x stock in DMSO) or DMSO was added to a black flat-bottom 96-well plate and mixed with 97  $\mu$ L reaction buffer. 1  $\mu$ L Suc-Leu-Tyr-AMC was added and the mixture was equilibrated at 32 °C for 15 min. The reaction was started by addition of 1  $\mu$ L *S. aureus* SaClpP (50 mM, final concentration 0.5  $\mu$ M). Fluorescence was recorded for 20 min and the measurements were carried out in triplicates. The recorded fluorescence over time signals were fitted to

$$F(t) = F_0 + A(1 - e^{-k_{obs} \cdot t})$$

using Microcal Origin 8.5. The resulting  $k_{obs}$  values were plotted against the inhibitor concentration and the slope ( $k_{obs}/[I]$ ) was determined via linear curve fitting.<sup>69</sup>

GFP degradation assays were performed in PZ buffer (25 mM HEPES, 200 mM KCl, 5 mM MgCl<sub>2</sub>, 1 mM DTT, 10% (v/v) glycerol, pH 7.6) with 60  $\mu$ L reaction volume at 30 °C. GFP fluorescence was monitored in white, flat-bottom well plates (Brand) by excitation at 485 nm and detection of emission at 535 nm using an Infinite F200 Pro (Tecan). Degradation reactions contained 0.4  $\mu$ M ClpX<sub>6</sub>, 0.2  $\mu$ M ClpP<sub>14</sub>, 0.41  $\mu$ M GFP-ssrA and an ATP regeneration system (4 mM ATP, 16 mM creatine phosphate, 20 U/mL creatine phosphokinase). For measuring the *S. aureus* protease activity the corresponding SaClpXP system was used. For measuring the *H. sapiens* protease activity HsClpP in combination with EcClpX was used. 0.6  $\mu$ L (1% of reaction volume) of inhibitor was added in different concentrations in DMSO. All reaction partners except the substrate were preincubated 10 min at 30 °C. The GFP-ssrA was added

afterwards to start the reaction. All data were recorded in triplicate measurements and in two independent experiments. The slope of the fluorescence over time signal was calculated from the corresponding time point of the half maximal fluorescence  $\pm$  5 next data points (1 min/data point) and 19 – 31 min for complete inhibited samples via linear regression using Microsoft Excel. DMSO treated control samples were normalized to 100% activity and the residual activity of inhibitor treated samples was determined.

### 5.2.3 Analytical gel filtration

25  $\mu$ M ClpP were incubated with 5-fold molar excess of inhibitor for 1 h at room temperature in a total volume of 200  $\mu$ L reaction buffer. The reaction mixture was subjected to a calibrated Superdex 200 10/300 GL column (GE Healthcare) connected to an Äkta purifier 10 system (GE Healthcare). The column was flushed with one column volume buffer A (20 mM HEPES, pH 7.0, 100 mM NaCl). UV absorption was recorded on-line at 280 nm and normalized with respect to the highest signal. The oligomerization state was determined by comparison of the elution volumes to the calibration curve of the column (gel filtration calibration kit, GE Healthcare).

### 5.2.4 High resolution intact protein mass spectrometry

To determine the degree of modification of ClpP by the inhibitors, 1  $\mu$ M protein was incubated with up to 50-fold molar excess of inhibitor for 1 h at room temperature. Measurements were performed on a Dionex Ultimate 3000 HPLC system coupled to Thermo LTQ-FT Ultra mass spectrometer with electrospray ionization source (spray voltage 4.0 kV, tube lens 110 V, capillary voltage 48 V, sheath gas 60 arb, aux gas 10 arb, sweep gas 0.2 arb). 5  $\mu$ L of reaction mixture were on-line desalted using a Massprep desalting cartridge (Waters). The mass spectrometer was operated in positive mode collecting full scans at high resolution ( $R = 200,000$ ) from  $m/z$  600 to  $m/z$  2000. Collected data was deconvoluted using Thermo Xcalibur Xtract algorithm. Masses were determined precisely by Gaussian fitting of the deconvoluted spectra using Microcal Origin 8.5.

### 5.2.5 Determination of acyl-enzyme intermediate stability

25  $\mu$ M ClpP were incubated with 5-fold molar excess of inhibitor for 1 h at room temperature in a total volume of 200  $\mu$ L reaction buffer. Excess inhibitor was removed on an analytical size exclusion chromatography column as described above. Fractions of 0.5 mL were collected and the fraction under the highest UV signal was immediately shock frozen in liquid nitrogen. Samples were prepared in triplicates. To determine the acyl-enzyme intermediate stability, samples were thawed and subjected to a time-resolved intact protein mass spectrometry-based assay. High resolution mass spectrometry data was collected every 24.5 min for more

than 12 h under the above mentioned conditions. The auto-sampler of the HPLC system was set to 32 °C. To ensure thorough temperature transfer from the auto sampler to the sample the space between vial and sample inlet was filled with water and pre-equilibrated to 32 °C prior to addition of the sample. The recorded spectra were deconvoluted using Thermo Xcalibur Xtract algorithm, the degree of modification was determined and plotted against time. Acyl-enzyme intermediate half-life  $t_{1/2}$  was determined by fitting to

$$y = A \cdot e^{\left(-\frac{x}{t}\right)}$$

and multiplying the resulting decay constant  $t$  with  $\ln 2$ .

#### 5.2.6 Hemolysis assay

5 mL of a *S. aureus* NCTC 8325 culture in lysogeny broth (LB) medium supplemented with 0.1% (w/v)  $K_2HPO_4$  were grown overnight at 37 °C. The following day a new 5 mL culture was inoculated 1:100 from the overnight culture. Bacteria were grown at 37 °C to an  $OD_{600}$  of 0.4 to 0.5. The suspension was then diluted to a concentration of  $3.4 \cdot 10^4$  bacteria per mL. 990  $\mu$ L of diluted suspension were added to culture tubes and 10  $\mu$ L inhibitor (100x stock in DMSO) or DMSO as a control were added. The culture tubes were closed tightly to ensure semi-aerobic conditions and the bacteria were grown for 19-20 h at 37 °C. The following day 100  $\mu$ L of culture was removed and diluted in 900  $\mu$ L broth. 100  $\mu$ L of this dilution were transferred to a transparent flat-bottom 96-well plate (Starlab) and  $OD_{600}$  was determined in a Tecan infinite M200 plate reader to monitor for growth inhibitory effects. Subsequently 800  $\mu$ L of the remaining overnight culture were harvested at 6200 x g for 10 min and 100  $\mu$ L of culture supernatant were transferred to a transparent flat-bottom 96-well plate (Starlab). 100  $\mu$ L B-medium were used as a negative control. A 10% erythrocyte suspension was prepared and 50  $\mu$ L were added to each well.  $OD_{600}$  was measured for 30 min at kinetic intervals of 1 min in a Tecan infinite M200 plate reader at 37 °C. The time point where hemolysis in the DMSO treated control sample was finished and  $OD_{600}$  reached a stable plateau was chosen for determination of  $EC_{50}$  values. The normalized hemolysis inhibition (I) was calculated according to

$$I = \frac{OD_{600}^{inhibitor} - OD_{600}^{DMSO}}{OD_{600}^{broth} - OD_{600}^{DMSO}} \cdot 100$$

and plotted against the negative logarithm of the inhibitor concentration.  $pEC_{50}$  values were determined by fitting to a dose response function using Microcal Origin 8.5. Experiments were performed in three biological replicates.

### 5.2.7 MTT assay

Human epithelial lung cancer cells (A549) cultivated in high glucose Dulbeccos's Modified Eagle's Medium supplemented with 10% (v/v) fetal bovine serum and 2 mM L-glutamine were seeded at a density of 7000 cells per well (100  $\mu$ L of a solution of 70000 cells/mL) in a transparent, flat-bottom 96-well plate. Cells were grown over night in a humidified atmosphere at 37 °C and 5% CO<sub>2</sub>. The next day the medium was removed and replaced by fresh medium supplemented with 100  $\mu$ M compound or 1% (v/v) DMSO as a control. The cells were incubated for 20 h. To determine metabolic activity of the cells, 20  $\mu$ L 3-(4,5-Dimethyl-2-thiazolyl)-2,5-diphenyl-2H-tetrazolium bromide solution (MTT, 5 mg/mL in PBS) were added to each well. The cells were incubated until full metabolic conversion of MTT to insoluble formazan salt was observed. The medium was completely removed and the formazan crystals were resuspended in 200  $\mu$ L DMSO and absorbance at 570 nm and at a reference wavelength of 630 nm was determined in an infinite F200 pro plate reader (Tecan). All data points were measured in triplicate. The data was normalized with respect to the DMSO control. Experiments were carried out in three biological replicates.

### 5.2.8 In situ analytical labeling

*S. aureus* NCTC 8325 was grown in lysogeny broth (LB) medium supplemented with 0.1% (w/v) K<sub>2</sub>HPO<sub>4</sub> and a quantity equivalent to 2 mL of OD<sub>600</sub> = 4 was harvested by centrifugation (10 min, 6000 g, 4 °C) 1 h after reaching stationary phase. After washing twice with PBS, the cells were resuspended in 200  $\mu$ L PBS.

198  $\mu$ L of cell suspension were incubated for 1 h with 2  $\mu$ L of probe in DMSO (ML16: 100x stock, final concentrations 100  $\mu$ M, 30  $\mu$ M, 10  $\mu$ M, 3  $\mu$ M; D3: 100x stock, final concentrations 30  $\mu$ M, 10  $\mu$ M, 3  $\mu$ M) at rt. A DMSO control was included.

After labeling, the cells were washed two times with PBS (2 x 1 mL) and resuspended in 200  $\mu$ L PBS. Cells were lysed by sonication under permanent cooling on ice with a Bandelin Sonopuls HD2070 homogenizer (4 x 30 s at 75% power, with pauses of 30 s between each run). Cell lysates were centrifuged (30 min, 20000 g, 4°C) to separate cytosolic and membrane fraction. The supernatant cytosolic fraction was transferred to a new vial. The click reaction was carried out with 88  $\mu$ L of proteome, so that after addition of all reagents a total volume of 100  $\mu$ L was reached. Therefore, 2  $\mu$ L rhodamine azide (5 mM in DMSO) was added to 88  $\mu$ L of proteome, followed by 2  $\mu$ L TCEP solution (53 mM in ddH<sub>2</sub>O) and 6  $\mu$ L TBTA (1.667 mM in *t*-BuOH/DMSO, 80/20). Samples were gently vortexed and the click reaction was initiated by the addition of 2  $\mu$ L CuSO<sub>4</sub> solution (50 mM in ddH<sub>2</sub>O). The reaction was incubated for 1 h at rt. For analytical SDS gel electrophoresis, 100  $\mu$ L 2x SDS loading buffer were added and 30  $\mu$ L were applied on gel. After electrophoresis, rhodamine azide labeled proteins were visualized using a Fujifilm

## PHENYL ESTER-BASED INHIBITORS OF CASEINOLYTIC PROTEASE P

LAS-4000 equipped with a Fujifilm Fujinon VRF43LMD3 lens and a 575DF20 filter (Fujifilm) operated in Cy3 fluorescence detection mode.

### 5.2.9 Western-Blot

After fluorescence scanning, the SDS-gel of the *in situ* labeling experiment was used for western-blot analysis. Proteome was blotted on a methanol-activated PVDF membrane for 50 min at 10 V (blotting buffer: 48 mM Tris, 39 mM glycine, 0.0375% SDS, 20% methanol) using a Bio-Rad Trans-Blot SD semi-dry transfer cell setup. The membrane was then blocked in blocking buffer (5% milk powder in PBS with 0.5% Tween-20), washed and incubated with serum of rabbit immunized with tagfree SaClpP (diluted 1:1000 into blocking buffer) for 15 h at 4 °C. The membrane was washed in PBS + 0.5% Tween-20, and then incubated with secondary antibody (goat anti-rabbit IgG-Atto 488 (Sigma Aldrich), diluted 1:10000 in blocking buffer) for 1 h at rt. The membrane was washed again with PBS + 0.5% Tween-20 and imaged using a Fujifilm LAS-4000 equipped with a Fujifilm Fujinon VRF43LMD3 lens and a Y515-Di filter (Fujifilm) operated in SYBR Green fluorescence detection mode.

### 5.2.10 Gel-free in situ target identification of ML16

*S. aureus* NCTC 8325 cells were grown in 20 mL lysogeny broth (LB) medium supplemented with 0.1% (w/v)  $K_2HPO_4$  at 37 °C until they reached stationary phase. Cells were then harvested at 6000 g for 10 min at 4 °C, washed with PBS and then resuspended in PBS to an  $OD_{600}$  of 40. 990  $\mu$ L of cell suspension were incubated with 10  $\mu$ L of ML16 (3 mM in DMSO; final concentration: 30  $\mu$ M) or DMSO for 1 h at rt. Cells were harvested and washed three times. The cells were reconstituted in 1 mL PBS and lysed by sonication with a Bandelin Sonopuls HD2070 device (4 x 30 sec, 75% power) under constant cooling on ice. The soluble protein fraction was isolated by centrifugation at 20000 g for 30 min at 4 °C. To 800  $\mu$ L of supernatant 20  $\mu$ L azide-PEG<sub>3</sub>-biotin (10 mM in DMSO), 10  $\mu$ L TCEP (53 mM in ddH<sub>2</sub>O) and 30  $\mu$ L TBTA (1.667 mM in *t*-BuOH/DMSO, 80/20) were added. Samples were gently vortexed and the click reaction was initiated by the addition of 10  $\mu$ L CuSO<sub>4</sub> solution (50 mM in ddH<sub>2</sub>O). The mixture was incubated for 1 h at rt. Afterwards proteins were precipitated by addition of 4 mL cold acetone and incubation overnight at -20 °C. The protein pellet was harvested by centrifugation at 9000 g for 15 min at 4 °C and washed twice with 1 mL of ice cold methanol. Proteins were reconstituted in 500  $\mu$ L PBS. 50  $\mu$ L avidin-agarose beads (Sigma) were prepared by washing three times with 1 mL 0.4% (w/v) SDS in PBS. All centrifugation steps were conducted at 400 g for 2 min at rt. The beads were added to the protein solution and incubated for 1 h at rt under constant inversion. Beads were subsequently washed three times with 1 mL 4% (w/v) SDS in PBS, two times with 1 mL 6 M urea in ddH<sub>2</sub>O and three times with 1 mL PBS. After the last washing step the beads were brought into 200  $\mu$ L digestion buffer

(20 mM HEPES, pH 7.5, 7 M urea, 2 M thiourea). Proteins were reduced (0.2  $\mu$ L 1 M DTT, 45 min, 37 °C) and alkylated (2  $\mu$ L, 30 min, rt, in the dark). The alkylation reaction was quenched by addition of 0.8  $\mu$ L 1M DTT and incubation for 30 min at rt. Proteins were pre-digested with 1  $\mu$ L LysC (Wako) for 4 h at rt. 600  $\mu$ L 50 mM TEAB buffer were added and the proteins were digested overnight with 1.5  $\mu$ L sequencing grade trypsin (Promega) at 37 °C. The following day the beads were settled and the supernatant was acidified with 20  $\mu$ L formic acid to a pH of 2 – 3. Peptides were desalted and dimethyl labeled using 50 mg SepPak C18 cartridges (Waters) and a vacuum manifold.<sup>83</sup> The cartridges were activated with 1 mL acetonitrile, washed once with 1 mL 80% (v/v) acetonitrile, 0.5% (v/v) formic acid and three times with 0.5% (v/v) formic acid. The samples were loaded on the cartridges and subsequently washed five times with 0.5% (v/v) formic acid. Peptides were labeled on column with either five times 1 mL labeling buffer “light” (90 mM sodium phosphate, pH 7.5, 30 mM NaBH<sub>3</sub>CN, 0.2% (v/v) CH<sub>2</sub>O) or five times 1 mL labeling buffer “heavy” (90 mM sodium phosphate, pH 7.5, 30 mM NaBD<sub>3</sub>CN, 0.2% (v/v) <sup>13</sup>CD<sub>2</sub>O). Cartridges were subsequently washed twice with 1 mL 0.5% (v/v) formic acid. The peptides were eluted with two times 200  $\mu$ L 80% (v/v) acetonitrile, 0.5% (v/v) formic acid. DMSO and ML16 treated samples were combined and dried by lyophilization. Peptides were reconstituted in 30  $\mu$ L 1% (v/v) formic acid and prepared for mass spectrometry by filtering through a 0.45  $\mu$ m nylon filter (VWR). Experiments were conducted in three independent replicates and a label switch from heavy to light label was included.

#### 5.2.11 Peptide mass spectrometry and data evaluation

10  $\mu$ L of digested peptide solution were analyzed on a LTQ Orbitrap XL mass spectrometer (Thermo) equipped with electro spray ionization (ESI) source operated in positive ionization mode coupled to a Dionex Ultimate 3000 HPLC system (Thermo). The samples were loaded on an Acclaim C18 PepMap100 (75  $\mu$ m ID x 2 cm) trap column at a flow rate of 5  $\mu$ L/min for 10 min in 0.1% formic acid and separated on an Acclaim C18 PepMap RSLC (75  $\mu$ m ID x 15 cm) separation column. Eluent A consisted of water with 0.1% (v/v) formic acid and 5% (v/v) DMSO in water (LC/MS grade), eluent B consisted of 0.1% (v/v) formic acid and 5% (v/v) DMSO in acetonitrile (LC/MS grade). Peptides were separated by applying a gradient ranging from 4% B to 35% B over 112 min at a flow of 200 nL/min. The mass spectrometer was operated in datadependent mode. Full scans were acquired in the Orbitrap at R = 60000 from m/z = 350 - 1400. The five most intense peaks were selected for collision induced fragmentation (CID) and analyzed in the ion trap at normal scan rate (isolation width: 2 ppm; activation time: 30 ms; normalized collision energy: 35; minimum signal threshold: 1000 counts; dynamic exclusion duration: 120 s). The following identification and assignment to proteins was performed using MaxQuant 1.5.1.2 software. Default settings for two-state dimethyl labeling were applied: dimethyl 0/0, dimethyl 8/8, maximum labeled amino acids per peptide: 3; missed cleavages: 2;

variable modification: oxidation (methionine); fixed modification: carbamidomethyl (cysteine); enzyme: trypsin/P; main search tolerance: 4.5 ppm; MS/MS tolerance: 0.5 Da; requantification: true; match between runs: true; Ile = Leu: true; false discovery rates: 0.01. Only unique peptides were used for quantification and minimum ratio count was set to 2. The data were searched against Uniprot *S. aureus* NCTC 8235 database (downloaded: 12/02/2014). Further settings were default. Data was further processed and visualized using Perseus software.<sup>84</sup> Reverse identifications, contaminants and hits identified by site only were omitted from further processing. H/L ratios were logarithmized. One sample Student's t-test was applied for statistical evaluation with Benjamini-Hochberg for FDR control.

## 5.3 In silico studies

### 5.3.1 Protein and compound preparation

The extended form of *S. aureus* ClpP (PDB-ID: 3V5E) was used as the starting structure for docking studies. Using the AMBER12 program and the AMBER99FF force field with default simulation conditions,<sup>85</sup> SaClpP was heated to 300 K over 100 ps and subsequently equilibrated at 300 K for another 10 ns. All calculations presented were performed using the program DynaCell<sup>86</sup> and the GROMOS53A1 force field,<sup>87</sup> and illustrations were created using VMD.<sup>88</sup> 3-dimensional structures of the compounds **AV170**, **ML21**, **ML74**, **ML89** and **ML90** were built using the programs ChemDraw and ChemDraw3D.<sup>89</sup> Force field parameters for the compounds were assigned based on GROMOS53A1-compatible topologies created by PRODRG<sup>90</sup> and all atom types, protonation states and charges were manually verified.

### 5.3.2 Docking calculations

For docking studies, five subunits of the protein were selected from the equilibrated starting structure, while keeping the larger binding site conserved. The subunits were reequilibrated for 1000 ps using backbone constraints of 100 kJ/(mol·nm) and the simulation setup described below. This final protein structure was then used as the starting structure for the following docking procedure. All compounds were docked into the ClpP catalytic site using the DynaDock docking procedure with default conditions.<sup>86</sup> The docking solutions were filtered using pharmacophoric constraints on the placement of the reactive ester group of the ligands in the oxyanion hole. This ensured that the ligand was placed such that the covalent binding reaction can occur. From this reduced set, the three energetically best ligand poses for each compound were further refined for 1000 ps using the simulation setup described below and the final refined structures were analyzed with respect to their structural binding properties.

### 5.3.3 Simulation settings

All simulations were performed using the simulation module of our in-house modeling program DynaCell. The same general simulation conditions were applied for the initial equilibration of the protein and the OPMD refinement simulations of the docking procedure. The GROMOS 53A1<sup>87</sup> force field was used as the energy function and a General Born implicit solvent model was applied.<sup>91-92</sup> Due to this implicit solvent model, no cutoffs were applied to the electrostatic and van-der-Waals interactions. Based on this energy function, the leapfrog algorithm<sup>93</sup> was used and a time step of 2 fs (1 fs during heating and for the OPMD refinement) was chosen. Additional stochastic forces were applied to keep the system stable.<sup>94</sup> A stochastic force constant of 10 kJ/(mol·nm) was used and a cutoff for the stochastic force calculations of 3 Å was chosen. The SHAKE algorithm<sup>95</sup> was applied to constrain all bond lengths. During heating, the temperature was controlled by velocity scaling and was subsequently kept at 300 K using the Berendsen's weak coupling method<sup>96</sup> and a coupling constant of 0.005. (The coupling constant was especially optimized for the settings of the simulations, i.e. solvent model, stochastic dynamics conditions, etc.<sup>87</sup>)



## II — HYDROXYLAMINE-BASED REVERSE POLARITY ACTIVITY-BASED PROTEIN PROFILING

Nina Bach generated the His<sub>6</sub>-TEV-PhoB construct. ABPP probes were synthesized by Barbara Hofbauer, Christian Fetzner and Jonas Drechsel.

## 1. INTRODUCTION

### 1.1 Post-translational modifications and protein phosphorylation

The central dogma of molecular biology states that information is encoded in DNA which is then transcribed into mRNA and finally translated into proteins.<sup>97</sup> While the DNA-encoded information is usually static and does not undergo physiological changes (except for somatic mutation in immune cells<sup>98</sup>), diversification of biological information starts at the transcriptional level: alternative splicing of the mRNA results in different protein products from the same DNA sequence after translation.<sup>99-100</sup> However, the creation of complexity does not stop at the protein level. Once proteins are synthesized, they are not static but rather can undergo a wide variety of post-translational modifications (PTMs). Two main pathways of PTMs can be distinguished: cleavage of the protein backbone, which e.g. results in active enzymes from inactive zymogens, and covalent addition of chemical groups to alter functionality, localization or solubility of a protein.<sup>18</sup> With the help of PTMs and diversification at the transcriptional level, the complexity of a proteome is believed to be up to two to three orders of magnitude higher than the respective encoding genome.<sup>18</sup> One of the most common PTMs is protein phosphorylation with its first accounts dating back more than one hundred years.<sup>101-102</sup> Protein phosphorylation is evolutionary highly conserved from eukaryotes to humans and enables spatial and temporal regulation of proteins.<sup>103</sup> Today it is known that protein phosphorylation can occur on nine amino acids: serine, threonine, tyrosine, cysteine, histidine, arginine, lysine, aspartate and glutamate. The most regularly encountered and best studied phosphorylation sites are serine, threonine and tyrosine.<sup>104</sup> Beyond these phosphoester residues there are also other types of phosphoamino acids in proteins: phosphoramidates like phosphohistidine, phosphoarginine and phospholysine have been reported.<sup>105-108</sup> Furthermore, there are the mixed phosphoanhydrides phosphoaspartate and phosphoglutamate (Fig. 12).<sup>109</sup>

### 1.2 Chemistry and biology of phosphoaspartate

From a chemical point of view, phosphoaspartate (pAsp) can be seen as the mixed anhydride of the carboxylic acid aspartic acid and phosphoric acid. Anhydrides are highly reactive compounds which makes phosphoaspartate a very labile chemical entity. Therefore, phosphoaspartate can be regarded as nature's equivalent to acyl chlorides and other activated species used in synthetic chemistry to generate acid derivatives. Compared to carboxyl groups at neutral pH the mixed carboxylic-phosphoric acid anhydride is activated by two effects: first, the carboxyl group has no negative net charge, making it less repulsive towards electron-rich nucleophiles. Second, the electron withdrawing phosphoryl group removes electron density from the carbonyl carbon.<sup>110</sup> Both effects make the carbonyl carbon in the mixed anhydride a

more reactive electrophile. Furthermore, the phosphoryl group is a much better leaving group than hydroxide. On the other hand, the phosphoryl group is also activated for nucleophilic substitution, since the electrophilicity of the phosphorus atom increases as well in the mixed anhydride.<sup>111</sup>

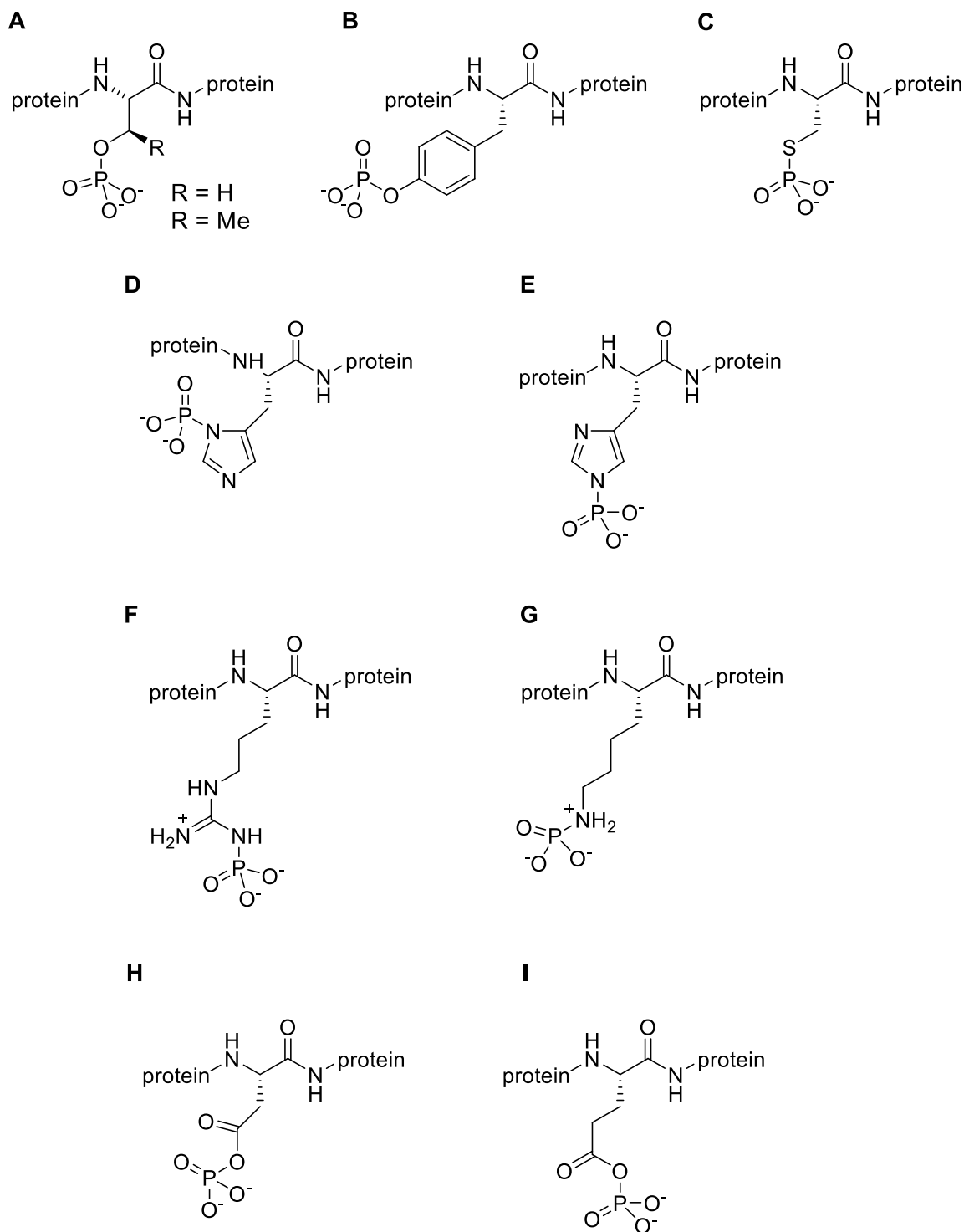


**Figure 12:** The nine phosphoamino acids found involved in protein phosphorylation. (A) phosphoserine and phosphothreonine; (B) phosphotyrosine; (C) phosphocysteine; (D) *N1*-phosphohistidine; (E) *N2*-phosphohistidine; (F) phosphoarginine; (G) phospholysine; (H) phosphoaspartate (I) phosphoglutamate

## HYDROXYLAMINE-BASED REVERSE POLARITY ABPP

Through this activation of the carboxyl and phosphoryl group, phosphoaspartate is reacting readily with nucleophiles like hydroxylamine and is also prone to hydrolysis.<sup>112</sup> At a neutral pH and 30 °C, 30% of phosphoaspartate is hydrolysed within 30 min.<sup>113</sup> For the model carboxylic-phosphoric acid anhydride acetyl phosphate, it has been shown that the rate of hydrolysis increases drastically at low and high pH but stays constant between pH 5 and 10.<sup>114</sup> The nucleophilic attack predominantly occurs at the carbonyl carbon at high or low pH leading to cleavage of the C-O bond, whereas attack at the phosphorus atom is favored at neutral pH conditions.<sup>114-115</sup> It has been suggested that the free energy of hydrolysis of acyl phosphates even surpasses that of ATP, making phosphoaspartate and phosphoglutamate excellent high-energy intermediates for biochemical reactions.<sup>109, 116</sup>

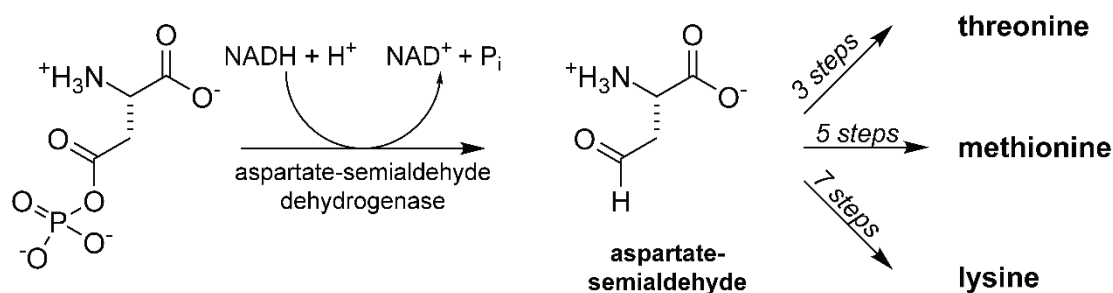


**Figure 13:** Phosphoaspartate is a key intermediate in the synthesis of threonine, methionine and lysine.

As such an intermediate, free phosphoaspartate is involved in the synthesis of lysine, threonine and methionine. Thereby, aspartate is first phosphorylated by aspartokinase to phosphoaspartate which then serves as a substrate for aspartate-semialdehyde dehydrogenase to form aspartate-semialdehyde (Fig. 13).<sup>109</sup> Furthermore, phosphoaspartate can be found as a reaction intermediate in the active sites of some enzymes. The most prominent example is the haloacid dehalogenase (HAD) superfamily.<sup>117</sup> This superfamily comprises the P-type ATPase ion pumps, phosphatases like phosphoserine phosphatase and phosphomutases like  $\beta$ -phosphomutases and phosphonoacetaldehyde hydrolase.<sup>117</sup> In all these enzymes the key catalytic step involves nucleophilic attack at the phosphorus atom to hydrolyze the active site phosphoaspartate, transferring the phosphate group to either a substrate molecule or water (Fig. 14). Beyond HAD superfamily proteins there is also report of a phosphoaspartate intermediate in the atypical protein kinase Rio2.<sup>118</sup>

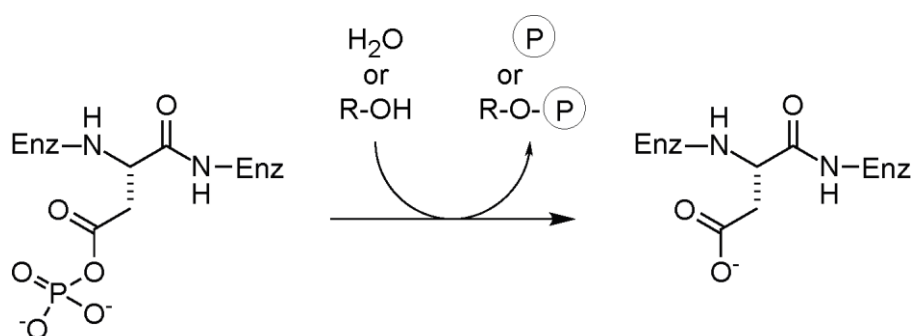


**Figure 14:** Phosphoaspartate in enzyme active sites. pAsp is subjected to nucleophilic attack at the phosphorus atom, resulting in the transfer of the phosphate moiety to water or substrate.

Beyond its role as a catalytic intermediate, phosphoaspartate is well known to play a crucial part in two-component signaling (TCS) pathways. TCS systems are best known in bacteria but are also involved in fruit ripening and development.<sup>119-120</sup> In classical TCS systems a membrane associated sensor histidine kinase (HK) reacts to an external stimulus through ATP-dependent autophosphorylation in *trans* (Fig. 15). The phosphate moiety is then transferred to a conserved aspartate residue in a downstream response regulator (RR). The RR comprises an N-terminal receiver domain, where the key aspartate residue is located, and a C-terminal effector domain. Upon aspartate phosphorylation the response regulator undergoes structural changes and the effector domain initiates the response.

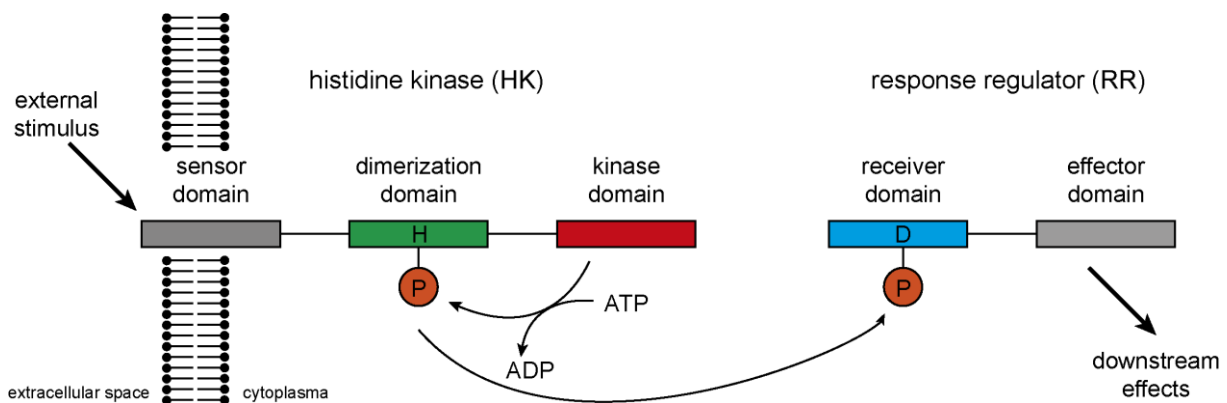


**Figure 15:** Classical bacterial two-component signaling system. Phosphotransfer from the sensor histidine kinase to the downstream response regulator is crucial for signal transduction. The phosphorylation status of the RR orchestrates the further downstream output effects.

More sophisticated phosphorelays involve a His-Asp-His-Asp phosphotransfer via hybrid kinases and His-containing phosphotransfer proteins. However, the final phosphate recipient is also a response regulator protein.<sup>120</sup> Response regulators may bind DNA and initiate effects on gene expression or directly interact with effector proteins. A well-studied transcription factor-like response regulator is *E. coli* PhoB. It is a member of the OmpR/PhoB family and is a key regulator of phosphate metabolism in *E. coli*.<sup>121</sup> About 400 genes have been shown to be influenced by inorganic phosphate concentrations in *E. coli*, many of these presumably under PhoB control.<sup>121-122</sup> PhoB is phosphorylated at Asp53 by the sensor histidine kinase PhoR and thereupon undergoes dimerization. Dimeric PhoB then binds to specific DNA binding sites in promoter regions and influences the transcription of its client genes.<sup>123</sup> TCSs have also been reported to be involved in the regulation of bacterial virulence, including host-microbe signaling.<sup>124-127</sup> Despite the central role of protein aspartate phosphorylation in cellular signaling pathways as well as in enzymatic catalysis, no global chemical proteomic profiling method is available so far.<sup>128</sup> Some methods recently published adapt known phosphoproteomic workflows to milder conditions, however this cannot guarantee protection from hydrolysis and does not exploit the chemical properties of the mixed anhydride bond.<sup>129-</sup>

### 1.3 Activity-based proteome profiling

To profile the reaction and interaction partners of small molecules in complex biological systems, the methodology of activity-based proteome profiling (ABPP) has become increasingly popular over the last years. ABPP has been used to examine the protein targets of electrophilic natural products, drugs, fragment sized molecules, environmental chemicals and endogenous metabolites in bacteria as well as in human cells.<sup>131-135</sup> ABPP protocols make use of small molecule-derived probes that are designed to make them suitable for target identification. A classical ABPP probe consists of an electrophilic reactive warhead, a reporter tag and a spacer region in between.<sup>136</sup> The reporter tag is usually either a fluorescent dye for visualization of protein targets after gel electrophoresis or an affinity tag, such as biotin that can be used for pulldowns and target enrichment. Since the introduction of such large entities significantly alters the physicochemical properties of a small molecule and usually makes the probe cell-impermeable, the method of choice today is the introduction of a small alkyne or azide group.<sup>137</sup> This approach does not interfere with cell permeability and allows for the *in situ* application of the probe and subsequent introduction of the reporter unit by bio-orthogonal chemistry, such as copper-catalyzed azide-alkyne cycloaddition (CuAAC, “click chemistry”).<sup>138-139</sup> If the molecule of interest does not contain a reactive moiety itself, a photo-crosslinking moiety can be introduced to covalently attach the probe to its target proteins by UV irradiation.<sup>140-141</sup> This kind of experimental design is usually termed affinity-based proteome profiling (AfBPP).

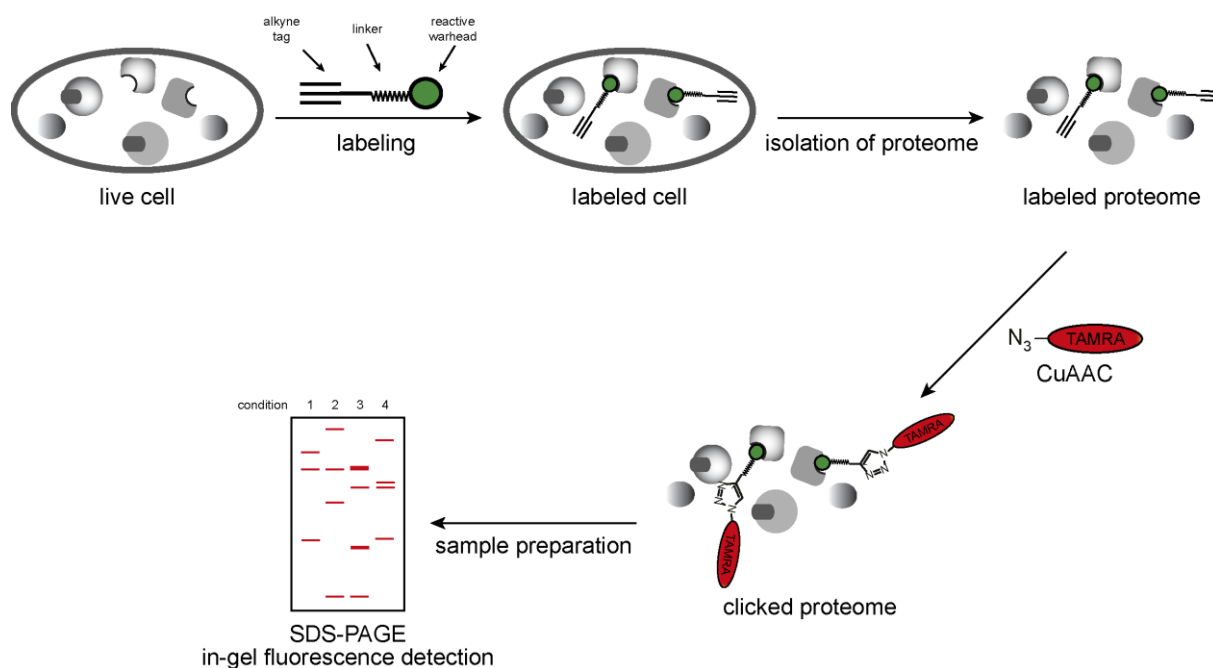


**Figure 16:** Workflow of an *in situ*, analytical ABPP experiment. Living cells are treated with probe, lysed and the labeled proteome is subjected to click chemistry. Readout is achieved by gel electrophoresis and fluorescence scanning. The workflow is suitable for the rapid determination of probe reactivity and labeling patterns.

There are numerous variations of the ABPP workflow: in general one can discriminate between gel-based and gel-free workflows and between mere visualization of the target proteins and their mass spectrometry-based identification. In a simple gel-based, analytical workflow live cells are treated with probe, the labeled proteome is isolated and a fluorescent dye is introduced by click chemistry. The proteome is then separated by gel electrophoresis and targets are visualized by fluorescence scanning (Fig. 16). Such a workflow is suitable for the rapid determination of probe reactivity and labeling patterns as well as the comparison of different conditions. However, it does not give information on the identity of the target proteins.

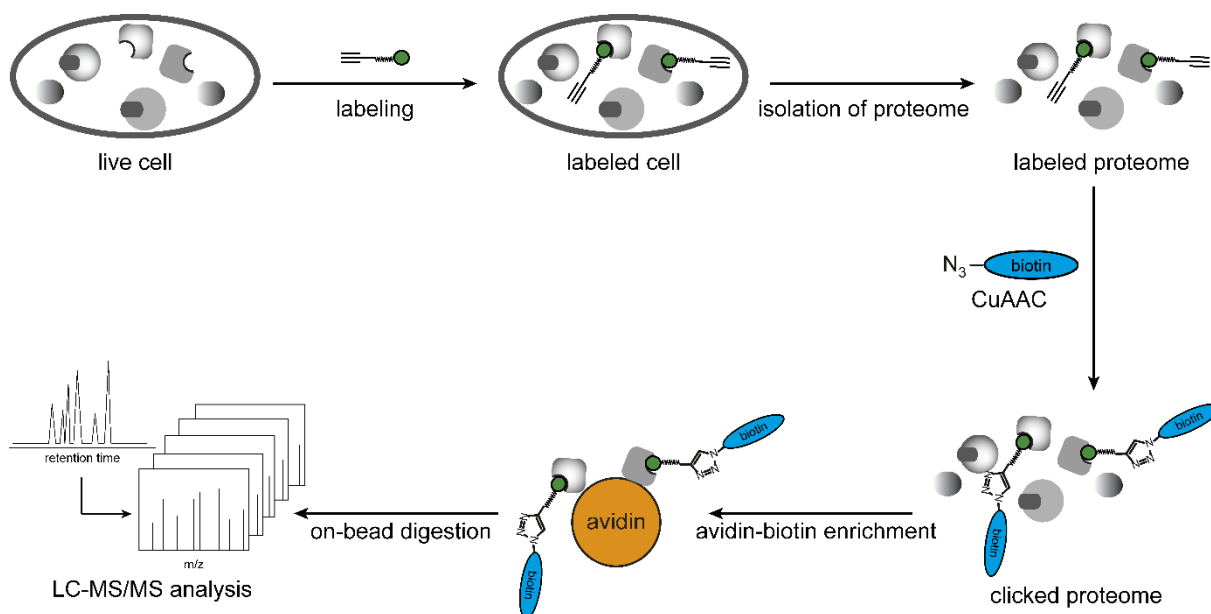


**Figure 17:** Concept of a preparative, MS-based target identification ABPP workflow. Enrichment via affinity capture of the labeled targets removes unlabeled proteins. The enriched proteins are digested with protease and the generated peptides are analyzed by LC-MS/MS.

More sophisticated experiments involve the introduction of a biotin affinity tag and enrichment of the labeled targets by affinity pulldown on avidin beads (Fig. 17). The targets are then digested on the beads and the generated peptides are subjected to analysis by liquid chromatography-coupled mass spectrometry (LC-MS/MS). This workflow allows for the identification of target proteins. Incorporation of quantitative methods like SILAC (stable isotope labeling of amino acids in cell culture), dimethyl labeling or label-free quantification (LFQ) moreover gives quantitative information on the enrichment of the targets compared to an untreated control sample and with that elimination of unspecific background. Larger quantities of the biological starting material are usually required for this workflow to yield sufficient amounts of proteome for a successful MS-based target identification.

Despite the rapid development of the ABPP toolbox over the last years, one blind-spot has been left for a long time: nucleophilic probes have not been considered. Only one study by *Cravatt et al.* published in 2017 reported the use of a hydrazine-derived probe for the global profiling of electrophilic centers in proteins which led to the discovery of the previously unknown

N-terminal glyoxylyl modification of proteins.<sup>142</sup> This study coined the term “reverse polarity ABPP” (rp-ABPP) for the use of nucleophilic instead of electrophilic probes.

## 2 SCOPE OF THIS WORK

The present study aims to develop a novel global chemoproteomic profiling methodology for the detection of protein aspartate phosphorylation. The intrinsic instability of the carboxylic-phosphoric acid anhydride precludes phosphoaspartate from detection via conventional proteomic and phosphoproteomic workflows. However, there are several methods to detect phosphoaspartate either directly or indirectly. Previous indirect detection methods are either based on the turnover of phosphoaspartate with the small molecule nucleophile hydroxylamine to form a hydroxamic acid derivative of aspartic acid (*N4*-hydroxyasparagine; *nhAsp*), or reductive cleavage by sodium borohydride to give homoserine.<sup>112, 143-144</sup> However, these previous methods were not applied on a global scale and could only be used for the study of individual proteins.<sup>118</sup> Direct detection methods involve Fourier transform infrared spectroscopy and <sup>31</sup>P-NMR and are also not suitable for global profiling.<sup>145-146</sup> To fill this methodological gap, a combination of ABPP technology and the turnover of phosphoaspartate with hydroxylamine was chosen. It is envisioned that the use of a hydroxylamine-based ABPP-probe should make it possible to convert the labile phosphoaspartate residues into stable derivatives, enrich the modified proteins and further detect them via mass spectrometry. The following chapter will demonstrate the conversion of the phosphoaspartate moiety by hydroxylamine and a hydroxylamine-derived probe in the model response regulator PhoB. Subsequently, an rp-ABPP workflow was established and applied in *B. subtilis* and *P. aeruginosa*.

### 3 RESULTS

#### 3.1 Conversion of phosphoaspartate in *E. coli* PhoB

In order to examine the conversion of phosphoaspartate with hydroxylamine to *N*4-hydroxyasparagine in a protein environment, the well-characterized RR PhoB from *E. coli* was recombinantly overexpressed as a His<sub>6</sub>-tagged construct in *E. coli* BL21. Purification was achieved by HisTrap affinity purification and size exclusion chromatography. The His<sub>6</sub>-tag could be removed by tobacco etch virus (TEV) protease cleavage, however, the tag did not influence the activity of the protein. PhoB was phosphorylated *in vitro* with acetyl phosphate as high-energy phospho-donor.<sup>123</sup> High resolution intact protein mass spectrometry was used to confirm the formation of phosphoaspartate (Fig. 18A).

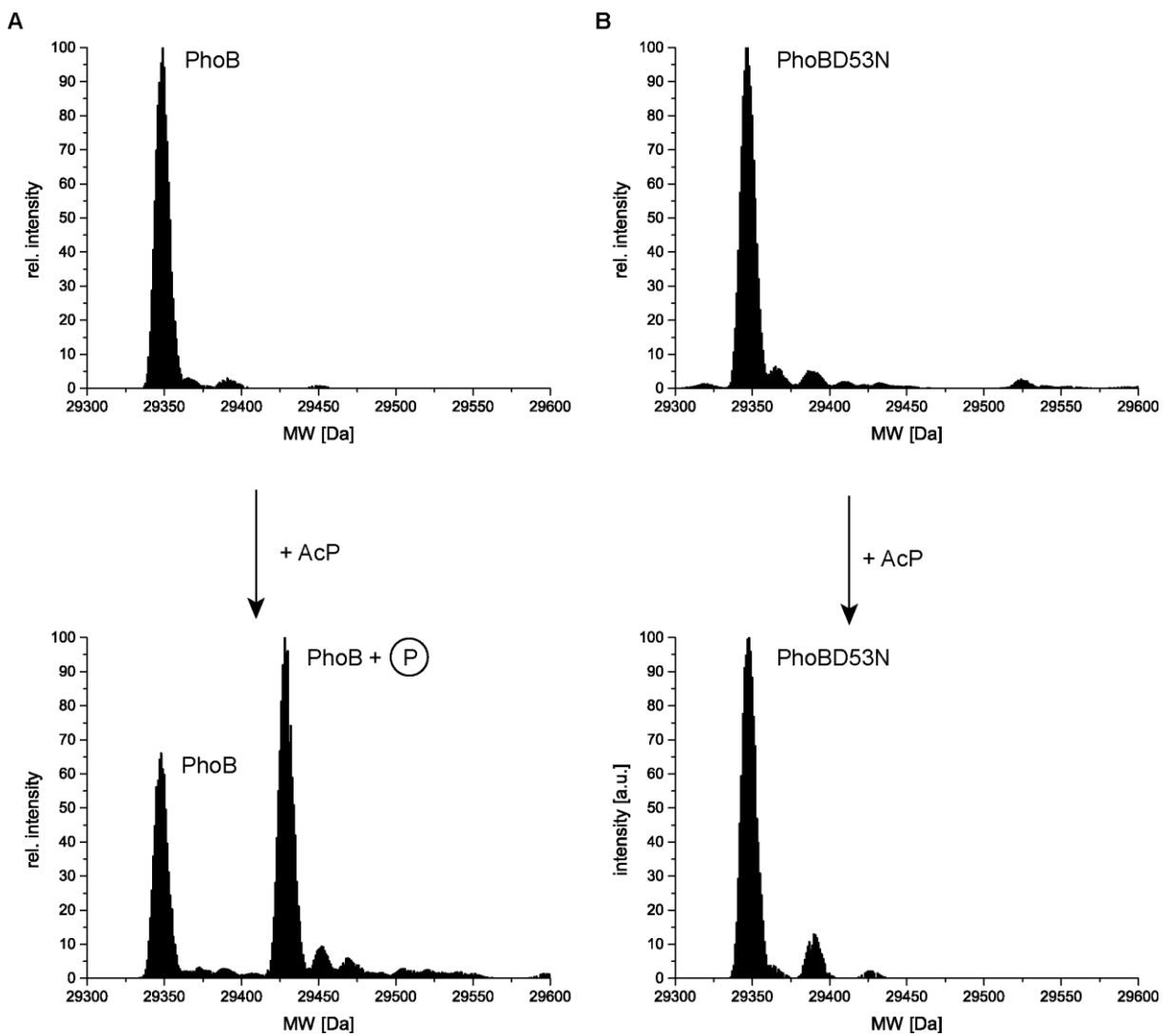


**Figure 18:** Site specific autophosphorylation of *E. coli* PhoB at Asp53. Intact protein mass spectrometry spectra of wt PhoB (A) and PhoBD53N (B) before and after treatment with acetyl phosphate (AcP).

## HYDROXYLAMINE-BASED REVERSE POLARITY ABPP

Deconvoluted spectra showed the formation of a covalent adduct of +80 Da, corresponding to the addition of a phosphate group to the protein (Fig. 18A). No such adduct was observed when a D53N mutant of PhoB was used, demonstrating that its formation is site specific and corresponds to the known phosphosite Asp53 (Fig. 18B). When excess phosphodonor was removed by spin-columns and the sample was treated with water, hydrolysis of pAsp was observed (Fig. 19A). In order to test the conversion of pAsp, the samples were treated for 1 h with 10% (v/v) of a 5 M  $\text{NH}_2\text{OH}\cdot\text{HCl}$  solution, the mass adduct corresponding to the phosphate adduct vanished and instead a novel covalent adduct with a mass of +15 Da was observed (Fig. 19B). This adduct corresponds to the formation of *N*4-hydroxyasparagine. As there is only one +15 Da adduct formed and multiple adducts are not observed, the adduct stems from specific turnover of the phosphoaspartate moiety and not an unspecific background reaction with the protein.

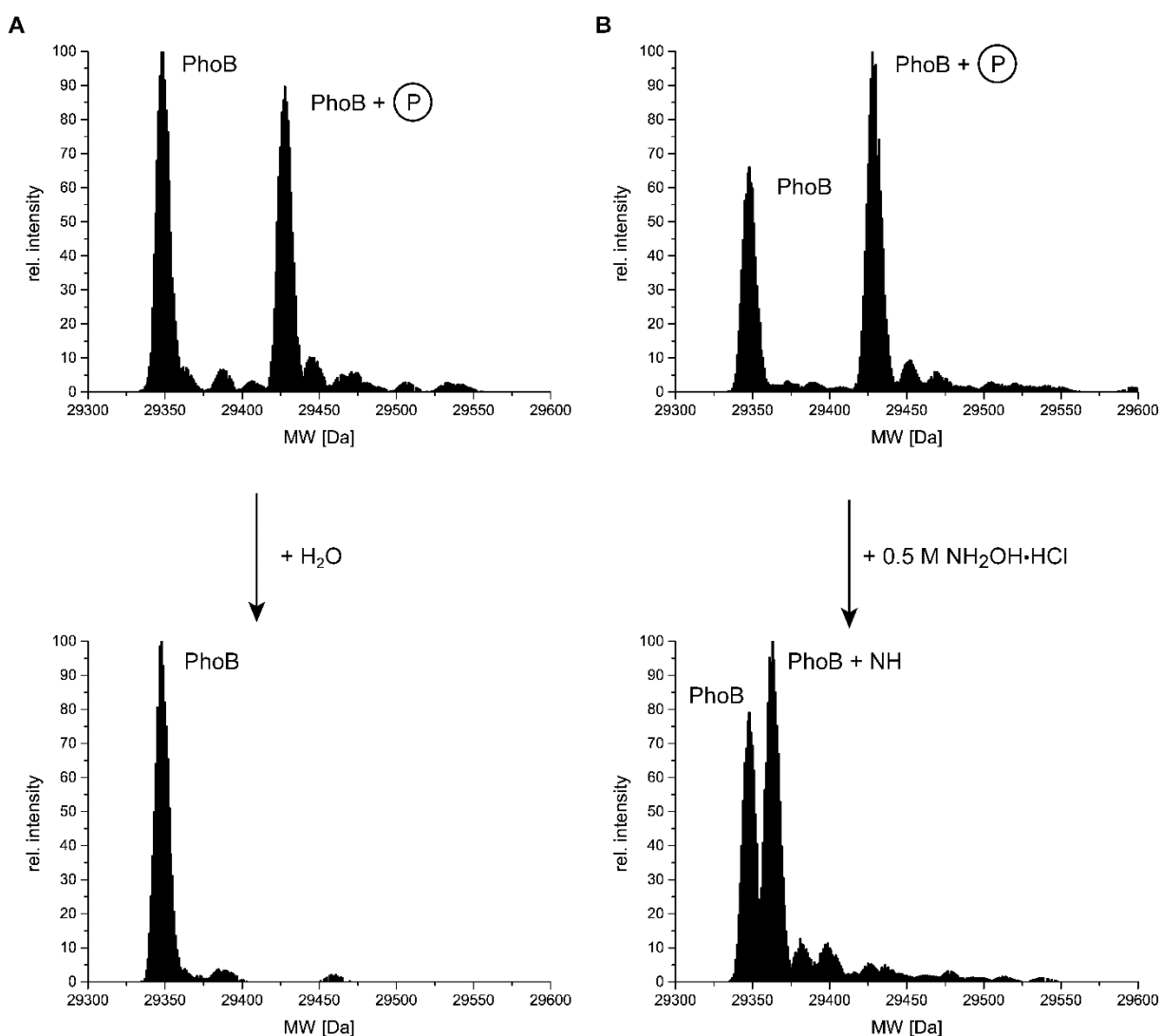


**Figure 19:** Hydrolysis and conversion of pAsp in *E. coli* PhoB. Intact protein mass spectrometry spectra of phosphorylated PhoB before and after treatment with water (A) or 10% (v/v) 5 M  $\text{NH}_2\text{OH}\cdot\text{HCl}$  (B). After treatment with hydroxylamine a mass adduct of +15 Da was observed, corresponding to an additional NH-group.

To further confirm the specificity of the reaction, non-phosphorylated PhoB was incubated with 10% (v/v) of a 5 M  $\text{NH}_2\text{OH}\cdot\text{HCl}$  solution (Fig. 20A). As expected, no adduct formation was observed, ruling out any unspecific reaction between the model protein and hydroxylamine. Addition of 10% (v/v) of a 5 M  $\text{NH}_2\text{OH}\cdot\text{HCl}$  solution to the reaction buffer (20 mM HEPES, pH 7.0) results in a final pH in the reaction mixture of pH 4.

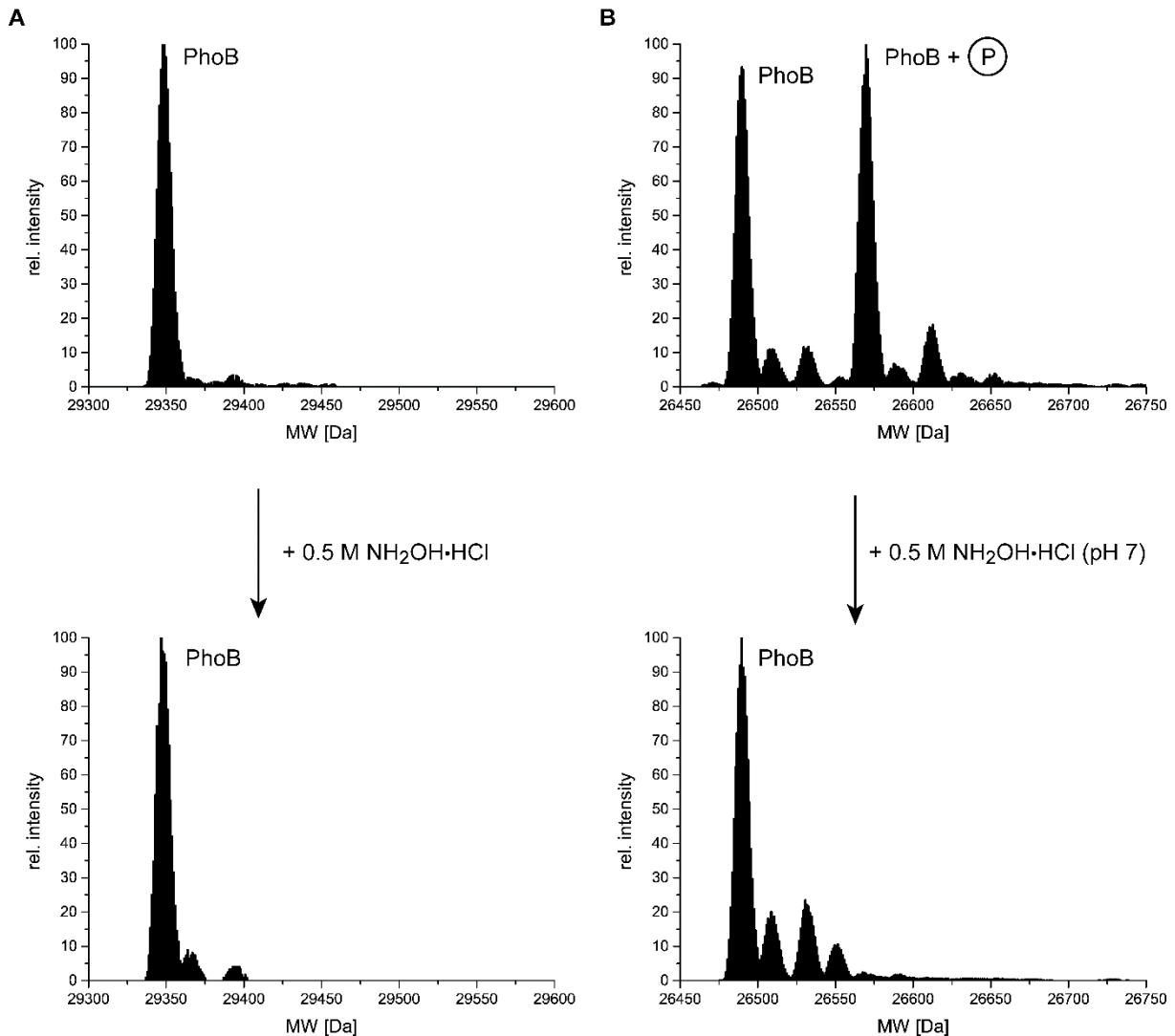


**Figure 20:** Controls for the selective turnover of phosphoaspartate by hydroxylamine. (A) No reaction between unphosphorylated PhoB and hydroxylamine was observed. (B) Treatment of phosphorylated PhoB with a neutralized hydroxylamine solution results in elimination of the phosphate moiety without formation of *N4*-hydroxyasparagine. Tag-free PhoB was used in (B).

In order to test for the pH-dependency of the reaction, the experiment was conducted with 10% (v/v) of a previously neutralized 5 M  $\text{NH}_2\text{OH}\cdot\text{HCl}$  solution, so that the reaction proceeded at neutral pH. No adduct formation was observed, instead, the phosphoaspartate adduct was removed completely (Fig. 20B). This observation is in line with the previously observed preference for nucleophilic attack at the phosphorus atom at neutral pH, leading to cleavage of the P-O bond of the anhydride.<sup>114-115</sup> Therefore, correct adjustment of the pH-value seems to be critical for the successful conversion of phosphoaspartate to *N4*-hydroxyasparagine

## HYDROXYLAMINE-BASED REVERSE POLARITY ABPP

(Fig. 21B). Time-resolved measurements showed that the turnover reaction proceeds quantitatively within about 30 min. Monitoring the total amount of modified PhoB (phosphorylated or *N4*-hydroxyasparagine) showed that the total amount of modified protein never exceeded the starting value of phosphorylated PhoB. This means that every newly formed hydroxamic acid modification must have arisen from a previously phosphorylated protein (Fig 21A).

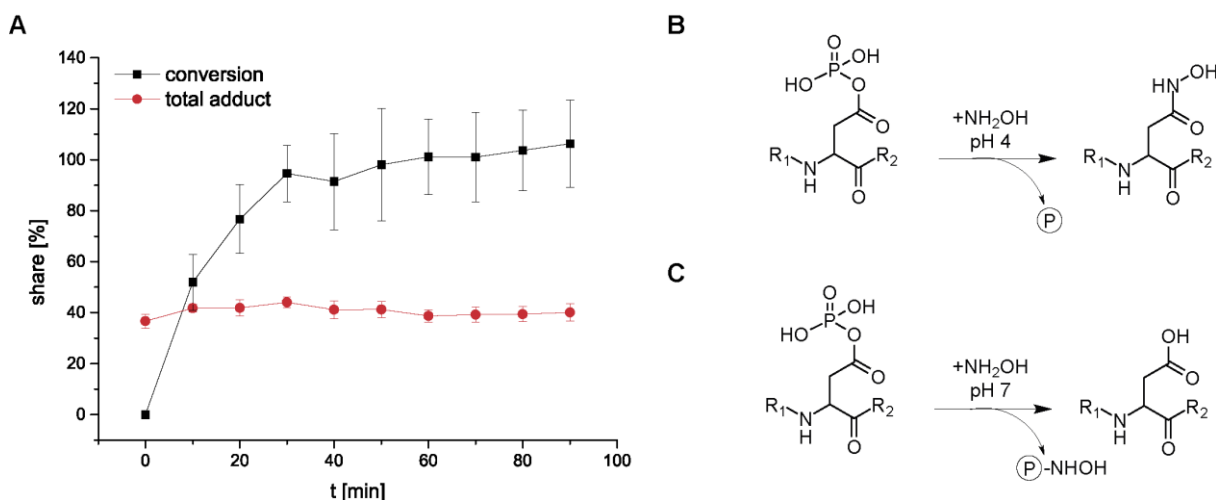


**Figure 21:** Time-resolved measurement of the conversion of pAsp to *N4*-hydroxyasparagine (**A**) and proposed reaction mechanism in dependence of the pH-value (**B-C**). Time courses were recorded in triplicates and results are given as mean  $\pm$  standard deviation.

With a working procedure for the conversion of pAsp to a stable derivative in hand, it was intended to prove that this method could also be applied to a more complex sample and that the modification could also be detected on the peptide level. As a prerequisite for this experiment, a digestion strategy, leading to the generation of a reporter peptide that carries Asp53, had to be developed. Due to long stretches without Arg or Lys residues, tryptic cleavage of PhoB does not deliver peptides carrying Asp53 that could be detected by standard LC-MS/MS settings. Chymotryptic cleavage resulted in peptides too short for MS/MS detection, due to unspecific cleavage after a series of Leu residues in direct proximity to Asp53. Therefore, a double digestion using trypsin and AspN protease was applied, leading to the formation of the desired semi-tryptic reporter peptides D(53)WMLPGGSGIQFIK and DLILLD(53)WMLPGGSGIQFIK, with a missed cleavage at Asp53. To study pAsp conversion in a complex biological background, PhoB was phosphorylated *in vitro* with acetyl phosphate, spiked into an orthogonal *B. subtilis* proteome and the mixture was subjected to treatment either with hydroxylamine or water as a control. Afterwards, the proteome was precipitated and further subjected to proteolytic cleavage using the developed digestion strategy combining trypsin and ApsN. The experiments showed that no aspartate phosphorylation was detectable when the mixture was mock treated, indicating that the phosphoaspartate moiety was too unstable for the applied steps of the proteomic workflow. Satisfyingly, conversion with

hydroxylamine to *N4*-hydroxyasparagine could be detected in three out of three replicates. Localization probability scores were very high in all replicates ( $> 0.99$ ), indicating that the site was identified unambiguously at Asp53. Interestingly, all modified peptides measured contained the missed AspN cleavage at position Asp53 (Fig. 22). No *N4*-hydroxyasparagine (*nhAsp*)-peptides with a correct cleavage at Asp53 were found. Therefore, modification of Asp53 seems to prevent recognition of the cleavage site by AspN protease leading to the generation of the missed cleavage reporter peptides. Spectral quality of the generated peptides was found to be very high and the modified Asp53 residue was covered in both the b- and y-ion series.

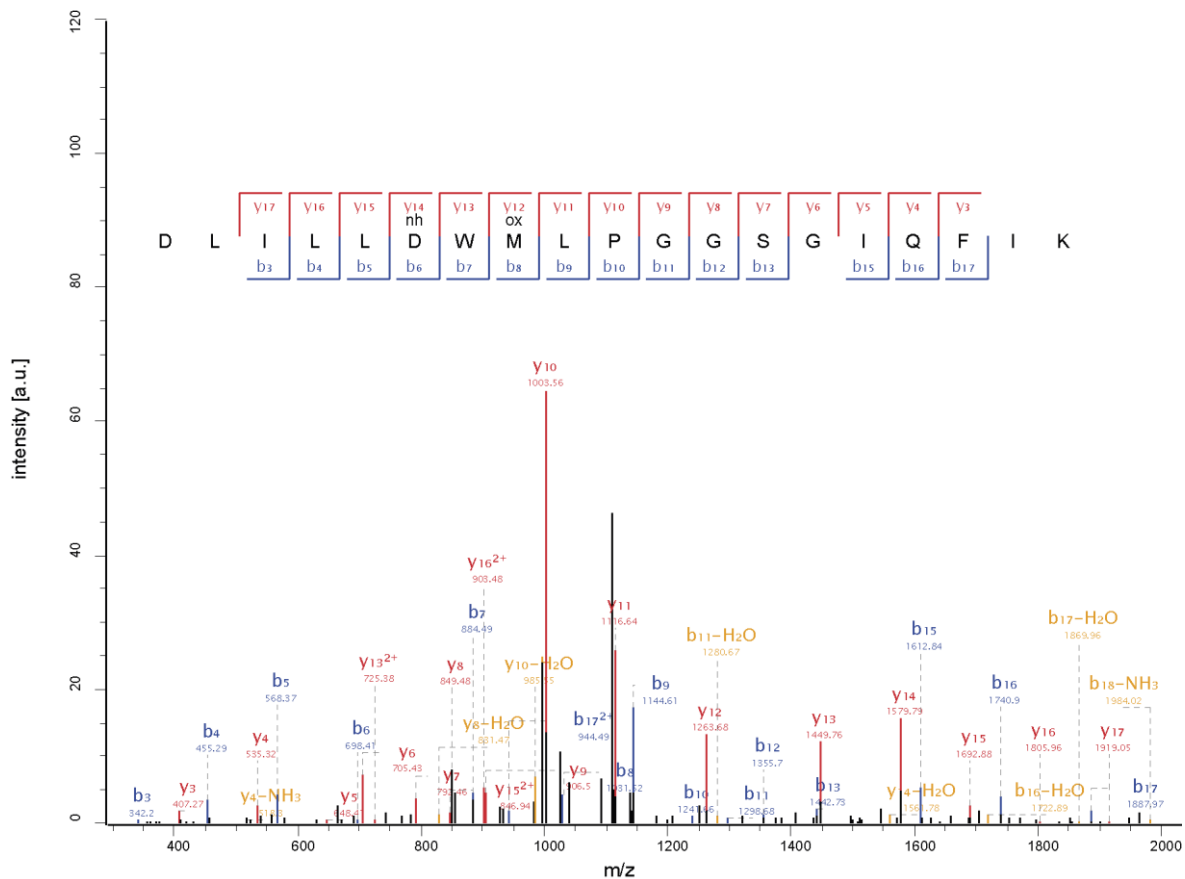


**Figure 22:** Peptide spectra of PhoB reporter peptide after conversion of phosphoaspartate with hydroxylamine in a complex sample. Phosphorylated *E. coli* PhoB was spiked in *B. subtilis* proteome and turned over with hydroxylamine. The sample was double digested with AspN and trypsin. (nh = *N4*-hydroxyasparagine; ox = oxidation).

These experiments demonstrate that PhoB could be established as a model protein for the turnover of aspartate phosphorylation with hydroxylamine. The turnover product *N4*-hydroxyasparagine could be detected on full-length protein by IP-MS and on the peptide level by LC-MS/MS experiments. Conversion of phosphoaspartate was successful in isolated PhoB as well as in a complex background proteome.

### 3.2 Development of an rp-ABPP protocol based on hydroxylamine

After it could be demonstrated that turnover of phosphoaspartate to *N*4-hydroxyasparagine is feasible in a complex biological background, the methodology should be transferred to a full proteome analysis of exponentially growing *B. subtilis*. To do so, bacteria were harvested and directly lysed in hydroxylamine-containing lysis buffer. This labeling strategy should assure immediate exposure of the proteome to the nucleophile in the moment of lysis. The precise adjustment of the pH-value was found to be a critical step for the conversion of phosphoaspartate in the model system PhoB. As within the bacterial cells the control of the pH-value cannot be assured, an *in situ* approach was not feasible. After lysis of the cells, the soluble fraction of the proteome was tryptically digested, separated on a HILIC (hydrophilic interaction chromatography) column and further subjected to LC-MS/MS analysis. Unfortunately, no differences between hydroxylamine and control treated samples could be detected, regarding the amount of *nhAsp* sites. Since phosphoaspartate is a rare and transient event, it is very likely that the full proteome approach failed due to an insufficient signal-to-noise ratio. Conventional phosphoproteomic methods use enrichment steps with affinity matrices like Fe<sup>3+</sup>-IMAC to overcome the problem of low abundance.<sup>147</sup> Reverse polarity ABPP with an alkyne-tagged hydroxylamine probe (**HA-yne**) would enable the enrichment of converted phosphoaspartate residues and with that could overcome the limitations of full proteome analysis. **HA-yne** was first tested in the PhoB model system (Fig. 23). The probe is prepared as a hydrochloride salt and therefore it can be used in the same way as NH<sub>2</sub>OH·HCl. IP-MS analysis revealed that **HA-yne** converted phosphoaspartate successfully at pH 4 (Fig. 23A). Moreover, time-resolved measurements showed that the reaction proceeds quantitatively within 1 h at room temperature (Fig. 23C).

After it could be demonstrated that **HA-yne** is a suitable probe for the conversion of phosphoaspartate, an rp-ABPP workflow should be established. The following section will highlight the key obstacles during the development of the workflow. All studies were carried out with *B. subtilis* in mid-exponential phase in analytical scale and readout was achieved by in-gel fluorescence scanning. Initial studies with the model protein PhoB showed that the pH-value plays a critical role for the successful conversion of phosphoaspartate.

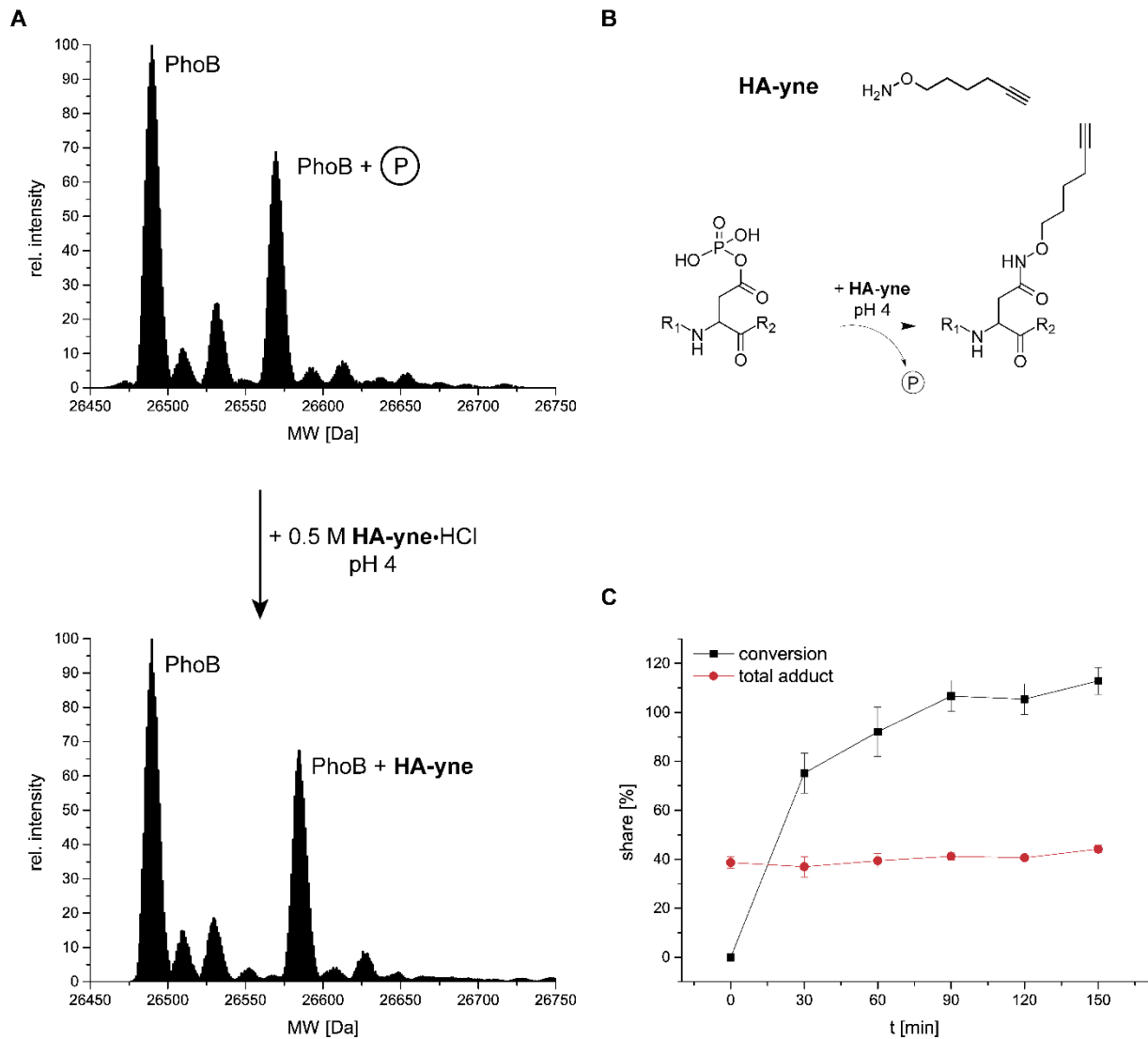


**Figure 23:** Hydroxylamine-based probe **HA-yne**. (A) Intact protein mass spectrometry of pAsp conversion by **HA-yne**. (B) Reaction of **HA-yne** with pAsp. (C) Time-resolved measurement of the conversion of pAsp by **HA-yne**. Time courses were recorded in triplicates and results are given as mean  $\pm$  standard deviation. Tag-free PhoB was used.

Therefore, pH-titration was carried out first to examine if these findings can be transferred to the proteome level (Fig. 24). Indeed, the labeling pattern was found to be highly pH-dependent: no labeling was observed at pH 4, whereas distinct labeling patterns were observed at pH 7 and pH 9. It is possible that the reaction profile of **HA-yne** is not limited towards phosphoaspartate. Other electrophilic centers like Asp/Glu ADP-ribosylation sites or unknown electrophilic PTMs might also be prone to nucleophilic attack by **HA-yne**.<sup>142, 148</sup> Moreover, one has to take into account that the reactivity of phosphoaspartate residues is also highly dependent of the protein environment. Therefore, not all pAsp-sites might behave like the model system PhoB.

## HYDROXYLAMINE-BASED REVERSE POLARITY ABPP

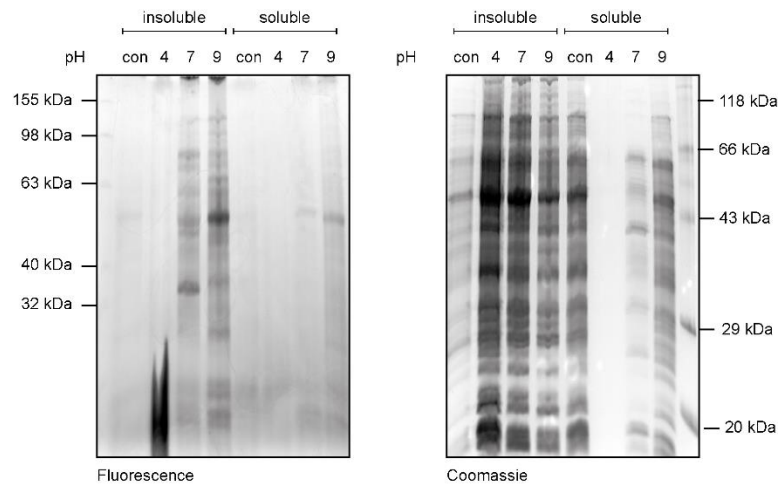


**Figure 24:** Analytical labeling of exponentially growing *B. subtilis* with 500 mM **HA-yne** at different pH-values. Labeling pattern and protein solubility are strongly pH dependent. (con = 20 mM HEPES, pH 7.0)

Another striking observation of the experiment was that most of the proteome was found in the insoluble fraction. A clear pH dependency of proteome solubility was observed. At pH 4 most of the proteome was found in the insoluble fraction, whilst at pH 7 and pH 9 more proteins remained soluble. Interestingly, labeling seemed to anti-correlate with solubility, as labeled proteins were found almost exclusively in the insoluble fraction. The acidic pH-value seemed to have destabilizing effects on the proteome, leading to complete precipitation before reaction between the probe and its targets could take place. Henceforth, several detergents were tested to stabilize the proteome with the goal to achieve labeling also at an acidic pH of 4 (Fig. 25). Complete proteome precipitation was observed without detergents when probe was present and labeling remained unsuccessful. Using 1% (w/v) LDAO in the lysis buffer resulted in a distinct and strong labeling pattern in both the soluble and insoluble fraction. Moreover, the protein amount seemed to be roughly equally distributed between soluble and insoluble fraction. Using 1% (v/v) NP-40 and 1% (w/v) DDM also had some stabilizing, but less pronounced effects. Slight labeling was visible in both the soluble and insoluble fraction, nonetheless almost the complete proteome remained in the insoluble fraction.

## HYDROXYLAMINE-BASED REVERSE POLARITY ABPP

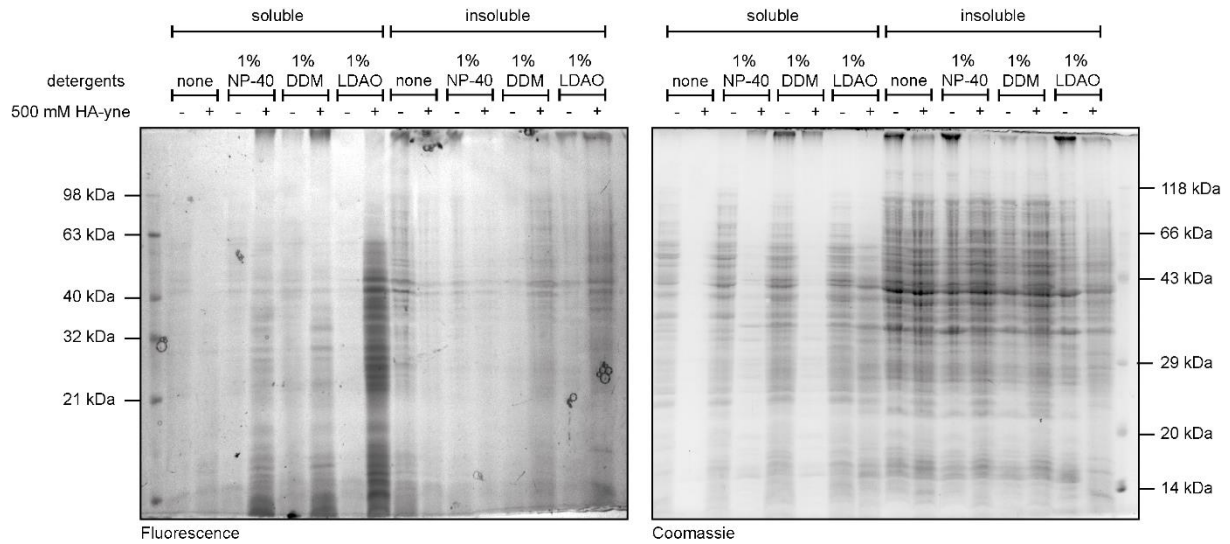


**Figure 25:** Testing of detergents for the optimization of labeling conditions at pH 4. Addition of 1% (w/v) LDAO led to the most efficient solubilization of the proteome as well as to the most pronounced labeling pattern.

Next, the dose-dependency of the labeling pattern of **HA-yne** was examined (Fig. 26). Two-fold serial dose-down from 500 mM downwards was prepared. Prior to lysis, the pH-value was carefully adjusted to pH 4 in all buffers, to ensure that changes in the labeling pattern are solely caused by probe concentration. In-gel fluorescence scanning revealed very strong labeling at a probe concentration of 500 mM and 250 mM in both the soluble and insoluble fraction. Some bands especially in the region of 30 to 40 kDa as well as a prominent band at 21 kDa appeared weakened at 250 mM. The labeling intensity deteriorated further at 125 mM and was almost completely lost at 62.5 and 31.25 mM.

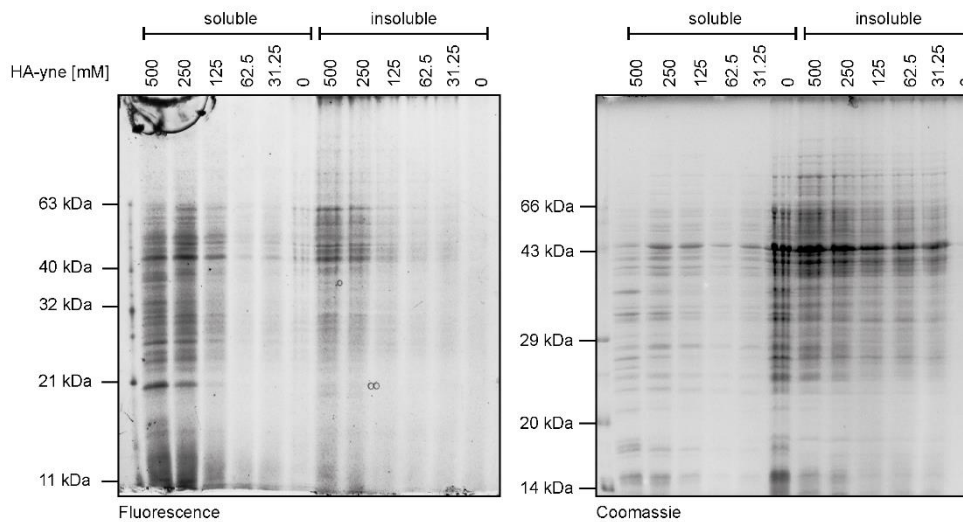


**Figure 26:** Dose-dependent labeling of exponentially growing *B. subtilis* with **HA-yne**.

Taking the pH-titration experiment into account, it can be assumed that the acidic pH-value in combination with the high probe concentration are responsible for proteome precipitation. Interestingly, the detected fluorescence intensity seemed not to correlate with protein

## HYDROXYLAMINE-BASED REVERSE POLARITY ABPP

abundance as detected by Coomassie staining. This indicates that the labeling pattern is not caused by unspecific non-covalent interaction with high abundant proteins.

Since the proteome was stabilized long enough for successful labeling by addition of the detergent LDAO and insoluble proteins can also be analyzed by MS-based proteomic workflows, no further focus was laid on the enhancement of protein solubility.

Based on the aforementioned results, a workflow for the MS-based target identification of **HA-yne** was designed (Fig. 27). Bacteria were harvested, washed and lysed in detergent-containing buffer with or without nucleophile. pH was carefully adjusted prior to lysis. Afterwards, soluble and insoluble fraction of the proteome were separated and the soluble fraction was precipitated. Both fractions were then washed to remove excess probe. Next, the fractions were combined again to remove any bias caused by altered solubility and clicked to biotin azide. Labeled proteins were then enriched on avidin beads and subsequently on-bead digestion was performed. The peptide mixture was analyzed via LC-MS/MS and enrichment factors compared to the control sample were determined by label-free quantification.

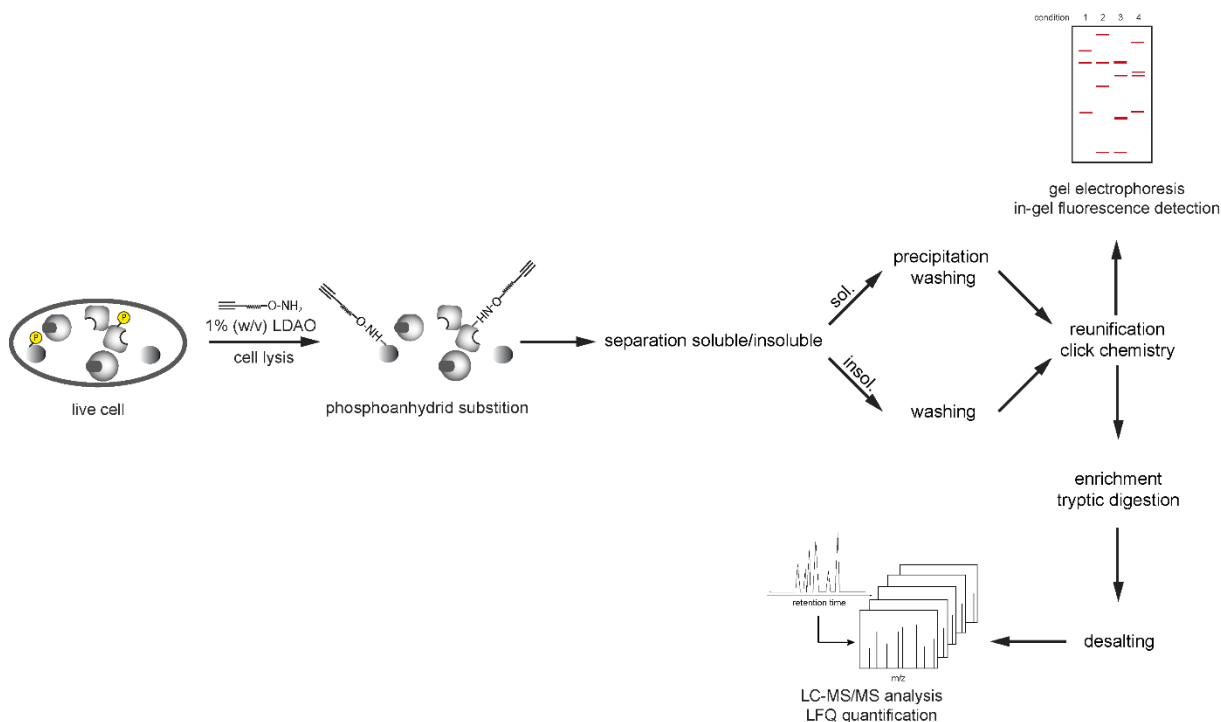


**Figure 27:** Scheme of the rp-ABPP workflow for quantitative target identification of the hydroxylamine-based probe **HA-yne**.

The newly developed workflow was applied to analyze the targets of **HA-yne** in exponentially growing *B. subtilis*. Furthermore, the technology was used to investigate the influence of the human opioid peptide dynorphin on the potential aspartate phosphorylation status of *P. aeruginosa*.

### 3.3 Target identification in exponentially growing *B. subtilis*

First quantitative target-ID experiments were carried out in exponentially growing *B. subtilis*. It was assumed that many regulatory processes, involving aspartate phosphorylation, would take place during this growth phase. The bacteria are constantly dividing in this phase and therefore many cellular processes need to be tightly regulated. Target-ID was carried out twice in three biological replicates and at five different concentrations of **HA-yne** (62.5 mM; 125 mM; 250 mM; 375 mM; 500 mM) (Fig. 28). This concentration screening should help to identify the most promising conditions for proteomic profiling. The probe displayed broad target reactivity and many proteins were found to be enriched. Therefore very strict cut-off criteria were applied and only protein IDs with an enrichment factor  $\geq 8$  and t-test p-value  $< 0.01$  were defined as high confidence targets of **HA-yne**. The number of high confidence targets peaked with 111 in the 125 mM sample (Fig. 28A). Gene ontology analysis of biological processes revealed that chemotaxis (12.83-fold enriched; p-value:  $1.88 \times 10^{-4}$ ) and flagellum-dependent cell motility (12.25-fold enriched; p-value:  $1.47 \times 10^{-3}$ ) associated proteins were significantly overrepresented in this dataset. Chemotaxis is the process by which bacteria react to attractants and repellents in their environment and regulate their movement. 37 out of 4185 (0.88%) reviewed proteins in *B. subtilis* strain 168 are annotated with aspartylphosphate modification in the Uniprot database. Four out of these 37 proteins (CheV; CssR; MalR; YfiK) were found among the high confidence targets, representing 3.6% of the dataset (Fig. 28B). At 500 mM concentration of **HA-yne**, proteins with the GO-term ribosome biogenesis were found to be overrepresented (7.26-fold enrichment; p-value  $3.83 \times 10^{-2}$ ), whereas no GO-term enrichment was found in the other datasets.

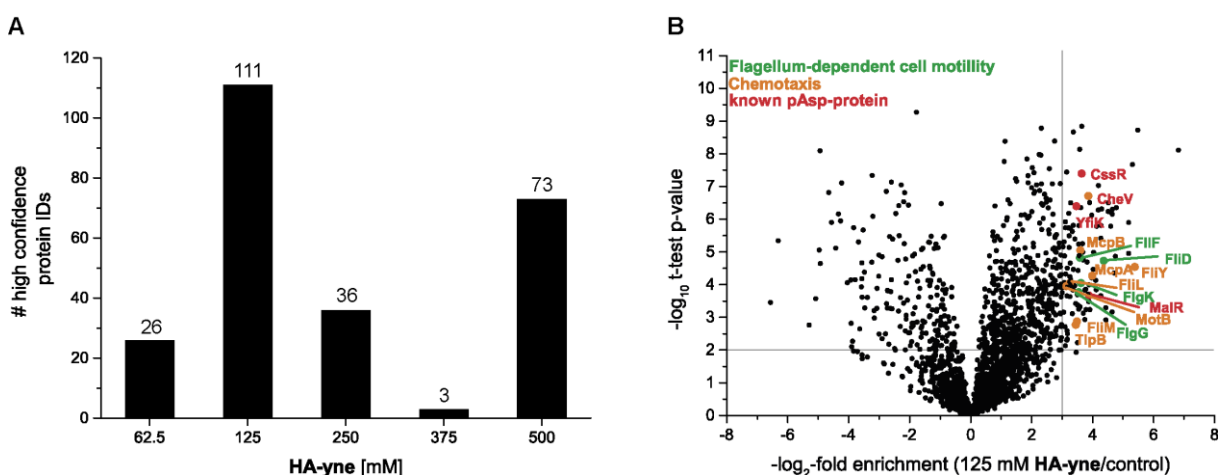


**Figure 28:** Target identification of probe **HA-yne** in exponentially growing *B. subtilis*. (A) Number of high confidence targets (enrichment factor  $\geq 8$  and t-test p-value  $< 0.01$ ) at different concentrations of **HA-yne**. (B) Volcano plot of target identification experiment with 125 mM **HA-yne**. Proteins with GO-term annotation “chemotaxis” and “flagellum-dependent cell motility” as well as known pAsp-proteins are highlighted among the high confidence targets. Experiments were carried out twice in three biological replicates.

## HYDROXYLAMINE-BASED REVERSE POLARITY ABPP

Aspartate phosphorylation plays a central role in chemotaxis and the regulation of flagellum dependent cell motility via the CheA-CheY phosphorelay system.<sup>149</sup> Therefore, the identification of these protein groups seemed to be very promising. With CheV, a central component of the chemotaxis machinery that is known to be aspartate phosphorylated, was identified. Interestingly, CheV is part of the signal adaptation process. The protein is phosphorylated by active histidine kinase CheA and in a feedback loop reduces the activity of CheA. This, in turn, leads to reduced phosphorylation of the response regulator CheY.<sup>149</sup> Signaling through CheY is also terminated by the phosphatase FliY.<sup>150</sup> This phosphatase was also identified as a high confidence target of **HA-yne**. In line with these results, the response regulator CheY was not found to be under the enriched targets of **HA-yne**. Among the enriched chemotaxis proteins also a group of methyl-accepting chemoreceptors (McpA; McpB and TlpB) was identified. These receptors form complexes with the histidine kinase CheA, but are not yet known to be phosphorylated themselves.<sup>149</sup>

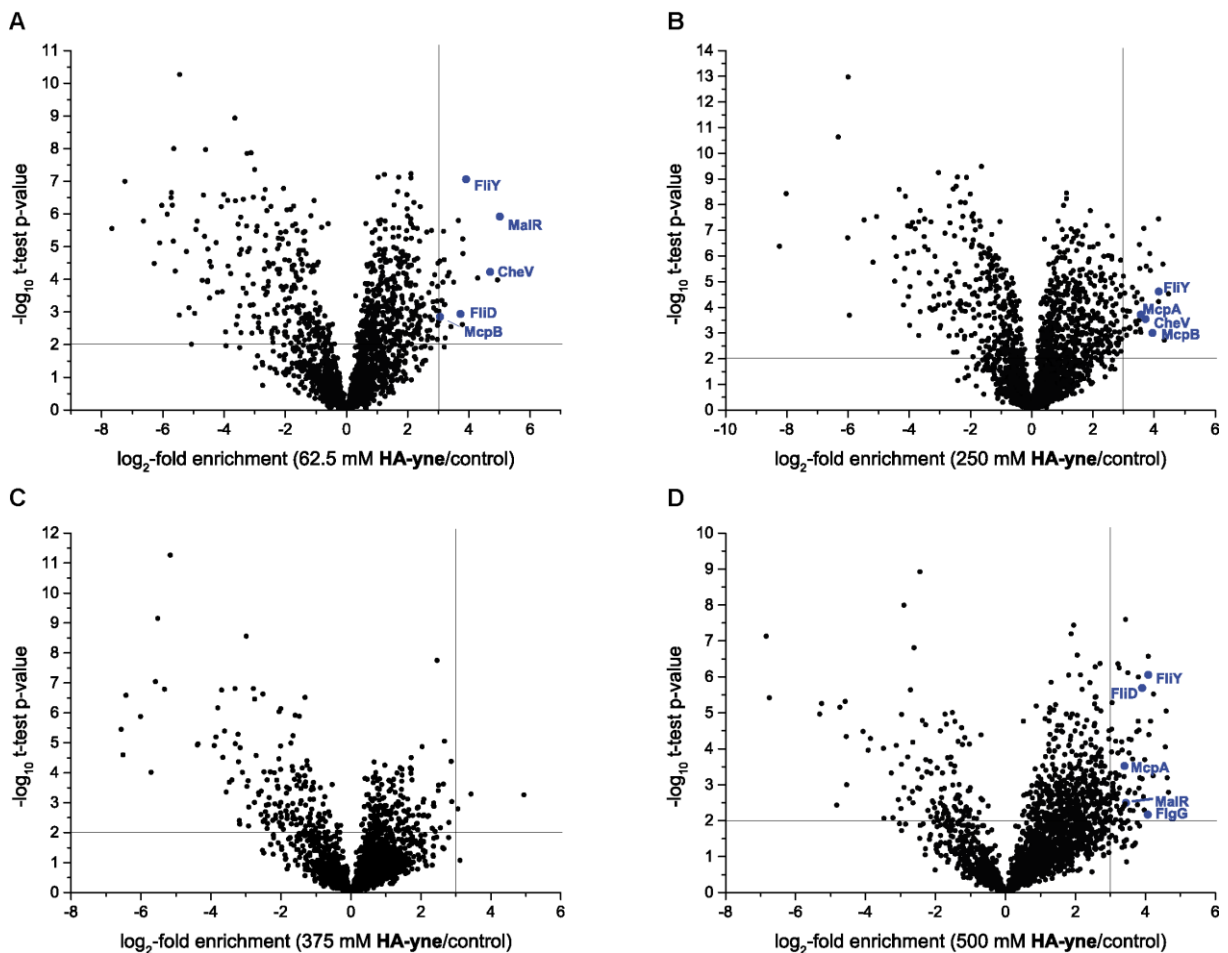


**Figure 29:** Volcano plots of target identification experiments with 62.5 mM (A), 250 mM (B), 375 mM (C) and 500 mM (D) **HA-yne**. Experiments were carried out twice in three biological replicates. High confidence targets are defined as proteins with an enrichment factor  $\geq 8$  and t-test p-value  $< 0.01$ . Redundant chemotaxis and flagellum-dependent cell motility associated targets and known pAsp-proteins identified as high confidence targets at 125 mM **HA-yne** are highlighted in blue.

To further narrow down the list of interesting target proteins, high confidence targets associated with chemotaxis, flagellum-dependent cell motility and known pAsp-proteins found at 125 mM probe concentration were also searched in datasets generated at different **HA-yne** concentrations. Satisfyingly, several of these proteins were also found in the other datasets (Fig. 29). The response regulator MalR and the chemotaxis protein CheV, with their known aspartylphosphate moieties, were found in three of the five experiments as one of the high confidence targets. Methyl-accepting chemotaxis proteins such as McpA or McpB could be identified in four of the five applied experimental conditions. Most striking is the redundancy of the phosphatase FliY, which is a top target in four of the five tested concentrations. Taken together, these studies show that a specific subset of proteins can be reproducibly labeled with hydroxylamine-based probe **HA-yne** and that known aspartate phosphorylated proteins are among the most enriched targets. Further studies will be needed to clarify the binding site of **HA-yne** and thereby identify the potential phosphoaspartate sites.

### 3.4 Target identification in *P. aeruginosa* under dynorphin treatment

Host-microbe interaction plays a crucial role in infectious processes and virulence regulation. The human opioid peptide dynorphin was shown to enhance virulence of the opportunistic pathogen *P. aeruginosa*.<sup>151</sup> Recently, it could be shown that dynorphin binds to ParS, a membrane-associated histidine kinase. ParS is the sensor kinase of the ParS/ParR two component signaling system.<sup>127</sup> After successfully establishing a quantitative target identification platform in *B. subtilis*, the rp-ABPP methodology was applied in *P. aeruginosa* to investigate putative changes in aspartate phosphorylation levels of ParR upon dynorphin treatment. To do so, *P. aeruginosa* cultures were treated with dynorphin or DMSO as a control for 30 min. Both samples were then either chased with **HA-yne** or buffer as a control. Subsequently, labeled proteins were quantified by LC-MS/MS analysis. This experimental set-up resulted in four different combinations of treatment and chase conditions: control-control; control-**HA-yne**; dynorphin-control and dynorphin-**HA-yne**. Comparing the dynorphin-**HA-yne** sample with the control-**HA-yne** sample will therefore allow for the identification of proteins that show increased reactivity towards **HA-yne** after treatment with dynorphin. However, the enrichment factor of the response regulator ParR did not change. Moreover, almost all identified proteins (2065 out of 2075) did not show any significant changes in reactivity towards **HA-yne** after dynorphin treatment. However, a very distinct subset of nine proteins was found to be significantly enriched (up to 470-fold) in the dynorphin-**HA-yne** over the control-**HA-yne** sample (Fig. 30A), among them, several uncharacterized proteins with putative hydrolase, lipase and peptidase activity (Q9HW54; Q9HXU5; Q9HZF5; Q9I5Z3 and Q9I6I3). Furthermore, SpeH was identified, a protein known to be involved in the synthesis of spermidine, a small molecule involved in protecting the membrane of *P. aeruginosa* from antibiotic stress. Most

## HYDROXYLAMINE-BASED REVERSE POLARITY ABPP

interestingly, three members of the *arn* operon (ArnA; ArnB and ArnC) were identified, which is known to be involved in anti-microbial peptide defense. Previous studies showed that the expression of members of the *arn* operon is upregulated upon dynorphin treatment.<sup>127</sup> To investigate whether the increased enrichment is due to higher unspecific background binding caused by higher protein levels, the control-chased samples were also compared (Fig. 30B). Satisfyingly, no enrichment of the target proteins was found in the dynorphin-control sample over the control-control sample, which speaks against an increased unspecific background binding to avidin beads caused by higher protein levels. Hence, it can be assumed that the significant enrichment of the proteins in the dynorphin-**HA-yne** over the control-**HA-yne** sample is caused by increased reactivity of these proteins towards the probe, induced by dynorphin treatment. Increased reactivity could be caused by electrophilic centers in PTMs on the mature protein, such as phosphoaspartate. Nonetheless, also the nascent polypeptide chain in its amino-acyl-tRNA bound state might be prone to nucleophilic attack by **HA-yne** at its ribosylated C-terminus.

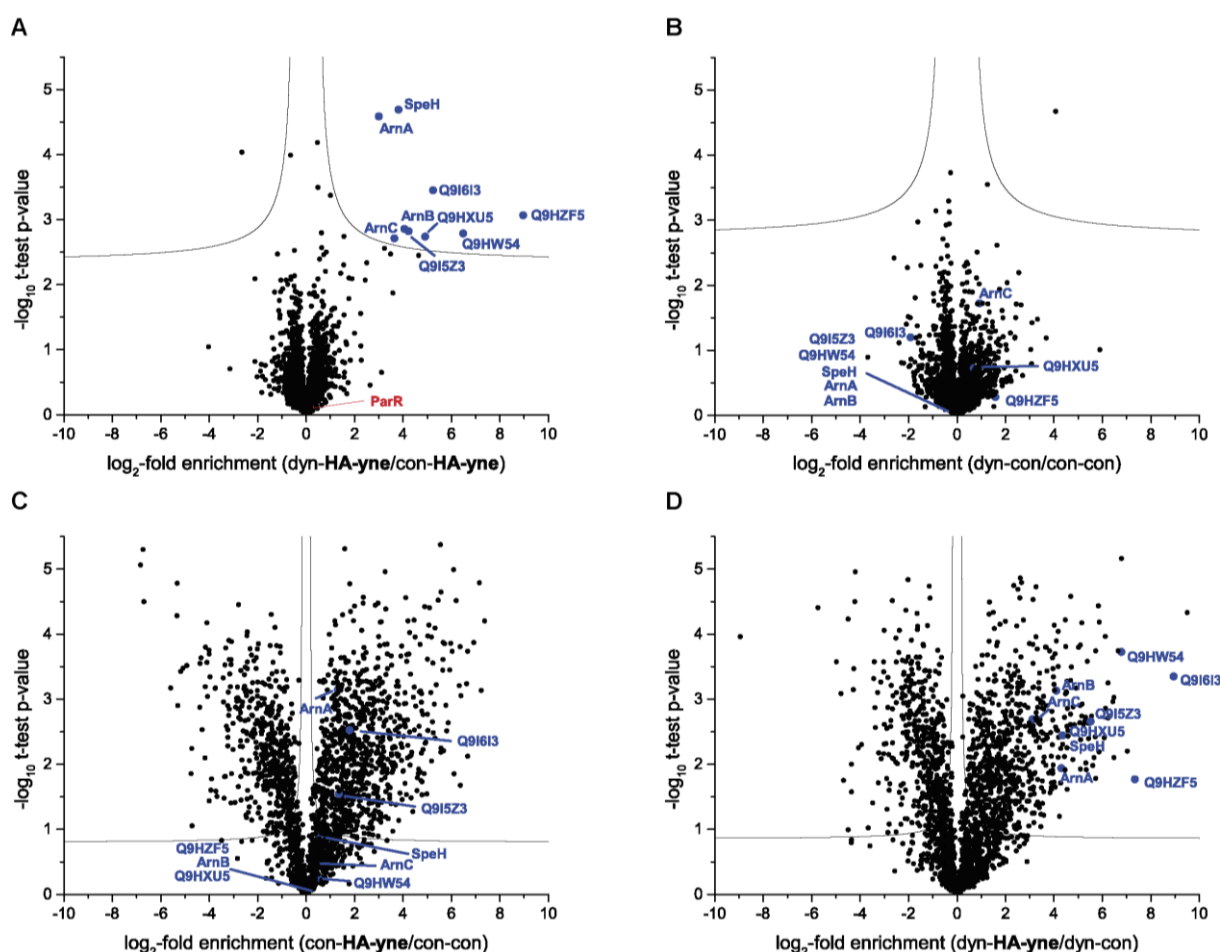


**Figure 30:** Rp-ABPP to assess changes in **HA-yne**-reactive centers of the proteome of *P. aeruginosa* after exposure to human opioid peptide dynorphin. **(A)** Volcano plot of label-free quantification data of **HA-yne** labeling after dynorphin treatment plotted against **HA-yne** labeling after control treatment. **(B)** Volcano plot of label-free quantification data of control-chase after dynorphin treatment plotted against control-chase after control treatment. **(C-D)** Enrichment of **HA-yne** labeled proteins after control **(C)** and dynorphin **(D)** treatment.

Comparison of the dynorphin-control with the control-control samples further confirmed that unspecific binding to the beads in general seems not to be altered upon dynorphin treatment, since background detection does barely change between the two sample sets (Fig. 30B). The volcano plots of the individual enrichments (control-**HA-yne**/control-control and dynorphin-**HA-yne**/dynorphin-control) nicely illustrate the increase of reactivity of the significantly enriched proteins upon dynorphin treatment (Fig. 30C-D). Taken together, these results indicate that a specific subset of proteins, some of which are involved in anti-microbial peptide defense, shows elevated reactivity towards the nucleophilic probe **HA-yne** after *P. aeruginosa* is exposed to dynorphin. It can be speculated that this increased reactivity is caused by electrophilic PTMs like phosphoaspartate. These findings provide a good basis for future validation, including the identification of the binding site of the probe in the respective proteins.

## 4 CONCLUSION AND OUTLOOK

Aspartate phosphorylation plays a crucial role in bacterial cell signaling and as an intermediate in catalytic processes. Due to its intrinsic instability the mixed anhydride bond is very labile and hard to detect using standard proteomic workflows. Therefore, a reverse polarity ABPP workflow based on the small molecule nucleophile hydroxylamine was developed. Using the well-characterized response regulator PhoB as a model system, it could be shown that aspartate phosphorylation can be converted to a stable hydroxamic acid derivative by hydroxylamine. Site specific and phosphorylation-dependent formation of this modification was monitored on the intact protein and on the peptide level by mass spectrometry. Various studies showed that the pH-value plays a crucial role for the efficient conversion of pAsp and needs to be adjusted to acidic conditions. Full proteome studies based on the conversion of pAsp to *nhAsp* were not successful, probably due to the low abundance of the modification. Identification numbers of *nhAsp* sites did not vary significantly between hydroxylamine and control-treated samples and therefore had to be regarded as unspecific noise. Phosphoproteomics of Ser/Thr/Tyr phosphorylation uses enrichment of phosphopeptides to overcome the problem of low abundance. An alkyne-tagged probe based on hydroxylamine (**HA-yne**) was used to develop a reverse polarity ABPP workflow for the enrichment of electrophilic **HA-yne**-reactive centers in proteins. Since earlier work by *Cravatt et al.* with a hydrazine-derived nucleophilic probe resulted in the identification of previously unknown electrophilic PTMs, it cannot be excluded that **HA-yne** also reacts with non-pAsp electrophilic PTMs. During method development key obstacles for a successful rp-ABPP workflow based on **HA-yne** were identified: (1) pH-value has a drastic influence on reactivity and thereby on the labeling pattern of the probe and (2) addition of a suitable detergent is key to achieve labeling at acidic pH. After overcoming these obstacles, labeling at an acidic pH-value, resembling the conditions of the *E. coli* PhoB model system, was achieved. The labeling was

demonstrated to be concentration dependent and did not correlate with protein abundance. The established workflow in combination with LFQ LC-MS/MS methodology was applied to identify the targets of **HA-yne** in exponentially growing *B. subtilis*. Chemotaxis associated proteins like the phosphatase FliY, methyl-accepting chemoreceptors like McpA/B and known pAsp-proteins like CheV and MalR were identified as the most promising targets of **HA-yne**. The probe depicted very broad reactivity and further studies will be needed to determine which target proteins are true pAsp-proteins. First, target-sites of the probe need to be determined by using specialized methods such as isoTop-ABPP that allow for the detection of probe-modified peptides.<sup>152</sup> The identified probe binding sites, then, need to be validated by biochemical and molecular biology methods. In the case of putative pAsp sites in chemotaxis proteins, the generation of genetic point mutants and their characterization in chemotaxis assays would be the method of choice. Further application of the rp-ABPP workflow aimed to quantify changes in the aspartate phosphorylation level of the response regulator ParR in *P. aeruginosa* after treatment with the human opioid hormone dynorphin. However, no change in enrichment of ParR could be detected between dynorphin and control-treated cells. This might be due to a wide variety of reasons. Either, the probe is not reactive towards ParR due to steric reasons, or phosphorylation levels already return to basal levels at the moment of **HA-yne** treatment. Dephosphorylation could be triggered by a negative feed-back by the ParS histidine kinase or accessory proteins, or might occur due to very fast hydrolysis.<sup>153</sup> Further time-dependent labeling studies will help to shed light on this aspect. Nonetheless, a very distinct subset of proteins changed greatly in reactivity towards **HA-yne** after treatment with the opioid peptide. Among these proteins are members of the *arn* operon that are known to be upregulated as a defense mechanism after exposure to dynorphin. To prove that the increased reactivity towards **HA-yne** is due to electrophilic PTMs like pAsp and not due to increased abundance, binding site identification studies will be needed. Once sites have been identified, their biological relevance will be assessed by generating genetic point mutations and exposure of the mutants to dynorphin. Furthermore, the rp-ABPP workflow can also be applied to a variety of other systems like vancomycin resistant enterococci where resistance is mediated by the VanS/VanR two-component signaling system.<sup>154</sup> It would be also possible to adapt the workflow for the study of human cancer cell lines to mine for potential pAsp sites also in higher organisms.

## 5 EXPERIMENTAL SECTION

### 5.1 *In vitro* studies on *E. coli* PhoB

#### 5.1.1 Protein purification

PhoB was expressed as N-terminal His<sub>6</sub>-tagged construct with TEV-cleavage site between tag and protein sequence encoded on a pET300 vector in *E. coli* BL21(DE3). Cells were grown in 1 L lysogeny broth (LB) medium at 37 °C until they reached OD<sub>600</sub>= 0.6 and expression was induced with 1:2000 (v/v) 1M IPTG. Protein expression was performed at 25 °C over night. Cells were harvest by centrifugation at 6000 rpm at 4 °C for 10 min. The cells were washed once with PBS, resuspended in lysis buffer (20 mM Trizma, pH 8.0; 150 mM NaCl; 2 mM  $\beta$ -mercaptoethanol; 10 mM imidazole; 0.4% (v/v) NP-40) and lysed by sonication (2x (7 min, 30% int.; 3 min, 80% int.) Bandelin Sonopuls) under constant cooling on ice. Cells debris was pelletized by centrifugation at 18000 rpm at 4 °C for 30 min. The cleared supernatant was loaded on a 5 mL HisTrap HP column (GE Healthcare) preequilibrated with 5 CV of wash buffer 1 (20 mM Trizma, pH 8.0; 150 mM NaCl; 2 mM  $\beta$ -mercaptoethanol; 10 mM imidazole) . After loading, the column was washed with 8 CV of binding buffer 1, 8 CV of binding buffer 2 (20 mM Trizma, pH 8.0; 1 M NaCl; 2 mM  $\beta$ -mercaptoethanol; 10 mM imidazole) and 8 CV of binding buffer 3 (20 mM Trizma, pH 8.0; 150 mM NaCl; 2 mM  $\beta$ -mercaptoethanol; 40 mM imidazole). Proteins were eluted with 8 CV of elution buffer (20 mM Trizma, pH 8.0; 150 mM NaCl; 2 mM  $\beta$ -mercaptoethanol; 500 mM imidazole) into fractions of 2.5 mL. Each collection tube contained 2.5 mL of binding buffer 1 to dilute the imidazole concentration. Samples were carefully concentrated and loaded onto a preequillibrated Superdex75 pg 16/60 column and separated over 1 CV in PhoB storage buffer (20 mM HEPES, pH 7.0; 150 mM NaCl; 0.1 mM EDTA; 0.1 mM DTT). Fractions containing ClpP were unified and concentrated carefully and stored after addition of 10% (v/v) glycerin in single-use aliquots at -80 °C.

For the generation of tag-free PhoB, the protein was dialyzed after His-affinity purification into 3 L of PhoB storage buffer (20 mM HEPES, pH 7.0; 150 mM NaCl; 0.1 mM EDTA; 0.1 mM DTT) for 20 h. The next day the protein sample was cleared of precipitation by centrifugation at 21100 g at 4 °C for 30 min. The soluble protein was incubated with 1:3 (w/w) TEV protease at 10 °C over night without shaking. Proteins were then carefully concentrated and subjected to gel filtration chromatography and further processed as described above.

## HYDROXYLAMINE-BASED REVERSE POLARITY ABPP

### 5.1.2 Generation of PhoBD53N

A D53N point mutant of *E. coli* PhoB was created using a QuikChange®-like protocol. The His<sub>6</sub>-TEV-PhoB construct in pET300 vector was used as template. 10 µL Phusion® polymerase GC or HF buffer (NEB), 1 µL dNTP-Mix (NEB), 1 µL template (100 ng/µL), 0.75 µL forward primer (GGATTTAATTCTCCTCAACTGGATGTTACCTGG), 0.75 µL reverse primer (CCAGGTAACATCCAGTTGAGGAGAATTAAATCC), 1.5 µL DMSO, 39.5 µL ddH<sub>2</sub>O and 0.5 µL Phusion® polymerase (NEB) were pipetted together. The reaction mixture was subjected to the following thermocycler program: 98 °C -> 3 min; 30 x (95 °C -> 0:45 min; 64 °C -> 0:30 min; 72 °C -> 7 min); 72 °C -> 8 min. Success of the PCR was confirmed on a preparative 1% (w/v) agarose gel via fluorescence detection after ethidium bromide staining. Gel bands were extracted using a gel extraction kit (Omega Bio-tek, Cat.-No.: 2500-01). 3 µL CutSmart® buffer (NEB) and 3 µL of DpnI (NEB) were added to 30 µL of extracted DNA and incubated for 1 h at 37 °C. 10 µL of the reaction solution were used for transformation into chemically competent *E. coli* BL21(DE3). GATC lightrun service (GATC Biotech) was used to confirm sequence conformity using T7 forward primer (TAATACGACTCACTATAGGG). Overexpression and purification of PhoBD53N were performed as described above.

### 5.1.3 *In vitro* phosphorylation and phosphoaspartate conversion of PhoB

A single-use aliquot of PhoB was carefully thawed on ice and reaction buffer (20 mM HEPES, pH 7.0; 0.1 mM DTT) was added to a final volume of 97 µL. Phosphorylation was started by addition of 1 µL of 1 M MgCl<sub>2</sub> and 2 µL of 1 M Li/K acetyl phosphate (Sigma, Cat.-No.: 01409). The reaction mixture was incubated at 37 °C without shaking. In the meantime gel filtration spin columns (Micro Bio-Spin™ 6 Columns, bio-rad, Cat.-No.: 732-6221) were equilibrated 4 times with 500 µL reaction buffer by centrifugation at 1000 g for 1 min at 4 °C. Acetyl phosphate was removed from the sample by adding the sample to the spin columns and centrifugation at 1000 g for 4 min at 4 °C. A small volume was taken from the sample, diluted 1:5 with reaction buffer and subjected to intact protein mass spectrometry to assess the degree of phosphorylation. The remaining sample was immediately further processed to minimize loss of phosphorylation. Nucleophile solutions were freshly prepared from hydrochloric salts (hydroxylamine hydrochloride: Sigma, Cat.-No.: 25-558-0; **HA-yne**: in house synthesis). 10% (v/v) of 5 M nucleophile or ddH<sub>2</sub>O as a control were added to the sample and the conversion reaction was let to proceed at room temperature for 1 h. The sample was subjected to intact protein mass spectrometry after dilution 1:5 with reaction buffer. For time-course experiments, samples were taken and diluted at every indicated time point and immediately measured. Time-resolved experiments were conducted in triplicates.

#### 5.1.4 Intact protein mass spectrometry

Measurements were conducted on a Thermo LTQ-FT Ultra mass spectrometer with electrospray ionization source (spray voltage 4.0 kV, tube lens 110 V, capillary voltage 48 V, sheath gas 60 arb, aux gas 10 arb, sweep gas 0.2 arb). Samples were on-line desalted on a Dionex Ultimate 3000 HPLC system equipped with a Massprep desalting cartridge (Waters). 3  $\mu\text{L}$  of 1:5 diluted reaction mixture were injected per measurement. The mass spectrometer was operated in positive ion mode and collected full scans at resolution  $R = 200,000$  from  $m/z$  600 to  $m/z$  2000. Spectra were deconvoluted with the help of Thermo Xcalibur Xtract.

#### 5.1.5 Phosphoaspartate conversion in PhoB in complex proteomic background

PhoB was carefully thawed on ice and phosphorylated for 90 min as described above. Success of the phosphorylation was confirmed by intact protein mass spectrometry. 15.6  $\mu\text{L}$  ( $\pm 5 \mu\text{g}$ ) of the phosphorylated PhoB solution were spiked into 144  $\mu\text{L}$  of soluble *B. subtilis* proteome (690 ng/ $\mu\text{L}$ ;  $\pm 100 \mu\text{g}$  of proteome). The mixture was immediately treated with 10% (v/v) freshly prepared 5M  $\text{NH}_2\text{OH}\cdot\text{HCl}$  in  $\text{ddH}_2\text{O}$  or  $\text{ddH}_2\text{O}$  as control and the reaction was let to proceed for 1 h at room rt. Subsequently, proteins were precipitated using the protocol by Wessel and Flügge.<sup>155</sup> From this point on all solvents were LC-MS grade. 600  $\mu\text{L}$  MeOH were added to 160  $\mu\text{L}$  protein mixture shortly vortexed and spun down. Then 225  $\mu\text{L}$   $\text{CHCl}_3$  were added, shortly vortexed and spun down. Next 450  $\mu\text{L}$   $\text{H}_2\text{O}$  were added, the mixture was agitated in a sonication bath for 7 min and then spun down. The upper layer was carefully removed and 450  $\mu\text{L}$  MeOH were added, the mixture shortly vortexed and spun down at 13000 rpm for 20 min. The supernatant was removed and the protein pellet was dried on air. Dried pellets were resuspended in 100  $\mu\text{L}$  50 mM Tris/HCl, pH 7.5 and the proteins were reduced (2  $\mu\text{L}$  50 mM DTT, 45 min, 450 rpm, rt) and alkylated (1  $\mu\text{L}$  550 mM iodoacetamide, 30 min, 450 rpm, rt). The reaction was quenched by addition of 12  $\mu\text{L}$  50 mM DTT for 30 min at 450 rpm at rt. Proteins were digested by addition of 2  $\mu\text{L}$  sequencing grade trypsin (0.5  $\mu\text{g}/\mu\text{L}$ , Promega) for 2 h at 450 rpm at 37 °C and subsequent addition of 4  $\mu\text{L}$  sequencing grade AspN (0.16  $\mu\text{g}/\mu\text{L}$ , Promega) over night at 450 rpm at 37 °C. The next day the samples were desalted on custom build stage tips. Two layers of Empore™ C18 material (3M) were packed in a 200  $\mu\text{L}$  pipette tip. The stage tip was activated with 70  $\mu\text{L}$  MeOH, washed with 70  $\mu\text{L}$  elution buffer (80% (v/v) ACN; 0.5% (v/v) formic acid) and washed with three times 70  $\mu\text{L}$  0.5% (v/v) formic acid. Samples was acidified to pH 2-3 with formic acid and loaded on the stage tip. After three washing steps with 70  $\mu\text{L}$  0.5% formic acid, peptides were eluted with two times 30  $\mu\text{L}$  elution buffer. The peptides were lyophilized over night and resuspended in 30  $\mu\text{L}$  1% (v/v) formic acid. Prior to measurement the sample was filtered through a 0.22  $\mu\text{m}$  PVDF filter (Millipore). 15  $\mu\text{L}$  of sample were analyzed LC-MS/MS on a LTQ Orbitrap XL mass spectrometer (Thermo) equipped with an electron spray ionization source. Samples on-line separated on an Ultimate

## HYDROXYLAMINE-BASED REVERSE POLARITY ABPP

3000 nano HPLC system (Dionex). The peptides were loaded on an Acclaim C18 PepMap100 trap column (75  $\mu\text{m}$  ID x 2 cm) for 7 min at 5  $\mu\text{l}/\text{min}$  in 0.1% (v/v) formic acid. Separation was performed on an Acclaim C18 PepMap RSLC (75  $\mu\text{m}$  ID x 15 cm) separation column with a gradient from 4% eluent B to 35% eluent B over 105 min at 200  $\text{nl}/\text{min}$  (eluent A: 0.1% (v/v) formic acid; 5% (v/v) DMSO in  $\text{H}_2\text{O}$ ; eluent B: 0.1% (v/v) formic acid; 5% (v/v) DMSO in ACN). The mass spectrometer was operated in positive ion mode and collected scans in data dependency. Full scans were acquired in Orbitrap mass analyzer at  $R = 60000$  from  $m/z = 350 - 1400$ . The five most intense peaks were selected for collision induced fragmentation (CID) and analyzed in the ion trap at normal scan rate (isolation width: 2  $m/z$ ; activation time: 30 ms; normalized collision energy: 35; minimum signal threshold: 1000 counts; dynamic exclusion duration: 120 s; exclusion of precursors with charge state  $< 2$ ). The recorded data were analyzed with MaxQuant 1.5.3.8. Data were searched on batch processing mode and the following settings were applied: variable modifications: oxidation (methionine); *N*4-hydroxyasparagine (aspartate) or phosphorylation (aspartate); fixed modification: carbamidomethyl (cysteine); enzyme: trypsin/P and AspN. All other settings were kept at default. The data were searched against a custom Uniprot *B. subtilis* strain 168 database including *E. coli* K12 PhoB sequence. Spiking experiments were carried out in triplicates.

### 5.2. rp-ABPP method development on analytical scale

To develop an rp-ABPP workflow, labeling was performed in exponentially growing *B. subtilis* on analytical scale. The following sections gives the basic principles of the labeling workflow, details were varied as described in section 3.2.

*B. subtilis* was grown to stationary phase in LB medium over night at 37  $^{\circ}\text{C}$  while shaking at 200 rpm. 50 mL day cultures were inoculated 1:100 with over night cultures. The cultures were grown at 37  $^{\circ}\text{C}$  while shaking at 200 rpm till they reached an  $\text{OD}_{600} = 0.5-0.6$ . Per condition to be tested, a volume equivalent to an  $\text{OD}_{600} = 4$  was harvested by centrifugation at 6000 g at 4  $^{\circ}\text{C}$  for 10 min and resuspended in ice-cold PBS at an  $\text{OD}_{600} = 4$ . The cells were aliquoted per condition to be tested into new 1.5 mL reaction tubes and pelleted again. Cells were resuspended in 100  $\mu\text{L}$  of the appropriate lysis buffer (basis: 20 mM HEPES pH 7.0; nucleophilic probe **HA-yne** was prepared freshly as 5 M solution and added to the buffer; pH was carefully titrated to the desired values). Cells were lysed by sonication (3 x 15 s; 80% int.) with cooling on ice. Insoluble fraction was pelleted by centrifugation at 21100 g at 4  $^{\circ}\text{C}$  for 30 min. The insoluble fraction was washed twice with PBS and stored at -20  $^{\circ}\text{C}$  until further processing. Meanwhile the soluble fraction was precipitated to remove excess probe by addition of 4-fold excess of acetone (-80 $^{\circ}\text{C}$ ) and incubation over night at -20  $^{\circ}\text{C}$ . The following day, the precipitate was pelletized by centrifugation at 9000 g at 4  $^{\circ}\text{C}$  for 10 min and washed twice in 100  $\mu\text{L}$  MeOH (-80  $^{\circ}\text{C}$ ). For the washing steps the pellets were resuspended by

sonication (10 s; 10% int.). Soluble and insoluble fraction were then both resuspended in 100  $\mu$ L 0.8% (w/v) SDS in PBS and 88  $\mu$ L of the solution were subjected to click chemistry (2  $\mu$ L rhodamine-azide (5 mM in DMSO); 2  $\mu$ L TCEP (52 mM in ddH<sub>2</sub>O); 6  $\mu$ L TBTA ligand (1.667 mM in 80/20 *t*-BuOH/DMSO). The click reaction mixture was shortly vortexed and spun down, click chemistry was started by addition of 2  $\mu$ L CuSO<sub>4</sub> (50mM in ddH<sub>2</sub>O). The click reaction was incubated for 1 h at rt in the dark. Click reaction was stopped by addition of 100  $\mu$ L sample loading buffer (63 mM Tris/HCl; 10% (v/v) glycerin; 2% (w/v) SDS; 0.0025% (w/v) bromophenol blue; 5% (v/v)  $\beta$ -mercaptoethanol) and the protein mixture was separated on a 12.5% SDS-polyacrylamide gel. Labeled protein bands were visualized by in-gel fluorescence scanning (Fujifilm LAS-4000 with Fujinon VRF43LMD3 lens and 575DF20 filter). Loading of the gel was controlled by staining with brilliant blue R250 solution.

## 5.3 Gel-free target identification

### 5.3.1 Labeling in exponentially growing *B. subtilis*

20 mL *B. subtilis* strain 168 over night cultures were grown to stationary phase in LB media at 37 °C while shaking at 200 rpm. 250 mL LB media day cultures were inoculated 1:100 and grown in 1 L non-baffled flasks at 37 °C while shaking at 200 rpm until they reached OD<sub>600</sub> = 0.5-0.6. Cells were harvested by centrifugation at 6000 rpm at 4 °C for 10 min. Cells were washed once with ice-cold PBS (centrifugation at 6000 g at 4 °C for 10 min) and subsequently resuspended in PBS at OD<sub>600</sub> = 40 and transferred to new 1.5 mL reaction tubes. Cells were pelletized again by centrifugation at 6000 g at 4 °C for 10 min. The cell pellets were resuspended in 1 mL of the appropriate lysis buffer with or without nucleophilic probe (basis: 20 mM HEPES pH 7.0; 1% (w/v) LDAO; nucleophilic probe **HA-yne** was prepared freshly as 5 M solution and added to the buffer; pH of nucleophile containing buffer was carefully adjusted to pH 4). Control and probe treated samples were always treated separately until LC-MS/MS measurement. Cells were immediately lysed by sonication (4 x 15 s; 80% int.) under cooling on ice. Next cell debris was pelletized by centrifugation at 21100 g at 4 °C for 30 min. The insoluble fraction was washed twice with PBS and stored at -20 °C until further processing. Meanwhile, the soluble fraction was precipitated to remove excess probe by addition of 4-fold excess of acetone (-80°C) and incubation over night at -20 °C. The following day the precipitate was pelletized by centrifugation at 9000 g at 4 °C for 10 min and washed twice in 1 mL MeOH (-80 °C). For the washing steps the pellets were resuspended by sonication (10 s; 10% int.). Soluble and insoluble fraction were then reunified in 1 mL 0.8% (w/v) SDS in PBS and 800  $\mu$ L of the solution were subjected to preparative click chemistry (20  $\mu$ L biotin-PEG3-azide (10 mM in DMSO); 10  $\mu$ L TCEP (52 mM in ddH<sub>2</sub>O); 30  $\mu$ L TBTA ligand (1.667 mM in 80/20 *t*-BuOH/DMSO). The click reaction mixture was shortly vortexed and spun down, click chemistry was started by addition of 10  $\mu$ L CuSO<sub>4</sub> (50mM in ddH<sub>2</sub>O). The click reaction was incubated

## HYDROXYLAMINE-BASED REVERSE POLARITY ABPP

for 1 h at rt in the dark. From this point on all solvents used were LC-MS grade. Click reaction was stopped by addition of 4-fold excess of acetone (-80°C) and precipitation of proteins over night at -20 °C. The following day, the precipitate was pelletized by centrifugation at 9000 g at 4 °C for 10 min and washed twice in 1 mL MeOH (-80 °C). For the washing steps the pellets were resuspended by sonication (10 s; 10% int.). Proteins were resuspended in 500 µL 0.4% SDS in PBS (pH 7.4). 50 µL avidin-agarose beads slurry were prepared by washing thrice with 1 mL 0.4% SDS in PBS (pH 7.4). Avidin agarose beads were always centrifuged at 400 g for 2 min at rt. Samples were added to the prepared beads and incubated under constant head-over-end inversion at rt for 1 h. The beads were then sedimented and the supernatant was removed. After that, the beads were washed thrice with 1 mL 0.4% SDS in PBS (pH 7.4), twice with 1 mL 6M urea and thrice with 1 mL PBS (pH 7.4). Subsequently, the beads were taken up in 200 µL digestion buffer (7 M urea, 2M thiourea in 20 mM HEPES, pH 7.5). Proteins were on-bead reduced (0.2 µL 1M DTT; 45 min; 37 °C; shaking at 850 rpm) and alkylated (2 µL 550 mM iodoacetamide; 30 min; rt; shaking at 850 rpm in the dark). The alkylation reaction was quenched with 0.8 µL 1 M DTT (30 min; rt; shaking at 850 rpm). Proteins were predigested with 1 µL LysC (Wako) for 2 h at rt while shaking at 450 rpm. 600 µL 50 mM TEAB (triethylammonium bicarbonate buffer, Sigma) were added prior to addition of 1.5 µL sequencing grade trypsin (0.5 µg/µL, Promega). Digestion was performed at 37 °C and shaking at 450 rpm over night. Digestion was quenched the following day by addition of 20 µL of formic acid (final pH ≤ 3). The beads were sedimented and the supernatant was desalted on 50 mg SepPak cartridges (Waters) using a vacuum manifold. Cartridges were activated with 1 mL ACN and washed with 1 mL elution buffer (80% (v/v) ACN; 0.5% (v/v) formic acid) and thrice with 1 mL 0.5% (v/v) formic acid. Samples were loaded slowly by gravity flow and the cartridges were washed five times with 1 mL 0.5% (v/v) formic acid. Peptides were eluted from the cartridges with two times 250 µL elution buffer. The eluate was lyophilized over night. Prior to measurement the peptides were resuspended in 30 µL 1% (v/v) formic acid and filtered through a 0.22 µm PVDF filter (Millipore). 2.5 µL were injected for measurement. All experiments were conducted twice in three biological replicates.

### 5.3.2 Labeling in dynorphin-treated *P. aeruginosa*

10 mL *P. aeruginosa* PAO1 over night cultures were grown in LB media at 37 °C while shaking at 200 rpm. 100 mL day cultures were grown in MOPS2 medium (50 mM MOPS, pH 7.2; 20 mM sodium succinate; 20 mM NH<sub>4</sub>Cl; 1 mM MgSO<sub>4</sub>; 10 mM KCl; 4 mM K<sub>2</sub>HPO<sub>4</sub>; 3.5 µM FeSO<sub>4</sub>). Cultures were inoculated 1:100 with over night cultures and grown in non-baffled flasks at 37 °C under constant shaking at 200 rpm until OD<sub>600</sub> = 0.8 - 1. From such a culture a volume equivalent to an OD<sub>600</sub> of 80 was harvested by centrifugation at 6000 g at 4 °C for 10 min and washed once in PBS. Bacteria were resuspended in 80 mL PBS (resulting in OD<sub>600</sub>

= 1) and split into two times 40 mL and given into two new 100 mL culture flasks. The cells were treated with 10  $\mu$ M dynorphin A (amino acids 1-17; f. c. DMSO: 0.2% (v/v); Proteogenix) or DMSO as a control for 30 min at 37 °C while shaking at 200 rpm.<sup>127</sup> After treatment the cells were harvested by centrifugation at 6000 g at 4 °C for 10 min. Bacteria were resuspended in 1 mL PBS and the samples were split again into two new 1.5 mL reaction tubes. One sample was designated to control treatment the other to labeling with **HA-yne**. The cells were pelletized again and then resuspended in 500  $\mu$ L of the designated lysis buffer (labeling: 20 mM HEPES pH 7.0; 1% (w/v) LDAO; + 2.5% (v/v) 5 M **HA-yne** pH adjusted to pH 4; control: 20 mM HEPES pH 7.0; 1% (w/v) LDAO). Cells were immediately lysed by sonication (4 x 15 s; 80% int.) and cell debris was pelletized by centrifugation at 10000 g at 4 °C for 30 min. From this point on the samples were processed as described in section 5.3.1 Except that samples were normalized a second time by BCA assay prior to enrichment on avidin agarose beads. For MS analysis samples were taken up in 25  $\mu$ L 1% (v/v) formic acid and 5  $\mu$ L were injected.

### 5.3.3 Label free quantification LC-MS/MS and data evaluation

Samples were analyzed by label free quantification on a Q Exactive Plus (Thermo Fisher) equipped with an EASY-spray source and coupled to Ultimate 3000 nano HPLC system (Dionex) for on-line liquid chromatograph. Peptides were loaded on an Acclaim C18 PepMap100 75  $\mu$ m ID x 2 cm trap column with 0.1% (v/v) TFA at a flow of 5  $\mu$ L/min. Samples were separated on an Acclaim Pepmap RSLC C18 (75  $\mu$ m ID x 50 cm) separation column over a gradient from 5% eluent B to 22% eluent B over 105 min and from 22% eluent B to 32% eluent B over 10 min at a flow of 300 nL/min (eluent A: 0.1% (v/v) formic acid in H<sub>2</sub>O; eluent B: 0.1% (v/v) formic acid in ACN). The mass spectrometer was operated in positive ion mode and collected scans in data dependency. Full scans were acquired in the Orbitrap mass analyzer (R: 70000; m/z: 300 - 1500; AGC target: 3 x 10<sup>6</sup>; maximum injection time: 80 ms). The 12 most intense precursors were selected for fragmentation by higher-energy collisional dissociation (HCD) and detection in the Orbitrap mass analyzer (isolation width: 1.6 m/z; normalized collision energy: 27; AGC target: 5 x 10<sup>4</sup>; minimum AGC target: 5 x 10<sup>3</sup>; R: 17500 dynamic exclusion duration: 60 s; isotope exclusion: on; exclusion of precursors with charge state < 2). Spectra were analyzed by MaxQuant 1.5.3.8 software, using a label-free quantification algorithm.<sup>156</sup> Data were searched against the respective databases (*B. subtilis* strain 168 or *P. aeruginosa* PAO1). The following settings were applied: variable modifications: oxidation (methionine), acetyl (protein N-terminal); fixed modification: carbamidomethyl (cysteine); enzyme: trypsin/P; LFQ min. ratio count: 1; min. ratio count: 1; match between runs: true. All other settings were kept at default. Collected data was further evaluated using Perseus 1.5.3.2.<sup>157</sup> Reverse identifications, contaminants and hits identified by site only were excluded from further processing. LFQ intensities were logarithmized and missing values were imputed

## HYDROXYLAMINE-BASED REVERSE POLARITY ABPP

from normal distribution (width = 0.3; down shift = 1.8). Statistical evaluation was performed using the volcano plot function applying a Student's t-test (both sided; number of randomization = 250; FDR = 0.05). GO-term analysis was performed using the geneontology.org web-based application.<sup>158</sup>

## BIBLIOGRAPHY

1. G20 Germany 2017, G20 Leaders' declaration - Shaping an interconnected World. **2017**.
2. Fleming, A., On the antibacterial actions of cultures of a penicillium with special reference to their use in the isolation of *B. influenzae*. *Brit J Exp Path* **1929**, *10*, 226-236.
3. Chambers, H. F.; Deleo, F. R., Waves of resistance: *Staphylococcus aureus* in the antibiotic era. *Nat Rev Microbiol* **2009**, *7* (9), 629-41.
4. Abraham, E. P.; Chain, E., An enzyme from bacteria able to destroy penicillin. *Nature* **1940**, *146*, 837.
5. Abraham, E. P.; Chain, E.; Fletcher, C. M.; Gardner E. D.; Heatley, N. G.; Jennings, M. A., Further observations on penicillin. *Lancet* **1941**, *238* (6155), 177.
6. Kirby, W. M., Extraction of a Highly Potent Penicillin Inactivator from Penicillin Resistant *Staphylococci*. *Science* **1944**, *99* (2579), 452-3.
7. Barber, M.; Rozwadowska-Dowzenko, M., Infection by penicillin-resistant staphylococci. *Lancet* **1948**, *2* (6530), 641-4.
8. Larson, E., Community factors in the development of antibiotic resistance. *Annu Rev Public Health* **2007**, *28*, 435-447.
9. OECD; WHO; FAO; OIE, Tackling antimicrobial resistance ensuring sustainable R&D. **2017**.
10. Alanis, A. J., Resistance to antibiotics: are we in the post-antibiotic era? *Arch Med Res* **2005**, *36* (6), 697-705.
11. The Review on Antimicrobial Resistance, Antimicrobial resistance: Tackling a crisis for the health and wealth of nations. **2014**.
12. Kluytmans, J.; van Belkum, A.; Verbrugh, H., Nasal carriage of *Staphylococcus aureus*: epidemiology, underlying mechanisms, and associated risks. *Clin Microbiol Rev* **1997**, *10* (3), 505-20.
13. Diekema, D. J.; Pfaller, M. A.; Schmitz, F. J.; Smayevsky, J.; Bell, J.; Jones, R. N.; Beach, M.; Group, S. P., Survey of infections due to *Staphylococcus* species: frequency of occurrence and antimicrobial susceptibility of isolates collected in the United States, Canada, Latin America, Europe, and the Western Pacific region for the SENTRY Antimicrobial Surveillance Program, 1997-1999. *Clin Infect Dis* **2001**, *32* Suppl 2, S114-32.
14. Czaplewski, L.; Bax, R.; Clokie, M.; Dawson, M.; Fairhead, H.; Fischetti, V. A.; Foster, S.; Gilmore, B. F.; Hancock, R. E.; Harper, D.; Henderson, I. R.; Hilpert, K.; Jones, B. V.; Kadioglu, A.; Knowles, D.; Olafsdottir, S.; Payne, D.; Projan, S.; Shaunak, S.; Silverman, J.; Thomas, C. M.; Trust, T. J.; Warn, P.; Rex, J. H., Alternatives to antibiotics—a pipeline portfolio review. *Lancet Infect Dis* **2016**, *16* (2), 239-51.
15. Dickey, S. W.; Cheung, G. Y. C.; Otto, M., Different drugs for bad bugs: antivirulence strategies in the age of antibiotic resistance. *Nat Rev Drug Discov* **2017**, *16* (7), 457-471.
16. Rasko, D. A.; Sperandio, V., Anti-virulence strategies to combat bacteria-mediated disease. *Nat Rev Drug Discov* **2010**, *9* (2), 117-28.

## BIBLIOGRAPHY

17. Clatworthy, A. E.; Pierson, E.; Hung, D. T., Targeting virulence: a new paradigm for antimicrobial therapy. *Nat Chem Biol* **2007**, *3* (9), 541-548.
18. Walsh, C. T.; Garneau-Tsodikova, S.; Gatto, G. J., Jr., Protein posttranslational modifications: the chemistry of proteome diversifications. *Angew Chem Int Ed Engl* **2005**, *44* (45), 7342-72.
19. Gottesman, S., Regulation by proteolysis: developmental switches. *Curr Opin Microbiol* **1999**, *2* (2), 142-7.
20. Wickner, S.; Maurizi, M. R.; Gottesman, S., Posttranslational quality control: folding, refolding, and degrading proteins. *Science* **1999**, *286* (5446), 1888-93.
21. Katayama-Fujimura, Y.; Gottesman, S.; Maurizi, M. R., A multiple-component, ATP-dependent protease from *Escherichia coli*. *J Biol Chem* **1987**, *262* (10), 4477-85.
22. Hwang, B. J.; Park, W. J.; Chung, C. H.; Goldberg, A. L., *Escherichia coli* contains a soluble ATP-dependent protease (Ti) distinct from protease La. *Proc Natl Acad Sci U S A* **1987**, *84* (16), 5550-4.
23. Katayama, Y.; Gottesman, S.; Pumphrey, J.; Rudikoff, S.; Clark, W. P.; Maurizi, M. R., The two-component, ATP-dependent Clp protease of *Escherichia coli*. Purification, cloning, and mutational analysis of the ATP-binding component. *J Biol Chem* **1988**, *263* (29), 15226-36.
24. Maurizi, M. R.; Clark, W. P.; Katayama, Y.; Rudikoff, S.; Pumphrey, J.; Bowers, B.; Gottesman, S., Sequence and structure of Clp P, the proteolytic component of the ATP-dependent Clp protease of *Escherichia coli*. *J Biol Chem* **1990**, *265* (21), 12536-45.
25. Maurizi, M. R.; Clark, W. P.; Kim, S. H.; Gottesman, S., Clp P represents a unique family of serine proteases. *J Biol Chem* **1990**, *265* (21), 12546-52.
26. Wickner, S.; Gottesman, S.; Skowyra, D.; Hoskins, J.; McKenney, K.; Maurizi, M. R., A molecular chaperone, ClpA, functions like DnaK and DnaJ. *Proc Natl Acad Sci U S A* **1994**, *91* (25), 12218-22.
27. Gottesman, S.; Clark, W. P.; de Crecy-Lagard, V.; Maurizi, M. R., ClpX, an alternative subunit for the ATP-dependent Clp protease of *Escherichia coli*. Sequence and in vivo activities. *J Biol Chem* **1993**, *268* (30), 22618-26.
28. Baker, T. A.; Sauer, R. T., ClpXP, an ATP-powered unfolding and protein-degradation machine. *Biochim Biophys Acta* **2012**, *1823* (1), 15-28.
29. Kim, Y. I.; Levchenko, I.; Fraczkowska, K.; Woodruff, R. V.; Sauer, R. T.; Baker, T. A., Molecular determinants of complex formation between Clp/Hsp100 ATPases and the ClpP peptidase. *Nat Struct Biol* **2001**, *8* (3), 230-3.
30. Yu, A. Y.; Houry, W. A., ClpP: a distinctive family of cylindrical energy-dependent serine proteases. *FEBS Lett* **2007**, *581* (19), 3749-57.
31. Bross, P.; Andresen, B. S.; Knudsen, I.; Kruse, T. A.; Gregersen, N., Human ClpP protease: cDNA sequence, tissue-specific expression and chromosomal assignment of the gene. *FEBS Lett* **1995**, *377* (2), 249-52.
32. Kang, S. G.; Ortega, J.; Singh, S. K.; Wang, N.; Huang, N. N.; Steven, A. C.; Maurizi, M. R., Functional proteolytic complexes of the human mitochondrial ATP-dependent protease, hClpXP. *J Biol Chem* **2002**, *277* (23), 21095-102.
33. Frees, D.; Qazi, S. N.; Hill, P. J.; Ingmer, H., Alternative roles of ClpX and ClpP in *Staphylococcus aureus* stress tolerance and virulence. *Mol Microbiol* **2003**, *48* (6), 1565-78.

34. Frees, D.; Sorensen, K.; Ingmer, H., Global virulence regulation in *Staphylococcus aureus*: pinpointing the roles of ClpP and ClpX in the sar/agr regulatory network. *Infect Immun* **2005**, *73* (12), 8100-8.
35. Pederson, K. J.; Carlson, S.; Pierson, D. E., The ClpP protein, a subunit of the Clp protease, modulates ail gene expression in *Yersinia enterocolitica*. *Mol Microbiol* **1997**, *26* (1), 99-107.
36. Webb, C.; Moreno, M.; Wilmes-Riesenberg, M.; Curtiss, R., 3rd; Foster, J. W., Effects of DksA and ClpP protease on sigma S production and virulence in *Salmonella typhimurium*. *Mol Microbiol* **1999**, *34* (1), 112-23.
37. Gaillot, O.; Pellegrini, E.; Bregenholt, S.; Nair, S.; Berche, P., The ClpP serine protease is essential for the intracellular parasitism and virulence of *Listeria monocytogenes*. *Mol Microbiol* **2000**, *35* (6), 1286-94.
38. Geiger, S. R.; Bottcher, T.; Sieber, S. A.; Cramer, P., A conformational switch underlies ClpP protease function. *Angew Chem Int Ed Engl* **2011**, *50* (25), 5749-52.
39. Gersch, M.; List, A.; Groll, M.; Sieber, S. A., Insights into structural network responsible for oligomerization and activity of bacterial virulence regulator caseinolytic protease P (ClpP) protein. *J Biol Chem* **2012**, *287* (12), 9484-94.
40. Gribun, A.; Kimber, M. S.; Ching, R.; Sprangers, R.; Fiebig, K. M.; Houry, W. A., The ClpP double ring tetradecameric protease exhibits plastic ring-ring interactions, and the N termini of its subunits form flexible loops that are essential for ClpXP and ClpAP complex formation. *J Biol Chem* **2005**, *280* (16), 16185-96.
41. Zhang, J.; Ye, F.; Lan, L.; Jiang, H.; Luo, C.; Yang, C. G., Structural switching of *Staphylococcus aureus* Clp protease: a key to understanding protease dynamics. *J Biol Chem* **2011**, *286* (43), 37590-601.
42. Hedstrom, L., Serine protease mechanism and specificity. *Chem Rev* **2002**, *102* (12), 4501-24.
43. Ye, F.; Zhang, J.; Liu, H.; Hilgenfeld, R.; Zhang, R.; Kong, X.; Li, L.; Lu, J.; Zhang, X.; Li, D.; Jiang, H.; Yang, C. G.; Luo, C., Helix unfolding/refolding characterizes the functional dynamics of *Staphylococcus aureus* Clp protease. *J Biol Chem* **2013**, *288* (24), 17643-53.
44. Sprangers, R.; Gribun, A.; Hwang, P. M.; Houry, W. A.; Kay, L. E., Quantitative NMR spectroscopy of supramolecular complexes: dynamic side pores in ClpP are important for product release. *Proc Natl Acad Sci U S A* **2005**, *102* (46), 16678-83.
45. Woo, K. M.; Chung, W. J.; Ha, D. B.; Goldberg, A. L.; Chung, C. H., Protease Tl from *Escherichia coli* requires ATP hydrolysis for protein breakdown but not for hydrolysis of small peptides. *J Biol Chem* **1989**, *264* (4), 2088-91.
46. Thompson, M. W.; Singh, S. K.; Maurizi, M. R., Processive degradation of proteins by the ATP-dependent Clp protease from *Escherichia coli*. Requirement for the multiple array of active sites in ClpP but not ATP hydrolysis. *J Biol Chem* **1994**, *269* (27), 18209-15.
47. Glynn, S. E.; Martin, A.; Nager, A. R.; Baker, T. A.; Sauer, R. T., Structures of asymmetric ClpX hexamers reveal nucleotide-dependent motions in a AAA+ protein-unfolding machine. *Cell* **2009**, *139* (4), 744-56.
48. Wojtyra, U. A.; Thibault, G.; Tuite, A.; Houry, W. A., The N-terminal zinc binding domain of ClpX is a dimerization domain that modulates the chaperone function. *J Biol Chem* **2003**, *278* (49), 48981-90.

## BIBLIOGRAPHY

49. Singh, S. K.; Rozycki, J.; Ortega, J.; Ishikawa, T.; Lo, J.; Steven, A. C.; Maurizi, M. R., Functional domains of the ClpA and ClpX molecular chaperones identified by limited proteolysis and deletion analysis. *J Biol Chem* **2001**, *276* (31), 29420-9.
50. Flynn, J. M.; Neher, S. B.; Kim, Y. I.; Sauer, R. T.; Baker, T. A., Proteomic discovery of cellular substrates of the ClpXP protease reveals five classes of ClpX-recognition signals. *Mol Cell* **2003**, *11* (3), 671-83.
51. Laachouch, J. E.; Desmet, L.; Geuskens, V.; Grimaud, R.; Toussaint, A., Bacteriophage Mu repressor as a target for the Escherichia coli ATP-dependent Clp Protease. *EMBO J* **1996**, *15* (2), 437-44.
52. Gottesman, S.; Roche, E.; Zhou, Y.; Sauer, R. T., The ClpXP and ClpAP proteases degrade proteins with carboxy-terminal peptide tails added by the SsrA-tagging system. *Genes Dev* **1998**, *12* (9), 1338-47.
53. Moore, S. D.; Sauer, R. T., The tmRNA system for translational surveillance and ribosome rescue. *Annu Rev Biochem* **2007**, *76*, 101-24.
54. Lee, C.; Schwartz, M. P.; Prakash, S.; Iwakura, M.; Matouschek, A., ATP-dependent proteases degrade their substrates by processively unraveling them from the degradation signal. *Mol Cell* **2001**, *7* (3), 627-37.
55. Kenniston, J. A.; Baker, T. A.; Fernandez, J. M.; Sauer, R. T., Linkage between ATP consumption and mechanical unfolding during the protein processing reactions of an AAA+ degradation machine. *Cell* **2003**, *114* (4), 511-20.
56. Aubin-Tam, M. E.; Olivares, A. O.; Sauer, R. T.; Baker, T. A.; Lang, M. J., Single-molecule protein unfolding and translocation by an ATP-fueled proteolytic machine. *Cell* **2011**, *145* (2), 257-67.
57. Grimaud, R.; Kessel, M.; Beuron, F.; Steven, A. C.; Maurizi, M. R., Enzymatic and structural similarities between the Escherichia coli ATP-dependent proteases, ClpXP and ClpAP. *J Biol Chem* **1998**, *273* (20), 12476-81.
58. Effantin, G.; Ishikawa, T.; De Donatis, G. M.; Maurizi, M. R.; Steven, A. C., Local and global mobility in the ClpA AAA+ chaperone detected by cryo-electron microscopy: functional connotations. *Structure* **2010**, *18* (5), 553-62.
59. Gersch, M.; Famulla, K.; Dahmen, M.; Gobl, C.; Malik, I.; Richter, K.; Korotkov, V. S.; Sass, P.; Rubsam-Schaeff, H.; Madl, T.; Brotz-Oesterhelt, H.; Sieber, S. A., AAA+ chaperones and acyldepsipeptides activate the ClpP protease via conformational control. *Nat Commun* **2015**, *6*, 6320.
60. Brandstetter, H.; Kim, J. S.; Groll, M.; Huber, R., Crystal structure of the tricorn protease reveals a protein disassembly line. *Nature* **2001**, *414* (6862), 466-70.
61. Otto, H. H.; Schirmeister, T., Cysteine Proteases and Their Inhibitors. *Chem Rev* **1997**, *97* (1), 133-172.
62. Szyk, A.; Maurizi, M. R., Crystal structure at 1.9Å of E. coli ClpP with a peptide covalently bound at the active site. *J Struct Biol* **2006**, *156* (1), 165-74.
63. Böttcher, T.; Sieber, S. A., Beta-lactones as privileged structures for the active-site labeling of versatile bacterial enzyme classes. *Angew Chem Int Ed Engl* **2008**, *47* (24), 4600-3.
64. Böttcher, T.; Sieber, S. A., Beta-lactones as specific inhibitors of ClpP attenuate the production of extracellular virulence factors of Staphylococcus aureus. *J Am Chem Soc* **2008**, *130* (44), 14400-1.

65. Böttcher, T.; Sieber, S. A., Structurally refined beta-lactones as potent inhibitors of devastating bacterial virulence factors. *Chembiochem* **2009**, *10* (4), 663-6.
66. Weinandy, F.; Lorenz-Baath, K.; Korotkov, V. S.; Böttcher, T.; Sethi, S.; Chakraborty, T.; Sieber, S. A., A beta-lactone-based antivirulence drug ameliorates *Staphylococcus aureus* skin infections in mice. *ChemMedChem* **2014**, *9* (4), 710-3.
67. Rathore, S.; Sinha, D.; Asad, M.; Böttcher, T.; Afrin, F.; Chauhan, V. S.; Gupta, D.; Sieber, S. A.; Mohammed, A., A cyanobacterial serine protease of *Plasmodium falciparum* is targeted to the apicoplast and plays an important role in its growth and development. *Mol Microbiol* **2010**.
68. Cole, A.; Wang, Z.; Coyaud, E.; Voisin, V.; Gronda, M.; Jitkova, Y.; Mattson, R.; Hurren, R.; Babovic, S.; Maclean, N.; Restall, I.; Wang, X.; Jeyaraju, D. V.; Sukhai, M. A.; Prabha, S.; Bashir, S.; Ramakrishnan, A.; Leung, E.; Qia, Y. H.; Zhang, N.; Combes, K. R.; Ketela, T.; Lin, F.; Houry, W. A.; Aman, A.; Al-Awar, R.; Zheng, W.; Wienholds, E.; Xu, C. J.; Dick, J.; Wang, J. C.; Moffat, J.; Minden, M. D.; Eaves, C. J.; Bader, G. D.; Hao, Z.; Kornblau, S. M.; Raught, B.; Schimmer, A. D., Inhibition of the Mitochondrial Protease ClpP as a Therapeutic Strategy for Human Acute Myeloid Leukemia. *Cancer Cell* **2015**, *27* (6), 864-76.
69. Gersch, M.; Gut, F.; Korotkov, V. S.; Lehmann, J.; Böttcher, T.; Rusch, M.; Hedberg, C.; Waldmann, H.; Klebe, G.; Sieber, S. A., The mechanism of caseinolytic protease (ClpP) inhibition. *Angew Chem Int Ed Engl* **2013**, *52* (10), 3009-14.
70. Gersch, M.; Kolb, R.; Alte, F.; Groll, M.; Sieber, S. A., Disruption of oligomerization and dehydroalanine formation as mechanisms for ClpP protease inhibition. *J Am Chem Soc* **2014**, *136* (4), 1360-6.
71. Kolb, R.; Bach, N. C.; Sieber, S. A., beta-Sultams exhibit discrete binding preferences for diverse bacterial enzymes with nucleophilic residues. *Chem Commun (Camb)* **2014**, *50* (4), 427-9.
72. Brötz-Oesterhelt, H.; Beyer, D.; Kroll, H. P.; Endermann, R.; Ladel, C.; Schroeder, W.; Hinzen, B.; Raddatz, S.; Paulsen, H.; Henninger, K.; Bandow, J. E.; Sahl, H. G.; Labischinski, H., Dysregulation of bacterial proteolytic machinery by a new class of antibiotics. *Nat Med* **2005**, *11* (10), 1082-7.
73. Sass, P.; Josten, M.; Famulla, K.; Schiffer, G.; Sahl, H. G.; Hamoen, L.; Brotz-Oesterhelt, H., Antibiotic acyldepsipeptides activate ClpP peptidase to degrade the cell division protein FtsZ. *Proc Natl Acad Sci U S A* **2011**, *108* (42), 17474-9.
74. Lee, B. G.; Park, E. Y.; Lee, K. E.; Jeon, H.; Sung, K. H.; Paulsen, H.; Rubsamen-Schaeff, H.; Brotz-Oesterhelt, H.; Song, H. K., Structures of ClpP in complex with acyldepsipeptide antibiotics reveal its activation mechanism. *Nat Struct Mol Biol* **2010**, *17* (4), 471-8.
75. Carney, D. W.; Compton, C. L.; Schmitz, K. R.; Stevens, J. P.; Sauer, R. T.; Sello, J. K., A Simple Fragment of Cyclic Acyldepsipeptides Is Necessary and Sufficient for ClpP Activation and Antibacterial Activity. *Chembiochem* **2014**, *15* (15), 2216-20.
76. Gominet, M.; Seghezzi, N.; Mazodier, P., Acyl depsipeptide (ADEP) resistance in *Streptomyces*. *Microbiology* **2011**, *157* (Pt 8), 2226-34.
77. Conlon, B. P.; Nakayasu, E. S.; Fleck, L. E.; LaFleur, M. D.; Isabella, V. M.; Coleman, K.; Leonard, S. N.; Smith, R. D.; Adkins, J. N.; Lewis, K., Activated ClpP kills persisters and eradicates a chronic biofilm infection. *Nature* **2013**, *503* (7476), 365-70.
78. Pahl, A.; Lakemeyer, M.; Vielberg, M. T.; Hackl, M. W.; Vomacka, J.; Korotkov, V. S.; Stein, M. L.; Fetzer, C.; Lorenz-Baath, K.; Richter, K.; Waldmann, H.; Groll, M.; Sieber, S. A., Reversible Inhibitors Arrest ClpP in a Defined Conformational State that Can Be Revoked by ClpX Association. *Angew Chem Int Ed Engl* **2015**, *54* (52), 15892-6.

## BIBLIOGRAPHY

79. Jenkinson, E. M.; Rehman, A. U.; Walsh, T.; Clayton-Smith, J.; Lee, K.; Morell, R. J.; Drummond, M. C.; Khan, S. N.; Naeem, M. A.; Rauf, B.; Billington, N.; Schultz, J. M.; Urquhart, J. E.; Lee, M. K.; Berry, A.; Hanley, N. A.; Mehta, S.; Cilliers, D.; Clayton, P. E.; Kingston, H.; Smith, M. J.; Warner, T. T.; University of Washington Center for Mendelian, G.; Black, G. C.; Trump, D.; Davis, J. R.; Ahmad, W.; Leal, S. M.; Riazuddin, S.; King, M. C.; Friedman, T. B.; Newman, W. G., Perrault syndrome is caused by recessive mutations in CLPP, encoding a mitochondrial ATP-dependent chambered protease. *Am J Hum Genet* **2013**, *92* (4), 605-13.
80. Gispert, S.; Parganlija, D.; Klinkenberg, M.; Drose, S.; Wittig, I.; Mittelbronn, M.; Grzmil, P.; Koob, S.; Hamann, A.; Walter, M.; Buchel, F.; Adler, T.; Hrabe de Angelis, M.; Busch, D. H.; Zell, A.; Reichert, A. S.; Brandt, U.; Osiewacz, H. D.; Jendrach, M.; Auburger, G., Loss of mitochondrial peptidase Clpp leads to infertility, hearing loss plus growth retardation via accumulation of CLPX, mtDNA and inflammatory factors. *Hum Mol Genet* **2013**, *22* (24), 4871-87.
81. Dahmen, M.; Vielberg, M. T.; Groll, M.; Sieber, S. A., Structure and Mechanism of the Caseinolytic Protease ClpP1/2 Heterocomplex from *Listeria monocytogenes*. *Angew Chem Int Ed Engl* **2015**, *54* (12), 3598-602.
82. Maglica, Z.; Kolygo, K.; Weber-Ban, E., Optimal efficiency of ClpAP and ClpXP chaperone-proteases is achieved by architectural symmetry. *Structure* **2009**, *17* (4), 508-16.
83. Boersema, P. J.; Raijmakers, R.; Lemeer, S.; Mohammed, S.; Heck, A. J., Multiplex peptide stable isotope dimethyl labeling for quantitative proteomics. *Nat Protoc* **2009**, *4* (4), 484-94.
84. Cox, J.; Mann, M., 1D and 2D annotation enrichment: a statistical method integrating quantitative proteomics with complementary high-throughput data. *BMC Bioinformatics* **2012**, *13 Suppl 16*, S12.
85. Case, D. D., T.; Cheatham, T. I.; Simmerling, C.; Wang, J.; Duke, R.; Luo, R.; Walker, R.; Zhang, W.; Merz, K.; Roberts, B.; Hayik, S.; Roitberg, A.; Seabra, G.; Swails, J.; Götz, A.; Kolossváry, I.; Wong, K.; Paesani, F.; Vanicek, J.; Wolf, R.; Liu, J.; Wu, X.; Brozell, S.; Steinbrecher, T.; Gohlke, H.; Cai, Q.; Ye, X.; Wang, J.; Hsieh, M.-J.; Roe, D.; Mathews, D.; Seetin, M.; Salomon-Ferrer, R.; Sagui, C.; Babin, V.; Luchko, T.; Gusarov, S.; Kovalenko, A.; Kollman, P. *AMBER 12*, University of California, San Francisco, **2012**.
86. Antes, I., DynaDock: A new molecular dynamics-based algorithm for protein-peptide docking including receptor flexibility. *Proteins* **2010**, *78* (5), 1084-104.
87. Oostenbrink, C.; Villa, A.; Mark, A. E.; van Gunsteren, W. F., A biomolecular force field based on the free enthalpy of hydration and solvation: the GROMOS force-field parameter sets 53A5 and 53A6. *J Comput Chem* **2004**, *25* (13), 1656-76.
88. Humphrey, W.; Dalke, A.; Schulten, K., VMD: visual molecular dynamics. *J Mol Graph* **1996**, *14* (1), 33-8, 27-8.
89. Cousins, K. R., Computer review of ChemDraw Ultra 12.0. *J Am Chem Soc* **2011**, *133* (21), 8388.
90. Schuttelkopf, A. W.; van Aalten, D. M., PRODRG: a tool for high-throughput crystallography of protein-ligand complexes. *Acta Crystallogr D Biol Crystallogr* **2004**, *60* (Pt 8), 1355-63.
91. Gallicchio, E.; Levy, R. M., AGBNP: an analytic implicit solvent model suitable for molecular dynamics simulations and high-resolution modeling. *J Comput Chem* **2004**, *25* (4), 479-99.
92. Gallicchio, E.; Paris, K.; Levy, R. M., The AGBNP2 Implicit Solvation Model. *J Chem Theory Comput* **2009**, *5* (9), 2544-2564.

93. Van Gunsteren, W. F.; Berendsen, H. J. C., A Leap-frog Algorithm for Stochastic Dynamics. *Mol Simul* **1988**, *1* (3), 173-185.
94. Fan, H.; Mark, A. E.; Zhu, J.; Honig, B., Comparative study of generalized Born models: protein dynamics. *Proc Natl Acad Sci U S A* **2005**, *102* (19), 6760-4.
95. Ryckaert, J.-P.; Ciccotti, G.; Berendsen, H. J. C., Numerical integration of the cartesian equations of motion of a system with constraints: molecular dynamics of n-alkanes. *J Comput Phys* **1977**, *23* (3), 327-341.
96. Berendsen, H. J. C.; Postma, J. P. M.; van Gunsteren, W. F.; DiNola, A.; Haak, J. R., Molecular dynamics with coupling to an external bath. *J Chem Phys* **1984**, *81* (8), 3684-3690.
97. Crick, F., Central dogma of molecular biology. *Nature* **1970**, *227* (5258), 561-3.
98. Gellert, M., Molecular analysis of V(D)J recombination. *Annu Rev Genet* **1992**, *26*, 425-46.
99. Black, D. L., Mechanisms of alternative pre-messenger RNA splicing. *Annu Rev Biochem* **2003**, *72*, 291-336.
100. Maniatis, T.; Tasic, B., Alternative pre-mRNA splicing and proteome expansion in metazoans. *Nature* **2002**, *418* (6894), 236-43.
101. Lipmann, F. A. L., P.A., Serinephosphoric acid obtained on hydrolysis of vitellinic acid *J Biol Chem* **1932**, *98*.
102. Levene, P. A. A., C., Zur Chemie der Paranucleinsäure. *Z Physiol Chem* **1900**, *31*, 543-555.
103. Pearlman, S. M.; Serber, Z.; Ferrell, J. E., Jr., A mechanism for the evolution of phosphorylation sites. *Cell* **2011**, *147* (4), 934-46.
104. Freschi, L.; Osseni, M.; Landry, C. R., Functional divergence and evolutionary turnover in mammalian phosphoproteomes. *PLoS Genet* **2014**, *10* (1), e1004062.
105. Attwood, P. V.; Piggott, M. J.; Zu, X. L.; Besant, P. G., Focus on phosphohistidine. *Amino Acids* **2007**, *32* (1), 145-56.
106. Besant, P. G.; Attwood, P. V.; Piggott, M. J., Focus on phosphoarginine and phospholysine. *Curr Protein Pept Sci* **2009**, *10* (6), 536-50.
107. Zetterqvist, O.; Engstrom, L., Isolation of N-e-[<sup>32</sup>P]phosphoryl-lysine from rat-liver cell sap after incubation with [<sup>32</sup>P]adenosine triphosphate. *Biochim Biophys Acta* **1967**, *141* (3), 523-32.
108. Ciesla, J.; Fraczyk, T.; Rode, W., Phosphorylation of basic amino acid residues in proteins: important but easily missed. *Acta Biochim Pol* **2011**, *58* (2), 137-48.
109. Attwood, P. V.; Besant, P. G.; Piggott, M. J., Focus on phosphoaspartate and phosphoglutamate. *Amino Acids* **2011**, *40* (4), 1035-51.
110. Denehy, E.; White, J. M.; Williams, S. J., Electronic structure of the sulfonyl and phosphoryl groups: a computational and crystallographic study. *Inorg Chem* **2007**, *46* (21), 8871-86.
111. Jencks, W. P., Mechanism of Reactions of Monosubstituted Phosphates in Water - Appearance and Reality. *ACS Symp Ser* **1992**, *486*, 102-114.
112. Lipmann, F.; Tuttle, L. C., A specific micromethod for the determination of acyl phosphates. *J Biol Chem* **1945**, *159* (1), 21-28.

## BIBLIOGRAPHY

113. Black, S.; Wright, N. G., Enzymatic reduction of beta-aspartyl phosphate to homoserine. *J Am Chem Soc* **1953**, *75* (22), 5766-5766.
114. Koshland, D. E., Effect of Catalysts on the Hydrolysis of Acetyl Phosphate. Nucleophilic Displacement Mechanisms in Enzymatic Reactions. *J Am Chem Soc* **1952**, *74* (9), 2286-2292.
115. Phillips, D. R.; Fife, T. H., Acid-catalyzed hydrolysis of acyl phosphates. *J Am Chem Soc* **1968**, *90* (24), 6803-6809.
116. Carpenter, F. H., The Free Energy Change in Hydrolytic Reactions: The Non-ionized Compound Convention. *J Am Chem Soc* **1960**, *82* (5), 1111-1122.
117. Allen, K. N.; Dunaway-Mariano, D., Phosphoryl group transfer: evolution of a catalytic scaffold. *Trends Biochem Sci* **2004**, *29* (9), 495-503.
118. Ferreira-Cerca, S.; Sagar, V.; Schafer, T.; Diop, M.; Wesseling, A. M.; Lu, H.; Chai, E.; Hurt, E.; LaRonde-LeBlanc, N., ATPase-dependent role of the atypical kinase Rio2 on the evolving pre-40S ribosomal subunit. *Nat Struct Mol Biol* **2012**, *19* (12), 1316-23.
119. Mizuno, T., Two-component phosphorelay signal transduction systems in plants: from hormone responses to circadian rhythms. *Biosci Biotechnol Biochem* **2005**, *69* (12), 2263-76.
120. West, A. H.; Stock, A. M., Histidine kinases and response regulator proteins in two-component signaling systems. *Trends Biochem Sci* **2001**, *26* (6), 369-76.
121. Hsieh, Y. J.; Wanner, B. L., Global regulation by the seven-component Pi signaling system. *Curr Opin Microbiol* **2010**, *13* (2), 198-203.
122. VanBogelen, R. A.; Olson, E. R.; Wanner, B. L.; Neidhardt, F. C., Global analysis of proteins synthesized during phosphorus restriction in Escherichia coli. *J Bacteriol* **1996**, *178* (15), 4344-66.
123. Creager-Allen, R. L.; Silversmith, R. E.; Bourret, R. B., A link between dimerization and autophosphorylation of the response regulator PhoB. *J Biol Chem* **2013**, *288* (30), 21755-69.
124. Crepin, S.; Chekabab, S. M.; Le Bihan, G.; Bertrand, N.; Dozois, C. M.; Harel, J., The Pho regulon and the pathogenesis of Escherichia coli. *Vet Microbiol* **2011**, *153* (1-2), 82-8.
125. Chekabab, S. M.; Jubelin, G.; Dozois, C. M.; Harel, J., PhoB activates Escherichia coli O157:H7 virulence factors in response to inorganic phosphate limitation. *PLoS One* **2014**, *9* (4), e94285.
126. Tiwari, S.; Jamal, S. B.; Hassan, S. S.; Carvalho, P.; Almeida, S.; Barh, D.; Ghosh, P.; Silva, A.; Castro, T. L. P.; Azevedo, V., Two-Component Signal Transduction Systems of Pathogenic Bacteria As Targets for Antimicrobial Therapy: An Overview. *Front Microbiol* **2017**, *8*, 1878.
127. Wright, M. H.; Fetzer, C.; Sieber, S. A., Chemical Probes Unravel an Antimicrobial Defense Response Triggered by Binding of the Human Opioid Dynorphin to a Bacterial Sensor Kinase. *J Am Chem Soc* **2017**, *139* (17), 6152-6159.
128. Hauser, A.; Penkert, M.; Hackenberger, C. P. R., Chemical Approaches to Investigate Labile Peptide and Protein Phosphorylation. *Acc Chem Res* **2017**, *50* (8), 1883-1893.
129. Lai, S. J.; Tu, I. F.; Wu, W. L.; Yang, J. T.; Luk, L. Y. P.; Lai, M. C.; Tsai, Y. H.; Wu, S. H., Site-specific His/Asp phosphoproteomic analysis of prokaryotes reveals putative targets for drug resistance. *BMC Microbiol* **2017**, *17* (1), 123.
130. Lapek, J. D., Jr.; Tomblin, G.; Kellersberger, K. A.; Friedman, M. R.; Friedman, A. E., Evidence of histidine and aspartic acid phosphorylation in human prostate cancer cells. *Naunyn Schmiedebergs Arch Pharmacol* **2015**, *388* (2), 161-73.

131. Gersch, M.; Kreuzer, J.; Sieber, S. A., Electrophilic natural products and their biological targets. *Nat Prod Rep* **2012**, *29* (6), 659-82.
132. Kreuzer, J.; Bach, N. C.; Forler, D.; Sieber, S. A., Target discovery of acivicin in cancer cells elucidates its mechanism of growth inhibition. *Chem Sci* **2014**, *6* (1), 237-245.
133. Lehmann, J.; Vomacka, J.; Esser, K.; Nodwell, M.; Kolbe, K.; Ramer, P.; Protzer, U.; Reiling, N.; Sieber, S. A., Human lysosomal acid lipase inhibitor lalistat impairs Mycobacterium tuberculosis growth by targeting bacterial hydrolases. *Medchemcomm* **2016**, *7* (9), 1797-1801.
134. Counihan, J. L.; Ford, B.; Nomura, D. K., Mapping proteome-wide interactions of reactive chemicals using chemoproteomic platforms. *Curr Opin Chem Biol* **2016**, *30*, 68-76.
135. Backus, K. M.; Correia, B. E.; Lum, K. M.; Forli, S.; Horning, B. D.; Gonzalez-Paez, G. E.; Chatterjee, S.; Lanning, B. R.; Teijaro, J. R.; Olson, A. J.; Wolan, D. W.; Cravatt, B. F., Proteome-wide covalent ligand discovery in native biological systems. *Nature* **2016**, *534* (7608), 570-4.
136. Nodwell, M. B.; Sieber, S. A., ABPP methodology: introduction and overview. *Top Curr Chem* **2012**, *324*, 1-41.
137. Lehmann, J.; Wright, M. H.; Sieber, S. A., Making a Long Journey Short: Alkyne Functionalization of Natural Product Scaffolds. *Chemistry* **2016**, *22* (14), 4666-78.
138. Rudolf, G. C.; Heydenreuter, W.; Sieber, S. A., Chemical proteomics: ligation and cleavage of protein modifications. *Curr Opin Chem Biol* **2013**, *17* (1), 110-7.
139. Rudolf, G. C.; Sieber, S. A., Copper-assisted click reactions for activity-based proteomics: fine-tuned ligands and refined conditions extend the scope of application. *Chembiochem* **2013**, *14* (18), 2447-55.
140. Eirich, J.; Orth, R.; Sieber, S. A., Unraveling the protein targets of vancomycin in living *S. aureus* and *E. faecalis* cells. *J Am Chem Soc* **2011**, *133* (31), 12144-53.
141. Kleiner, P.; Heydenreuter, W.; Stahl, M.; Korotkov, V. S.; Sieber, S. A., A Whole Proteome Inventory of Background Photocrosslinker Binding. *Angew Chem Int Ed Engl* **2017**, *56* (5), 1396-1401.
142. Matthews, M. L.; He, L.; Horning, B. D.; Olson, E. J.; Correia, B. E.; Yates, J. R., 3rd; Dawson, P. E.; Cravatt, B. F., Chemoproteomic profiling and discovery of protein electrophiles in human cells. *Nat Chem* **2017**, *9* (3), 234-243.
143. Marmelstein, A. M.; Moreno, J.; Fiedler, D., Chemical Approaches to Studying Labile Amino Acid Phosphorylation. *Top Curr Chem (Cham)* **2017**, *375* (2), 22.
144. Purich, D. L., Use of sodium borohydride to detect acyl-phosphate linkages in enzyme reactions. *Methods Enzymol* **2002**, *354*, 168-77.
145. Andersson, J.; Barth, A., FTIR studies on the bond properties of the aspartyl phosphate moiety of the Ca<sup>2+</sup>-ATPase. *Biopolymers* **2006**, *82* (4), 353-7.
146. Schlemmer, H.; Sontheimer, G. M.; Kalbitzer, H. R., P-31 Nuclear Magnetic-Resonance Spectroscopy of the Phosphorylated Tetrapeptide Gly-Gly-Asp-Ala. *Magn Reson Chem* **1988**, *26* (3), 260-263.
147. Grimsrud, P. A.; Swaney, D. L.; Wenger, C. D.; Beauchene, N. A.; Coon, J. J., Phosphoproteomics for the masses. *ACS Chem Biol* **2010**, *5* (1), 105-19.
148. Zhang, Y.; Wang, J.; Ding, M.; Yu, Y., Site-specific characterization of the Asp- and Glu-ADP-ribosylated proteome. *Nat Methods* **2013**, *10* (10), 981-4.

## BIBLIOGRAPHY

149. Porter, S. L.; Wadhams, G. H.; Armitage, J. P., Signal processing in complex chemotaxis pathways. *Nat Rev Microbiol* **2011**, *9* (3), 153-65.
150. Szurmant, H.; Muff, T. J.; Ordal, G. W., Bacillus subtilis CheC and FliY are members of a novel class of CheY-P-hydrolyzing proteins in the chemotactic signal transduction cascade. *J Biol Chem* **2004**, *279* (21), 21787-92.
151. Zaborina, O.; Lepine, F.; Xiao, G.; Valuckaite, V.; Chen, Y.; Li, T.; Ciancio, M.; Zaborin, A.; Petrof, E. O.; Turner, J. R.; Rahme, L. G.; Chang, E.; Alverdy, J. C., Dynorphin activates quorum sensing quinolone signaling in Pseudomonas aeruginosa. *PLoS Pathog* **2007**, *3* (3), e35.
152. Weerapana, E.; Wang, C.; Simon, G. M.; Richter, F.; Khare, S.; Dillon, M. B.; Bachovchin, D. A.; Mowen, K.; Baker, D.; Cravatt, B. F., Quantitative reactivity profiling predicts functional cysteines in proteomes. *Nature* **2010**, *468* (7325), 790-5.
153. Georgellis, D.; Kwon, O.; De Wulf, P.; Lin, E. C., Signal decay through a reverse phosphorelay in the Arc two-component signal transduction system. *J Biol Chem* **1998**, *273* (49), 32864-9.
154. Chancey, S. T.; Zahner, D.; Stephens, D. S., Acquired inducible antimicrobial resistance in Gram-positive bacteria. *Future Microbiol* **2012**, *7* (8), 959-78.
155. Wessel, D.; Flugge, U. I., A method for the quantitative recovery of protein in dilute solution in the presence of detergents and lipids. *Anal Biochem* **1984**, *138* (1), 141-3.
156. Cox, J.; Hein, M. Y.; Luber, C. A.; Paron, I.; Nagaraj, N.; Mann, M., Accurate proteome-wide label-free quantification by delayed normalization and maximal peptide ratio extraction, termed MaxLFQ. *Mol Cell Proteomics* **2014**, *13* (9), 2513-26.
157. Tyanova, S.; Temu, T.; Sinitcyn, P.; Carlson, A.; Hein, M. Y.; Geiger, T.; Mann, M.; Cox, J., The Perseus computational platform for comprehensive analysis of (prote)omics data. *Nat Methods* **2016**, *13* (9), 731-40.
158. Ashburner, M.; Ball, C. A.; Blake, J. A.; Botstein, D.; Butler, H.; Cherry, J. M.; Davis, A. P.; Dolinski, K.; Dwight, S. S.; Eppig, J. T.; Harris, M. A.; Hill, D. P.; Issel-Tarver, L.; Kasarskis, A.; Lewis, S.; Matese, J. C.; Richardson, J. E.; Ringwald, M.; Rubin, G. M.; Sherlock, G., Gene ontology: tool for the unification of biology. The Gene Ontology Consortium. *Nat Genet* **2000**, *25* (1), 25-9.

## CURRICULUM VITAE

**Mathias Willibald Hackl**, born November 10<sup>th</sup> 1987 in Munich, Germany

Doctoral studies	01/2014 – 01/2018 Chair of Organic Chemistry II at the Technische Universität München under supervision of Prof. Dr. Stephan A. Sieber.
Master thesis	06/2013 – 12/2013 Chair of Organic Chemistry II at the Technische Universität München under supervision of Prof. Dr. Stephan A. Sieber. <i>“Methods for the examination of small molecule-protein interactions under native conditions and fluorescence labeling of ClpP and ClpX”</i>
Master studies	09/2011 – 12/2013 Biochemistry (minors: bioorganic chemistry and oncology) at the Technische Universität München
Bachelor studies	09/2008 – 06/2011 Biochemistry at the Technische Universität München. Bachelor Thesis with Prof. Dr. Bernhard Küster at the Chair of Proteomics and Bioanalytics. <i>“Establishment, optimization and application of an IMAC-based protocol for phosphopeptide enrichment”</i>
School education	09/1998 – 07/2007 Heinrich-Heine Gymnasium, Munich Higher education entrance qualification (“Abitur”)  09/1994 – 07/1998 Grund- und Teilhauptschule Putzbrunn I, Putzbrunn
Alternative national service	09/2007 – 05/2008 Städtisches Klinikum München, Krankenhaus Harlaching, Munich



LICENSE AGREEMENT

20.11.2017 RightsLink® by Copyright Clearance Center



# RightsLink®

[Home](#)
[Create Account](#)
[Help](#)




**ACS Publications**  
Most Trusted. Most Cited. Most Read.

**Title:** Phenyl Esters Are Potent Inhibitors of Casinolytic Protease P and Reveal a Stereogenic Switch for Deoligomerization

**Author:** Mathias W. Hackl, Markus Lakemeyer, Maria Dahmen, et al

**Publication:** Journal of the American Chemical Society

**Publisher:** American Chemical Society

**Date:** Jul 1, 2015

Copyright © 2015, American Chemical Society

**LOGIN**

If you're a copyright.com user, you can login to RightsLink using your copyright.com credentials. Already a RightsLink user or want to learn more?

**PERMISSION/LICENSE IS GRANTED FOR YOUR ORDER AT NO CHARGE**

This type of permission/license, instead of the standard Terms & Conditions, is sent to you because no fee is being charged for your order. Please note the following:

- Permission is granted for your request in both print and electronic formats, and translations.
- If figures and/or tables were requested, they may be adapted or used in part.
- Please print this page for your records and send a copy of it to your publisher/graduate school.
- Appropriate credit for the requested material should be given as follows: "Reprinted (adapted) with permission from (COMPLETE REFERENCE CITATION). Copyright (YEAR) American Chemical Society." Insert appropriate information in place of the capitalized words.
- One-time permission is granted only for the use specified in your request. No additional uses are granted (such as derivative works or other editions). For any other uses, please submit a new request.

BACK
CLOSE WINDOW

Copyright © 2017 Copyright Clearance Center, Inc. All Rights Reserved. [Privacy statement](#). [Terms and Conditions](#). Comments? We would like to hear from you. E-mail us at [customerscare@copyright.com](mailto:customerscare@copyright.com).